



Skolkovo Institute of Science and Technology

MULTISCALE MODELING OF GRAPHENE NANOBUBBLES

*Doctoral Thesis*

by

EVGENY IAKOVLEV

DOCTORAL PROGRAM IN MATHEMATICS AND MECHANICS

Supervisor  
Professor Iskander Akhatov

Co-supervisor  
Doctor Petr Zhilyaev

Moscow - 2021

© Evgeny Iakovlev 2021

I hereby declare that the work presented in this thesis was carried out by myself at Skolkovo Institute of Science and Technology, Moscow, except where due acknowledgement is made, and has not been submitted for any other degree.

Candidate (Evgeny Iakovlev)

Supervisor (Prof. Iskander Akhatov)

## Abstract

Van der Waals two dimensional heterostructures are systems created by stacking two-dimensional crystals such as graphene, boron nitride, and MoS<sub>2</sub>. The layers are attracted to each other by van der Waals forces. The essential property of such structures is an atomically flat surface. Also, two-dimensional heterostructures recently actively studied because they have a great potential to develop materials with any required properties.

While creating these heterostructures, inevitably, some contamination can be trapped between layers leading to the formation of the bubble. The structure consisting of the atomically flat substrate, the upper two-dimensional crystal, and the trapped matter is called van der Waals nanobubble. At first, these nanobubbles were treated as negative manufacturing defects. Eventually, a large number of interesting properties of the nanobubbles were found, such as extreme internal pressure and giant pseudo magnetic field. Also, nanobubbles are spots of intense photoluminescence emission caused by a strained-induced shift in the band structure.

In this study, the properties of the van der Waals nanobubbles are studied by the example of graphene nanobubbles - the van der Waals nanobubbles with graphite as a substrate and the graphene as the upper layer.

In current study, molecular dynamics simulations are performed to investigate the graphene nanobubbles filled with argon with a radius up to 33 nm. These calculations allow verifying the universal shape scaling, i.e., the constant height of the bubble to the footprint radius of the nanobubble, which is found experimentally. Also, it is discovered that argon exists in solid-state inside nanobubbles. However, the trapped argon is at such temperature and pressure, insufficiently enough for crystallization in the bulk system. The 'pancake' nanobubbles are found, i.e., the nanobubbles with relatively low height to radius ratio, which are at the metastable states - nanobubbles with a radius less than 10 nm.

The molecular dynamics simulations can be performed only for small nanobubbles up to 50 nm. For the investigation of larger nanobubbles, other approaches should be implemented. Thus, the theoretical model based on the continuum approach is developed, which covers a wide range of nanobubbles radii. It uses a combination of the theory of elasticity of membranes, the equations of state of matter, and molecular dynamics simulations to evaluate some macro parameters such as elastic modulus and adhesion energies. The properties of the nanobubble are obtained by minimization of the total energy of the bubble consisting of the elastic energy of the upper graphene sheet, the free energy of the trapped fluid, and the adhesion energy between the substrate the graphene, and the trapped matter. The proposed model is applied to a graphene nanobubble filled with argon and ethane at different temperatures. The model allows finding a correlation between the size of the nanobubble and the state of trapped matter. Also, it gives the profile of the nanobubble and the stresses and strains of the upper graphene sheet, which are consistent with molecular dynamics simulations and experimental studies. The model reveals new phenomena, and we called it the 'forbidden region' - the range of radii where no stable bubble can be found. This region separates bubbles with a different state of trapped matter. In this study, we consider gas and liquid states, thus smaller bubbles contain liquid state matter, and bigger bubbles contain gas

state. Finally, the classical density functional theory is applied to get more precise thermodynamical properties of the trapped matter and to take into account the inhomogeneity of the fluid.

The study can be used as a reference for the theoretical investigation of the van der Waals nanobubbles. The developed continuum model can be adapted for any type of van der Waals nanobubble by substituting parameters for a given type of substrate, upper two-dimensional crystal, and trapped matter. The molecular dynamics simulations yield more detailed information about the system, but the continuum approach covers a wider range of sizes of the nanobubbles.

The van der Waals nanobubbles have a great potential to study. Their variety of unique properties can be used in some industrial applications. This work is an attempt to get a deeper physical understanding of the formation of nanobubbles. The author hopes that this research will benefit the science of nanoscale systems.

## Publications

1. Evgeny Iakovlev, Petr Zhilyaev, and Iskander Akhatov. Atomistic study of the solid state inside graphene nanobubbles. *Scientific reports*, 7(1):1–7, 2017
2. ES Iakovlev, PA Zhilyaev, and I Sh Akhatov. Obtaining the state of matter inside graphene nanobubble from its shape. In *Journal of Physics: Conference Series*, volume 1147, page 012006. IOP Publishing, 2019a
3. Petr Zhilyaev, Evgeny Iakovlev, and Iskander Akhatov. Liquid–gas phase transition of ar inside graphene nanobubbles on the graphite substrate. *Nanotechnology*, 30(21):215701, 2019
4. Evgeny Iakovlev, Petr Zhilyaev, and Iskander Akhatov. Modeling of the phase transition inside graphene nanobubbles filled with ethane. *Physical Chemistry Chemical Physics*, 21(33):18099–18104, 2019b
5. TF Aslyamov, ES Iakovlev, I Sh Akhatov, and PA Zhilyaev. Model of graphene nanobubble: Combining classical density functional and elasticity theories. *The Journal of Chemical Physics*, 152(5):054705, 2020
6. ES Iakovlev, PA Zhilyaev, and I Sh Akhatov. Adhesion energy of ethane–graphite interface: Atomistic study. In *Journal of Physics: Conference Series*, volume 1556, page 012052. IOP Publishing, 2020

## Conferences

1. Shaping the Future: Big Data, Biomedicine and Frontier Technologies (April 25-26, 2017, Skoltech, Russia)
2. Generation-Y (October, 27-1, 2017, Sochi, Russia)
3. XXXIII International Conference on Equations of State for Matter (March 1-6, 2018, Elbrus, Russia)
4. International Summer School-Conference “Advanced Problems in Mechanics” (June 24-29, 2018, Saint Petersburg, Russia)
5. MRS Fall Meeting and Exhibit (November, 25-30, 2018, Boston, USA)
6. XXXIV Interaction of Intense Energy Fluxes with Matter (March 1-6, 2019, Elbrus, Russia)
7. XII Russian Congress on the fundamental problems of theoretical and applied mechanics (August 19-24, 2019, Ufa, Russia)
8. Symposium for Computational Materials Program of Excellence (September 4-6, Skoltech, Russia)
9. International Congress on Graphene, 2D Materials and Applications (September 30-October 4, Sochi, Russia)

*Dedicated to my parents.*

# Contents

<b>1</b>	<b>Introduction</b>	<b>10</b>
1.1	Relevance of work . . . . .	10
1.2	Research topic status . . . . .	11
1.3	Goals and objectives . . . . .	12
1.4	Novelty of the work . . . . .	13
1.5	Theoretical and practical impact . . . . .	13
1.6	Methodology and research methods . . . . .	14
<b>2</b>	<b>Background</b>	<b>15</b>
2.1	Graphene nanobubbles history . . . . .	15
2.2	2D heterostructures . . . . .	15
2.3	Van der Waals nanobubbles . . . . .	16
2.4	Confined fluid . . . . .	22
2.5	Molecular dynamics . . . . .	24
2.6	Interatomic potentials . . . . .	25
2.6.1	Tersoff potential . . . . .	27
2.6.2	AIREBO potential . . . . .	29
2.6.3	TraPPE-UA . . . . .	30
<b>3</b>	<b>Thesis Objectives</b>	<b>31</b>
3.1	Atomistic study . . . . .	32
3.1.1	Potential verification . . . . .	32
3.1.2	Contribution . . . . .	33
3.2	The shape of the bubble and the state of the trapped matter . . . . .	42
3.2.1	Contribution . . . . .	42
3.3	Prepare to continuum approach: adhesion energy . . . . .	49
3.3.1	Contribution . . . . .	49
3.4	Continuum approach: argon case . . . . .	55
3.4.1	Contribution . . . . .	55
3.5	Continuum approach: ethane case . . . . .	64
3.5.1	Contribution . . . . .	64
3.6	Continuum approach: DFT implementation . . . . .	71
3.6.1	Contribution . . . . .	71
<b>4</b>	<b>Conclusion</b>	<b>83</b>
4.1	Summary . . . . .	83
4.2	Outlook . . . . .	84

<b>Glossary</b>	<b>86</b>
<b>Bibliography</b>	<b>87</b>

# Chapter 1

## Introduction

### 1.1 Relevance of work

The system consisting of the substrate, outer [two dimensional \(2D\)](#) crystal, and matter trapped inside, we define as a [van der Waals \(vdW\)](#) nanobubble. The special case of a van der Waals nanobubble is [graphene nanobubble \(GN\)](#) when 2D crystal is graphene. Graphene nanobubbles studies are a novel and rapidly developing area that includes solid state physics, surface physics, and high pressure chemistry. Investigation of graphene nanobubbles on an atomic scale is actual in fundamental science and industry projects.

Recently, classical MD methods are used as a standard tool for developing models of such atomic systems. The advantages of numerical modeling are the possibility of tracking trajectories of atoms and molecules and further calculating macro-parameters of the system, such as pressure, temperature, elastic modulus, etc. Thus, it is possible to describe the properties of the whole system by observing the behavior of the separate atoms. That is why we use MD analysis to study graphene nanobubbles since it is a highly non-homogeneous system. Experimental studies only indirectly measure the inner structure of the nanobubble and the pressure of trapped matter, while MD calculations make it possible to evaluate these values directly.

Although the [molecular dynamics \(MD\)](#) method has significant potential for predictive capability, this method has natural limitations such as the number of

particles in the simulation box. Present-day supercomputers, such as the Joint Supercomputer Center of the Russian Academy of Sciences, can simulate systems consisting of millions of atoms. It corresponds to a nanobubble with a radius of 30-40 nm. In order to study bigger systems, it is necessary to develop continuum models based on macroscopic elastic equations, equations of states of the matter, and so on. These models use parameters, which can be obtained from experiment or MD calculations or *ab-initio* calculations.

## 1.2 Research topic status

The recent popular research subject is the creation of 2D heterostructures [Geim and Grigorieva \[2013\]](#), [Novoselov et al. \[2016\]](#). The van der Waals heterostructures consisting of atomic planes are made layer by layer. During this process of creation, foreign atoms could be trapped in the space between the layers, which leads to the formation of bubbles and blisters of nanoscopic scale [Levy et al. \[2010\]](#), [Khestanova et al. \[2016\]](#).

There are three different approaches of graphene nanobubbles investigation:

- experimental studies, which allows to directly or implicitly measure the parameters of the nanobubbles;
- MD studies allow to model and directly observe physical processes inside GNs;
- semi-analytical approach is based on theories from different areas: the theory of elasticity, thermodynamics, and interaction of the matter.

Experiments reveal a lot of interesting properties of graphene nanobubbles. For example, the nanobubbles can be used as chemical reactors of nanometer scale. In work [Lim et al. \[2013\]](#) authors show that water inside graphene nanobubbles becomes much more reactive and starts to interact with the diamond substrate. In another work [Mu et al. \[2012\]](#) graphene nanobubbles are found to be able to visualize chemical reactions in real-time.

There are other promising aspects of graphene studies: the connection between magnetic, electronic, and mechanical properties of graphene. In work [Levy et al.](#)

[2010] authors show that graphene nanobubbles generate gigantic pseudo-magnetic fields up to 300 tesla. In other works Lu et al. [2012], Georgiou et al. [2011] the curvature of graphene nanobubbles is controlled by an external electric field.

Also, the investigation is rapidly developing of van der Waals nanobubbles generated by irradiation of highly energetic ions Zamborlini et al. [2015], Larciprete et al. [2016]. The authors show that inside nanobubbles, the clusters with irradiated atoms are formed.

The MD study is performed in work Ghorbanfekr-Kalashami et al. [2017], the small graphene nanobubbles with a radius up to 20 nm are investigated. The authors used sophisticated potential ReaxFF Van Duin et al. [2001], authors performed MD calculations with a different type of trapped matter. Also, similar systems are considered in the work Algara-Siller et al. [2015]. This research shows that matter behavior in confinement significantly differs from bulk matter behavior.

Also, relevant and interesting topic is interactions between vdW nanobubbles. Thus, in Lu et al. [2012] a junction of the nanobubbles is investigated. Of significant interest is a dependence on the shape of vdW nanobubbles and the type of matter trapped inside. In the work Ghorbanfekr-Kalashami et al. [2017], it is shown experimentally and theoretically that there is a connection between the shape and content of graphene nanobubbles.

### 1.3 Goals and objectives

1. Investigation of the profile of graphene nanobubbles with dependence on the size of graphene nanobubble and the matter trapped inside
2. Investigation of adhesion properties between graphene and argon/methane
3. Development of a continuum approach, which allows to model nanobubbles of any sizes
4. Investigation of connection between the shape of the nanobubble and the trapped substance
5. Comparison of continuum and MD approaches

## 1.4 Novelty of the work

In this work, the properties of vdW nanobubbles are studied on the example of graphene nanobubbles. An attempt is made to find general patterns in systems consisting of the substrate, 2D crystal, which is attracted to substrate by vdW forces, and trapped matter between the substrate and 2D crystal.

At the time of the beginning of this work, no known to author studies used the MD methods to model graphene nanobubbles with a setup close to the experimental one. For the first time, we observed that matter could crystallize at such temperature and pressure in nanobubbles with sizes up to 33 nm (and probably more), where the matter has to be liquid. This phenomenon is a manifestation of the strong influence of confinement.

Despite that there were studies [Khestanova et al. \[2016\]](#), where a semi-analytical approach is suggested for nanobubbles, a comprehensive model, which takes into account the state of the trapped matter, was still missing. For the first time, in this thesis a model is proposed that considers the system's energy as a contribution of three parts: energy of vdW interaction between the substrate, the graphene sheet, and the trapped matter; elastic energy of graphene sheet; the energy of trapped matter. This model allows investigating the complex connection between the shape of the bubble, trapped matter state, the pressure inside, stresses in the upper graphene sheet, adhesion energy.

Also, our model is improved by applying [density functional theory \(DFT\)](#) to take into account the inhomogeneity of the trapped matter. This model makes it possible to describe the inner structure of the bubble and evaluate the effect of the nanoconfinement.

## 1.5 Theoretical and practical impact

Investigating the state of trapped matter inside graphene nanobubble of different sizes and analyzing the stresses inside graphene sheet during the formation of the nanobubble are the main theoretical results of this study. The critical aspect also is the development of a continuum model, which, together with the MD approach,

allows to consider nanobubbles of various sizes and investigate the inner structure of the bubble on different scales.

The significant practical impact is contribution to understanding the connection between the shape of the bubble and its inner structure. The insight into the formation of graphene and other vdW nanobubbles is the crucial factor in creating clear 2D heterostructures.

The indicator of the significance of the work is the nomination of paper [Iakovlev et al. \[2017\]](#) as one of the best in relevant topics "Editor's choice: 2D materials and heterostructures". Also, editors of the Physical Chemistry Chemical Physics journal chose article [Iakovlev et al. \[2019b\]](#) as hot research "selected by the Editors as a 2019 HOT PCCP article".

## 1.6 Methodology and research methods

MD simulations are performed in [large-scale atomic/molecular massively parallel simulator \(LAMMPS\)](#) software package [Plimpton \[1995\]](#) on different supercomputers. The continuum model is implemented by minimizing the energy functional. The code is written in python. The Broyden–Fletcher–Goldfarb–Shanno (BFGS) method is used to get optimal coefficients of Chebyshev polynomials, which correspond to equilibrium bubble. Density functional theory is used to take into account the inhomogeneity of trapped matter inside graphene nanobubbles.

"All models are wrong, but some are useful"

George E. P. Box

## Chapter 2

# Background

Here is a comprehensive review of the literature related to the topic of this work. The main methods used in this work are described. Also the history of graphene nanobubbles studies is mentioned. Then, MD methods are discussed including description of potentials used in the work.

## 2.1 Graphene nanobubbles history

## 2.2 2D heterostructures

The history of graphene nanobubbles is not straightforward. It starts when Andrei Geim's group in Manchester actively started to study two dimensional (2D) heterostructures [Geim and Grigorieva \[2013\]](#). 2D heterostructure is a material which consists of the stack of two dimensional crystals, attracted one by another with van der Waals forces. This type of material is also called van der Waals heterostructures. Isolated atomic planes are not so interesting in sense of industrial applications, as they are very active and reactive and it is really complicated to obtain the pure atomic crystals. But if one has stack of the crystals planes - it is stable and also it reveals many unusual properties.

Different types of 2D crystals can be used in van der Waals heterostructures: graphene, MoS<sub>2</sub>, hBN, WSe<sub>2</sub>, fluorographene and etc. The main idea of construction is to take the monolayer and put it on the top of another monolayer or several layer

crystal. This concept Geim and his group called "Lego". The strong covalent bonds make the material strong in-plane of the crystal, and relatively weak van der Waals forces are enough to keep the stack stable. The first experiment that showed the possibility of creating a stable van der Waals heterostructure is [Ponomarenko et al. \[2011\]](#). The authors showed a strong Anderson localization and the corresponding metal–insulator transition in pure graphene. To do that they created two closely-spaced but electrically isolated graphene monolayers sandwiched in boron nitride.

The main feature of 2D heterostructures is atomically flat and clean from any contamination surface because of strong van der Waals adhesion between the layers [Haigh et al. \[2012\]](#). However, there can be some remained water or hydrocarbons presented on the surface while preparing the samples. Thus the van der Waals forces push this trapped substance between the layers into the nano or submicron-size bubbles. After formation of the bubbles, the surface remains atomically sharp and absolutely clean. For scientists these bubbles are the manifestation that the surface of 2D heterostructures between the bubbles is perfectly clean. For example, the authors [Kretinin et al. \[2014\]](#) found that devices created by encapsulating graphene with molybdenum or tungsten disulfides and hBN exhibit the self-cleaning effect between graphene, hBN and dichalcogenides. The contamination is found to be captured into the "large pockets" and leaves the rest of surface clean. This attribute is proved by measuring the carrier mobility, which is high for clean surface (about  $60000 \text{ cm}^2 \text{ V}^{-1} \text{ s}^{-1}$ ) and low for poor quality graphene (about  $1000 \text{ cm}^2 \text{ V}^{-1} \text{ s}^{-1}$ ).

## 2.3 Van der Waals nanobubbles

The formed onto the surface bubbles are called van der Waals nanobubbles, or in case there the upper 2D crystal is graphene - graphene nanobubbles. There are a lot of interesting properties are discovered associated with them.

The comprehensive research is performed by [Khestanova et al. \[2016\]](#). Authors studied different types of substrates (hBN, graphite and  $\text{MoS}_2$ ) and upper 2D layers (graphene, hBN and  $\text{MoS}_2$  monolayers). Special technique is developed to prepare

samples which includes standart dry-peeling technique [Mayorov et al. \[2011\]](#), followed by annealing the prepared heterostructure for 20-30 minutes, that results into formation of the bubbles. Then the surface with hundreds of the bubbles is analyzed using [atomic force microscopy \(AFM\)](#).

Different sizes and shapes of the nanobubbles are detected depending on the type of the substrate and upper 2D layer. Most bubble are with radius less than 500 nm with round footprint. The bigger bubbles tend to be in pyramidal shapes, with either triangular or trapezoidal bases. Also authors in [Khestanova et al. \[2016\]](#) defined convenient geometrical parameter that characterizes the bubble - the height to radius aspect ratio  $H/R$ . This value is useful to implement in order to compare shapes of the bubbles for different types of materials. They found that the ratio is universal for different radii ranges for particular types of the bubbles. For example, for graphene and hBN nanobubbles on the hBN substrate the value  $H/R = 0.11$ . But there is a deviation from the rule for nanobubbles with radius less than 50 nm. For MoS<sub>2</sub> monolayer the  $H/R$  parameter is larger - around 0.14 for MoS<sub>2</sub> substrate and 0.16 for hBN substrate. The difference in these values attributes to different Young's modulus of monolayers and to different adhesion energies between the substrate and the upper layers.

The first continuum approach is developed in study [Khestanova et al. \[2016\]](#) which formulates the energy of the system as a sum of different parts: the elastic energy of the 2D crystal, the van der Waals energy associated with detaching of the monolayer from the substrate and the free energy of the substance inside the bubble of volume  $V$ .

$$E_{tot} = E_{el} + E_{vdW} + E_b(V) \quad (2.1)$$

Then by minimizing this energy with respect to radius  $R$  and the maximum height  $h_{max}$  and denoting pressure as  $P = -\partial E_b / \partial V$ , one can obtain the expression for the geometrical parameter  $H/R$  assuming the absence of the external strain:

$$\frac{h_{max}}{R} = \left( \frac{\pi\gamma}{5c_1 Y} \right)^{\frac{1}{4}}, \quad (2.2)$$

where  $c_1$  is a dimensionless constant which depends on the shape  $h(r)$ ,  $Y$  is a Young's modulus of graphene,  $\gamma$  is a adhesion energy, which is decomposed as:

$$\gamma = \gamma_{GS} - \gamma_{Gb} - \gamma_{Sb}, \quad (2.3)$$

where  $\gamma_{GS}$ ,  $\gamma_{Gb}$ ,  $\gamma_{Sb}$  are adhesion energies between the substrate and graphene, graphene and trapped matter and the substrate and the matter inside the bubble, respectively.

The equation 2.2 shows the dependence of the geometry of the bubble on the elastic properties of the 2D crystal and adhesion energies. The stronger adhesion between the layers in the heterostructure - the thicker the bubble, and in contrast, the harder the 2D crystal - the flatter the bubble.

Also this article [Khestanova et al. \[2016\]](#) provides method of how to evaluate the pressure inside the bubble using an AFM tip. Authors used nanoindentation method [Roos et al. \[2010\]](#), which implies indentation of the bubble with an AFM tip and recording the response - force-displacement curves. The new energy of the system with the indented bubble consists of the van der Waals energy, elastic energy with indentation correction, internal energies, and work done by an external force by the tip:

$$E_{tot} = -F\delta + E_{el}(R, \delta) + E_{vdW}(R) + E_V[V(R, \delta)]. \quad (2.4)$$

After minimizing the energy with respect to  $R$  and  $\delta$ , assuming that inside the bubble there is incompressible fluid, one can get the simple relation between the force and the indentation depth:

$$F = 2c(v)\sigma\delta \quad (2.5)$$

where  $c(v)$  is a constant which depends on the Poisson ratio of the upper 2D layer.

The real force-displacement curves are not linear, as a contact area between the tip and the membrane is finite. If one takes into account the non-linearity, the new approximation can be derived:

$$\frac{F}{\delta} = d(v)Y \frac{h_{max}^2}{R^2} \quad (2.6)$$

where  $d(v)$  is another constant which depends on the Poisson ratio. Finally, the equation for dependence of the pressure due to elastic deformations:

$$P_{el}(r) = \frac{1}{r} \frac{\partial}{\partial r} [r \sigma_{rr}(r) \partial_r h(r)], \quad (2.7)$$

where  $\sigma_{rr}$  is the radial stress. Thus, authors [Khestanova et al. \[2016\]](#) fit real experimental data with derived equations and evaluate pressure inside the bubbles. For rather big MoS<sub>2</sub> and graphene nanobubbles with radius 250-800 nm the van der Waals pressure is of the order of several MPa. To evaluate hydrostatic pressure of the trapped matter (most probably hydrocarbons in the study) inside the bubble the elastic contribution has to be taken into account also. For the bubbles discussed above the value of elastic pressure can reach 20 MPa. Also, using this technique the elastic modulus of the 2D crystal can be measured. The Young's modulus of graphene is evaluated as  $420 \pm 20 \text{ N m}^{-1}$  and for MoS<sub>2</sub> -  $210 \pm 20 \text{ N m}^{-1}$ , which is higher than the obtained values before using nanoindentation method:  $350 \pm 50 \text{ N m}^{-1}$  for graphene [Hone et al. \[2008\]](#) and  $180 \pm 80 \text{ N m}^{-1}$  for MoS<sub>2</sub> [Bertolazzi et al. \[2011\]](#). Authors attribute this difference to the fact that membrane is strained up to  $\approx 1 \%$  in the observed nanobubbles.

The electronic properties of graphene sheet change in the stressed state. Thus the van der Waals nanobubble is a great example of the system which contains strained graphene. There is a sequence of works, which are devoted to studying of the electronic properties of graphene nanobubbles. In [Levy et al. \[2010\]](#) the giant strained-induced pseudo-magnetic field up to 300 tesla is observed in graphene nanobubbles. The electronic states can be adjusted using pseudo-magnetic fields. In the work [Levy et al. \[2010\]](#) the strained graphene in the nanobubbles are studied using [scanning tunneling microscopy \(STM\)](#). The Landau levels are found which can be formed in graphene in presence of the magnetic field around 300 tesla. Using the graphene nanobubbles, it is possible to study electronic properties in strained crystal under inaccessible extreme magnetic field.

In another work Qi et al. [2014] pseudo-magnetic field in graphene nanobubbles using MD method is studied. The authors use MD simulations to calculate the geometry of graphene membrane placed against the round aperture inflated by some gas. Then they use continuum mechanics equations of infinitesimal strain tensor:

$$e_{ij} = \frac{1}{2} \left( \frac{\partial u_i}{\partial X_j} + \frac{\partial u_j}{\partial X_i} \right) + \frac{1}{2} \left( \frac{\partial u_k}{\partial X_i} \frac{\partial u_k}{\partial X_j} \right) \quad (2.8)$$

where  $(X_i)$  is the Cartesian coordinates and  $(u_i)$  is a displacement field.

From MD simulations it is possible to get the displacements of the carbon atoms and by substituting them into 2.8 obtain strain tensor.

Pseudo-magnetic field reflects the changing of the bond length between carbon atoms and, as a result, the perturbation of the electrons near the Fermi level. The tight-binding (TB) method is able to describe all low energy electronic properties of graphene. The highest magnitude of the pseudo-magnetic field concentrates near the edges of the aperture. That is because near the boundaries the most bent graphene part is located. The tilted  $p_z$  orbitals, curvature, and stretched bonds affect the pseudo-magnetic field the most. In contrast, at the center of the bubble, weak pseudo-magnetic field due to isotropic strain profile can be observed. This strong localization can be used in strain engineering in order to guide electrons into the channel-like geometries by the blisters edges.

Trapped water inside graphene nanobubbles on a diamond substrate exhibits activity high enough to etch the diamond surface Lim et al. [2013]. After putting a graphene layer onto the diamond, the system is annealed to the temperature 1275 K. It results in a large number of graphene nanobubbles with water trapped inside. At such temperature the bonds between the substrate and graphene layer is high enough to make inside "hydrothermal anvil cell", thus superheated water makes square holes in the diamond substrate. Also trapped substance between graphene layers is studied by a Fourier transform infrared (FTIR) spectroscopy *in-situ*. The vibrational bands keep the same for the temperature up to 773 K, that means that water is inside the bubble.

There is another type of the nanobubbles: graphene nanobubbles on the metallic substrate. The type of adhesion has different physical nature - bonds between

carbon and metal atoms are covalent or ionic [Das et al. \[2013\]](#), nevertheless these bubbles capture the basic principle of formation: competition between the elastic forces of graphene and the adhesion forces between graphene and the substrate. One of the way of producing these type of bubbles is bombarding the graphene membrane on Ir substrate by low-energy argon ions [Zamborlini et al. \[2015\]](#). The ions penetrate through the membrane and form clusters. Then the system is annealed and the surface is studied by low energy electron microscopy (LEEM) [Bauer \[1994\]](#), synchrotron-based photoemission electron microscopy (XPEEM) [Locatelli and Menteş \[2015\]](#), and scanning tunneling microscopy (STM). If annealing is performed at 1080°C then the nanobubbles with radius of tens of nm and few nm of height are formed. Thus the sizes are controlled by the temperature of treatment. The result bubbles are found to be filled with solid aggregates of argon atoms [Zamborlini et al. \[2015\]](#).

Another study [Larciprete et al. \[2016\]](#) where argon atoms are intercalated under the graphene membrane on Ni(111) and Gr substrate. After annealing the authors obtained the nanosized blisters evenly distributed on the surface. The strain in the graphene layer is non-uniform. It is attributed to the inhomogeneous graphene elastic properties.

Graphene nanobubbles are a great example of system with curved graphene. The curvature changes electronic and optical properties of the crystal. In the article [Kim et al. \[2015\]](#) argon ions are intercalated between graphene and Pt substrate. It is shown that such graphene nanobubbles are spots of intense phonon excitation and electron tunneling above the phonon energy. This happens due to the increasing the distance between the graphene layer and the substrate and following reduction of the interaction. Thus, graphene nanobubbles can be used to control the local phonon properties. Also this study explains that electron properties could differs from the expected in graphene nanodevices due to imperfections in graphene or substrate while assembling.

Another work [Tyurnina et al. \[2019\]](#) describes the possibility of using the van der Waals nanobubbles with monolayer transition metal dichalcogenides as spots of photoluminescence with adjustable wavelength. Strain can change optical and electronic

properties of 2D layer. Here it creates "artificial atoms", which work as exciton condensers and responsible for photoluminescence mechanism. In the study [Tyurnina et al. \[2019\]](#) MoS<sub>2</sub> is used as upper 2D layer and substrates are PtSe<sub>2</sub>, WS<sub>2</sub>, MoS<sub>2</sub>, or graphite. It is demonstrated that the intensity of the photoluminescence can be adjusted varying different substrates. Also it is found that photoluminescence is quenched in the flat area, where the 2D crystal and the substrate are in good contact, that makes the bubbles the only areas with high intensity of emission. Using different monolayers transition metal dichalcogenides and substrates it is possible to adjust desired by the application photoluminescence.

## 2.4 Confined fluid

The one more aspect, van der Waals nanobubbles are interesting, is the state of the trapped matter and conditions in which the matter is. It is noticeable that the matter inside the bubble is an example of the strong confinement. It can significantly affect the behaviour of the substance. For example, in [Nair et al. \[2012\]](#) it was shown that the permeability in graphene based membranes through the nanometer size pores differs significantly for different types of substance. This membrane was almost impermeable for liquids, vapors, and gases, including helium, but water penetrates in 10<sup>10</sup> times faster than helium. This behaviour is absolutely unexpected for regular filtration through the medium. Such behaviour authors attribute to the ability of the monolayer of water to flow with low friction in 2D pores formed by graphene sheets. In contrast, other types of matter are locked down by water contamination or narrowing of pores due to low humidity.

Another work [Holt et al. \[2006\]](#) shows that permeability inside the carbon nanotubes with diameter less than 2 nm differs from the predicted Knudsen diffusion model. For gas permeability is by more than an order of magnitude, for water - 3 orders of magnitude. Authors made comparison of their experiments results with MD simulations measurements and it agrees well. Moreover the MD calculations revealed the mechanism of the flow: the molecules are arranged into the "wires" inside the tube. Thus the high permeability can be described either by proposed

mechanism or by nearly frictionless surface.

There are many works show abnormal behaviour of water inside strong confinement. "Soft dynamics" of water in carbon nanotubes (CNTs) was discovered by neutron scattering [Kolesnikov et al. \[2004\]](#). This kind of dynamics described by flexible hydrogen bonds in water molecule and anharmonic intermolecular potentials. Then MD study revealed that water inside the CNT forms rolled sheet that is uniaxial with the CNT. And inside that tubes water molecules form the chain that is very mobile.

Confinement between two graphene sheets can be used in situ transmission electron microscopy (TEM) [Yuk et al. \[2012\]](#). This technique allows to observe liquid films in more realistic conditions, also giving higher resolution. Another works [Park et al. \[2015\]](#) shows usage of graphene liquid cells in order to investigate biological objects, such as viruses, using TEM. This method allows to observe objects in their native buffer solution at room temperature with nanometer scale spatial resolution. In another work [Wojcik et al. \[2015\]](#) graphene cells are used to study alive cells without exposing of vacuum.

Water captured between the two graphene layers is shown to present in the absolutely new phase with a symmetry different from the conventional tetrahedral geometry of hydrogen bonding between water molecules [Algara-Siller et al. \[2015\]](#). The shape of the confined water is quadratic that is why authors called that phase "square ice". The density of the water inside that confinement is very high with lattice constant 2.83 Å. The water between graphene sheets presents in the form of bi- or tri-layer crystals.

Reactions in the confinement is another interesting topic to study. It is the direct application of graphene nanobubbles, natural way to capture different substances, localize it and observe the consequent reaction. For example, in [Sutter et al. \[2010\]](#) the graphene-metal interface is modified by intercalation of oxygen molecules. This leads to distancing the graphene layer from the metal substrate and consequently restoring the Dirac cones inherent to isolated graphene later.

In the study [Mu et al. \[2012\]](#) there is suggested way to visualize chemical reactions. A graphene island is grown on the Pt(111) substrate at high temperature,

when cooling the large wrinkles are formed due to different expansion coefficients of graphene and the Pt substrate. Then the gas flow exposes the prepared surface and after raising the pressure, the gas starts to penetrate into the wrinkle. The CO intercalation leads to enlarging distance between graphene and the substrate, that can be detected by real-time low-energy electron microscopy (LEEM) and photoemission electron microscopy (PEEM) by changing the diffraction intensity. Also the reaction of the CO with O<sub>2</sub> molecules can be visualized using LEEM/PEEM and in situ X-ray photoelectron spectroscopy (XPS). The confined CO molecules are influenced by strong confinement - CO molecules are able to desorb from the Pt surface at room temperature.

Iodine intercalated into single wall CNT is found to form a helical chains [Fan et al. \[2000\]](#). Such strong confinement initiates the charge transferring between iodine atoms and carbon atoms in the CNT. That produces iodine ions in that are very active and easily oxidize particles at the ends of the tube and defects in the CNT.

## 2.5 Molecular dynamics

Molecular dynamics simulation is a calculation of trajectory of atoms, molecules or particles by integrating the equations of motion [Norman and Stegailov \[2013\]](#), [Frenkel and Smit \[2001\]](#), [Tuckerman \[2010\]](#). In classical molecular dynamics the Newton's second laws of motion is solving for each atom or particle in simulation box:

$$m_i \frac{d^2 r_i}{dt^2} = F_i(r_1, \dots, r_N), \quad (2.9)$$

where  $m_i$ ,  $r_i$  and  $F_i$  — the mass, the coordinate and the force acting on the  $i$ th particle, respectively. Forces acting on particles are calculated via interatomic potential  $U(r_1, \dots, r_N)$ :

$$F_i = -\frac{\partial U(r_1, \dots, r_N)}{\partial r_i} \quad (2.10)$$

There are different options how to solve these equations of motion, but most used method is velocity Verlet integration in second-order approximation:

$$\begin{aligned} v_i(t + \frac{\Delta t}{2}) &= v_i(t) + \frac{F_i}{m_i} \frac{\Delta t}{2}, \\ r_i(t + \Delta t) &= r_i(t) + v_i(t + \frac{\Delta t}{2}) \Delta t, \\ v_i(t + \Delta t) &= v_i(t + \frac{\Delta t}{2}) + \frac{F_i(t + \Delta t)}{m_i} \frac{\Delta t}{2}. \end{aligned} \quad (2.11)$$

Statistical mechanics methods allow to get macro parameters of the system from atoms or particles trajectories:

$$T = \frac{2}{3(N-3)} \left\langle \sum_{i=1}^N m_i v_i^2 / 2 \right\rangle, \quad (2.12)$$

where  $N$  – the number of the particles in simulation box,  $v_i$  — the velocity of the particle. Also the pressure can be calculated using the coordinates of the particle and their pair interaction, it is called virial theorem:

$$P = \frac{NT}{V} + \frac{1}{3} \left\langle \sum_i \sum_{i < j} F(r_{ij}) \cdot r_{ij} \right\rangle. \quad (2.13)$$

Interatomic potential  $U(r_1, \dots, r_N)$  is the key detail in molecular dynamics simulation. The choose of the potential influence how realistic is the system modeled. Also different potentials requires different computational costs, which may differ in tens and hundreds of times. In the next section the main interatomic potentials used in this work will be discussed.

## 2.6 Interatomic potentials

In current work the carbon, argon and hydrocarbons interactions have to be taken into consideration. Generally, interactions can be divided into intramolecular and intermolecular.

Long intermolecular interaction between atoms, which have dipole-dipole physical nature, is usually described by van der Waals forces (see Figure 2-1). Such interaction is well described by the Lennard-Jones potential:

$$E_{LJ} = 4\epsilon \left[ \left( \frac{\sigma}{r_{ij}} \right)^{12} - \left( \frac{\sigma}{r_{ij}} \right)^6 \right], \quad (2.14)$$

where  $\sigma$  — equilibrium distance between particles,  $\epsilon$  — the depth of the energy well. The term  $\frac{1}{r^6}$  characterizes the attractive due to dipole-dipole interaction. And term  $\frac{1}{r^{12}}$  characterizes the repulsion behaviour, the 12 power is chosen for convenient of integration operation. There are more physically interpreted form of that term - it is the Buckingham potential [Buckingham \[1938\]](#), where this term takes form  $e^{-r/r_0}$ . This more precise form of the intermolecular interaction is important for modeling of the matter at high pressures.

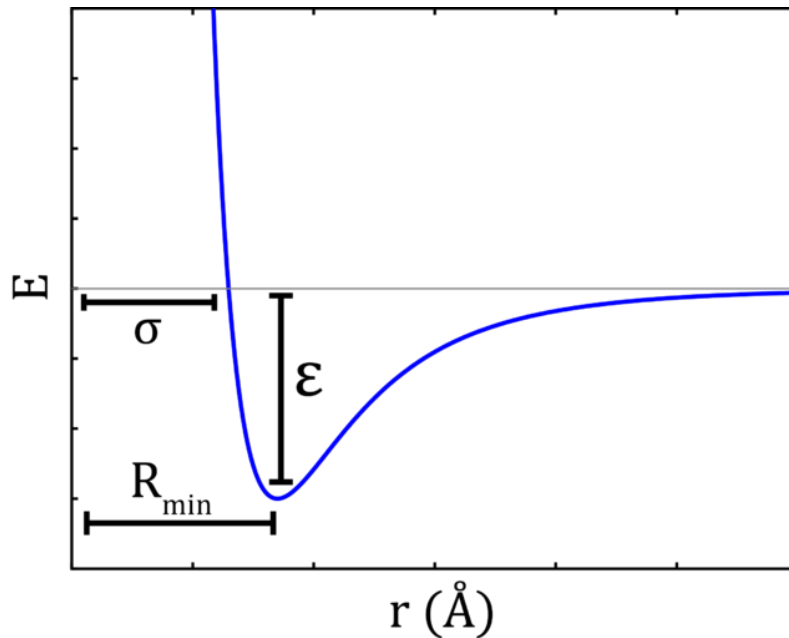


Figure 2-1: Typical curve of the Lennard-Jones potential. The depth of the potential well —  $\epsilon$ ; the distance, where the energy of the interaction is zero —  $\sigma$ .  $R_{\min}$  — the distance, where the minimum of the energy landscape located.

More complex potentials are required to describe interaction between carbon atoms, as the nature of carbon atom implies different orbital hybridisation depending on the local environment. In MD simulations in this work two types of the potentials are used: Tersoff [Tersoff \[1988, 1989\]](#) and AIREBO [Stuart et al. \[2000\]](#), [Brenner et al. \[2002\]](#), [O'Connor et al. \[2015\]](#). These interatomic potentials describe the mechanical

properties of graphene, which is a key factor for this work.

### 2.6.1 Tersoff potential

The mathematical models are used in MD simulations to describe interatomic potentials: energies of the interaction between atoms in the system, calculations of the forces on the interacting particles. The general property of these models is Taylor expansion for the energy as a function of atoms positions:

$$E = \sum_i V_1(r_i) + \sum_{i<j} V_2(r_i, r_j) + \sum_{i<j<k} V_3(r_i, r_j, r_k) + \dots \quad (2.15)$$

where  $V_1$ ,  $V_2$ ,  $V_3$  - the one body, two body and three body potentials and depend on the coordinates of each atom. The first member is related to the external forces and can be neglected if we consider only interatomic forces.  $V_2$  is the term which describes well the dense structures, such as noble gases Ar, Kr, Xe and so on. However, this type of potential is not suitable for description of the strongly covalent systems. No pair potential is capable to describe stabilized crystal structure. To make it possible one needs to add term  $V_3$ . Together with term  $V_2$  they can make a reasonably accurate model for the real physical systems.

The Tersoff potential is many-body potential, which takes into account local environment of the atoms for the calculation of the force acting on the atom. Thus, for example, if there are 4 carbon atoms near the carbon atom - it will form a sp<sup>3</sup> hybridized bonds, if there are 3 atoms - sp<sup>2</sup> hybridized bonds and so on. It allows to model systems with any atoms configuration. For the first time this potential was invented for the silicon atom, but then for carbon also. The general potential form is the following:

$$E = \sum_i E_i = \frac{1}{2} \sum_{i \neq j} V_{ij}, \quad (2.16)$$

$$V_{ij} = f_C(r_{ij})[f_R(r_{ij}) + b_{ij}f_A(r_{ij})], \quad (2.17)$$

$$f_R(r) = Ae^{-\lambda_1 r}, \quad (2.18)$$

$$f_A(r) = -Be^{-\lambda_2 r}, \quad (2.19)$$

where the energy of the system is decomposed into the energies of the different sites  $E_i$  and the energies of the separate bonds  $V_{ij}$ ,  $r_{ij}$  — the distance between atoms  $i$  and  $j$ ,  $f_A$  and  $f_R$  — the attractive and repulsive part of the potential respectively, and  $f_C$  is a smooth cutoff function:

$$f_C(r) = \begin{cases} 1, & r < R - D, \\ \frac{1}{2} - \frac{1}{2} \sin\left[\frac{\pi}{2}(r - R)/D\right], & R - D < r < R + D, \\ 0, & r > R + D. \end{cases} \quad (2.20)$$

It should be noted, that the  $R$  and  $D$  parameters are adjusted in a way that in closed pack structures, such as graphite or diamond, only nearest neighbours bonds are taken into the account. Cutoff function  $f_C$  is decreasing gradually from 1 to 0 in the interval from  $R - D$  to  $R + D$ . The main term of the potential is  $b_{ij}$ , it is responsible for the strength of the bond. Also it depends on the local environment and decreases for large number of the neighbours. This dependence is described by the  $b_{ij}$ , which can decrease or increase depending on the local environment of the atom:

$$b_{ij} = \frac{1}{(1 + \beta^n \zeta_{ij}^n)^{1/2n}}, \quad (2.21)$$

$$\zeta_{ij} = \sum_{k \neq i, j} f_C(r_{ij} g(\theta_{ijk})) e^{[\lambda_3^3 (r_{ij} - r_{ik})^3]}, \quad (2.22)$$

$$g(\theta) = 1 + \frac{c^2}{d^2} - \frac{c^2}{[d^2 + (h - \cos \theta)^2]}. \quad (2.23)$$

Here term  $\zeta_{ij}$  depends on the number of the neighbours of the atom  $i$ , considering the distance between atoms  $r_{ij} - r_{ik}$  and the angle  $\theta$ . Function  $g(\theta)$  has the local

minimum for  $h = \cos \theta$ , the  $d$  parameter describes how strong dependence on the angle is and the  $c$  parameter expresses the strength of the angle effect.

This potential and its parameters are fit to predict theoretical and experimental data of real or hypothetical structures of silicon, carbon, etc. So the energy of the bond, for example in crystal structure, is equal to the experimental measurements, also the length of the bond has to be the same as in the diamond lattice and etc. This potential was calibrated by Tersoff [Tersoff \[1988\]](#) in a way that the vacancy formation in diamond corresponds to at least 4 eV, close to the value found by Bernholc [Bernholc et al. \[1988\]](#).

Parameters of the potential in [Tersoff \[1988\]](#) was tested by the calculation of the bond energy in different stable carbon structures, calculation of the elastic modules, phonon spectrum, energy of the formation of the defects, potential barriers for vacancy migration in graphite or diamond. The results of the calculations are in agreement with experimental data and *ab-initio* simulations. The distance to the nearest neighbour in the graphite in calculations with Tersoff potential is 1.46 Å, that is close to the theoretical value 1.42 Å. One more advantage of the potential is the possibility to describe the difference in the energy strength in diamond and graphite structures: for diamond it is -7.39 eV, and for graphite -7.37 eV.

## 2.6.2 AIREBO potential

AIREBO potential [Stuart et al. \[2000\]](#) is Adaptive Intermolecular Reactive Empirical Bond Order. This potential is able to describe carbon and hydrocarbon systems. The main part of the potential is the REBO part, which is in fact the Tersoff potential described above. But in AIREBO also van der Waals energy and torsional interaction are included. In general form:

$$E = \frac{1}{2} \sum_i \sum_{j \neq i} \left[ E_{ij}^{\text{REBO}} + E_{ij}^{LJ} + \sum_{k \neq i, j} \sum_{l \neq i, j, k} E_{kijl}^{\text{TORSION}} \right]. \quad (2.24)$$

This potential allows to model formation and breaking of the bonds, to study the reactions flow. It also makes it possible to model in MD simulations gas and liquid hydrocarbons, thin films and saturated systems.

### 2.6.3 TraPPE-UA

TraPPE-UA is Transferable Potentials for Phase Equilibria-United Atom [Martin and Siepmann \[1998\]](#). This potential is created to describe hydrocarbons and it is developed in a way to be computationally efficient. This is done by introducing the pseudo atoms, the typical ones are CH<sub>4</sub>, CH<sub>3</sub>, CH<sub>2</sub>, CH and C. However, the polar atoms are treated as individual sites. The potential energy consists of bonded and non-bonded parts. Bonded term is responsible for interactions in the molecule and includes bonds, angles and torsions. The nonbonded term consists of regular Lennard-Jones potential and for some polar more complex molecules the Coulomb interaction is turned on:

$$u_{NB}(r_{ij}) = 4\epsilon_{ij} \left[ \left( \frac{\sigma_{ij}}{r_{ij}} \right)^{12} - \left( \frac{\sigma_{ij}}{r_{ij}} \right)^6 \right] + \frac{q_i q_j}{4\pi\epsilon_0 r_{ij}} \quad (2.25)$$

This part is applied only for sites between molecules or sites inside one molecule separated for more than 4 bonds. The simplicity of this potential makes it very efficient.

"If you can't explain it to a six year old, you don't understand it yourself."

Albert Einstein

## Chapter 3

# Thesis Objectives

This chapter defines the goals and derives the specific questions to be addressed in our research. Each section is represented by one article published in the journal. Before the paper, there is a small introduction that describes how the article fits into the general idea of the thesis.

## 3.1 Atomistic study

The first approach to describe the formation of the graphene nanobubbles is to perform MD simulations. The studied trapped matter is argon at room temperature. The MD method allows the calculation of all system parameters, such as pressure, the density of the trapped argon, observe the structure of the matter and calculate stress and strain tensors of graphene. However, the MD study also has several limitations that need to be considered. For example, the boundary effect of the simulation box can strongly affect the results of the simulation. Also, this method has computational limitations. Thus our resources allow us to simulate a few million carbon atoms with AIREBO potential.

The main result of this part is the observation of the solid argon inside the graphene nanobubbles at such pressures and temperatures, where argon has to be liquid. This result shows the strong effect of the confinement on trapped matter created by the graphene walls. Also, the inner structure of the matter is studied. The argon is shown to be at the close-packed hexagonal structure. Also, the profiles of the bubbles are calculated, and the phenomenon of universal shape scaling is approved, which is found experimentally and from semi-analytical findings.

### 3.1.1 Potential verification

The crucial part of all molecular dynamics simulations is the right choice of potential. In this work, we used AIREBO to describe carbon-carbon interaction. In the calculations, the graphene layer is stretched and curved. So we decided to check the mechanical elastic moduli and compare them with other molecular dynamics studies and experimental measurements.

In order to verify AIREBO potential, we performed molecular dynamics calculations of stretching the graphene sheet in both the zigzag direction and the armchair direction.

The cutoff for REBO part potential is set to 3.0 Å. The timestep for calculation is 0.5 fs. The simulation is performed under the NVT ensemble at 300 K. The engineering shear strain rate is  $10^{-3}$  ps<sup>-1</sup>. The result stress-strain curve (see Figure 3-1)

is in good agreement with another molecular dynamics study [Zhao et al. \[2009\]](#). The Young's modulus derived from the MD simulation is 1.01 TPa, which is consistent with experimental data [Lee et al. \[2008\]](#).

### 3.1.2 Contribution

My contribution to this work: carried out all MD calculations and data analysis, took part in results discussion, and writing the manuscript.

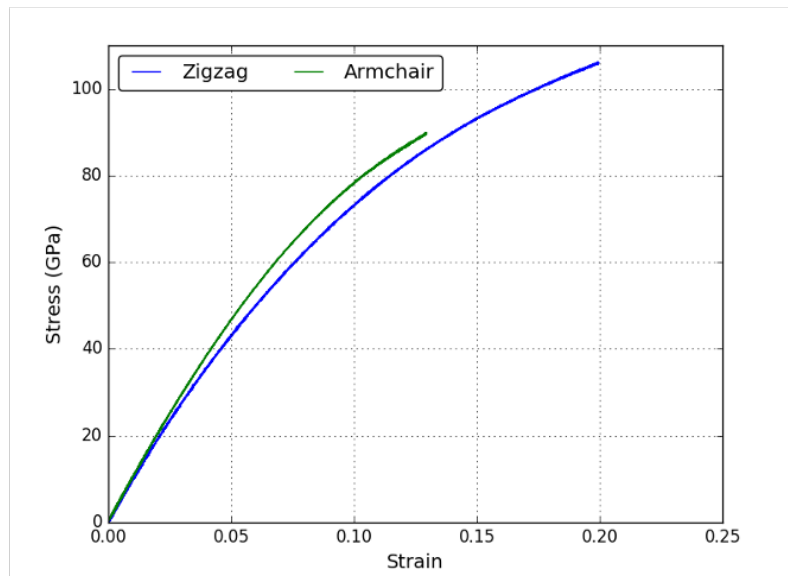


Figure 3-1: Graphene strain-stress curve obtained from molecular dynamics simulation of graphene sheet tensile test in both the zigzag direction and the armchair direction at 300 K.

# SCIENTIFIC REPORTS

OPEN

## Atomistic study of the solid state inside graphene nanobubbles

Evgeny Iakovlev , Petr Zhilyaev & Iskander Akhatov

A two-dimensional (2D) material placed on an atomically flat substrate can lead to the formation of surface nanobubbles trapping different types of substances. In this paper graphene nanobubbles of the radius of 7–34 nm with argon atoms inside are studied using molecular dynamics (MD). All modeled graphene nanobubbles except for the smallest ones exhibit an universal shape, i.e., a constant ratio of a bubble height to its footprint radius, which is in an agreement with experimental studies and their interpretation using the elastic theory of membranes. MD simulations reveal that argon does exist in a solid close-packed phase, although the internal pressure in the nanobubble is not sufficiently high for the ordinary crystallization that would occur in a bulk system. The smallest graphene bubbles with a radius of 7 nm exhibit an unusual “pancake” shape. Previously, nanobubbles with a similar pancake shape were experimentally observed in completely different systems at the interface between water and a hydrophobic surface.

Graphene is a basic material used to create various heterostructures that have been actively studied and have shown potential for many electronic and optical applications<sup>1–4</sup>. These structures are usually created layer by layer, and sometimes, atoms and molecules can be trapped between layers, which results in bubbles, blisters and nanodrums of nanoscale height<sup>5–10</sup>. The formation of these enclosures were first considered undesirable defects of the surface. However, later studies showed that they possess several interesting properties, including a giant pseudo magnetic field<sup>5,6</sup> and extreme internal pressure<sup>7–9</sup>, and their presence can adjust phonon–electron interactions<sup>11</sup>. These structures can also be used as hydrothermal reactors<sup>12</sup>, as surface modifiers<sup>7</sup> and for the visualization of chemical reactions<sup>13</sup>. Graphene nanobubbles and blisters on metallic substrates produced by bombarding with noble gas ions<sup>14,15</sup> are actively studied and could be used for novel gas storage technologies.

A high pressure of up to 1 GPa<sup>9</sup> is assumed to be present in the substance trapped inside the heterostructures. These pressures can lead to a phase transition that is strongly affected by the surface interaction between the substrate and the two-dimensional (2D) crystal. This confinement ordering has already been discovered in carbon nanotubes both experimentally<sup>16</sup> and theoretically<sup>17</sup>. However, because of the small radius of the nanotube and, consequently, the small number of atoms and molecules inside it, it is more appropriate to treat such a phase transition as an ordering of atoms and molecules. The phase transition inside nanobubbles leads to intermediate states wherein the system consists of billions of atoms, and its thermodynamic behavior is understood and largely determined by the interaction with the interface.

The pressure inside graphene nanobubbles is determined by their shape and hence could be experimentally evaluated using atomic force microscopy (AFM). In the work<sup>8</sup> the consistent experimental AFM study of geometry of nanobubbles in 2D materials was performed. It was shown that the shape of the nanobubbles with the radius more than 50 nm exhibits universal scaling, i.e. the ratio of the bubble height (H) to the radius of its footprint (R) is constant in a wide range of bubble sizes and depends only on type of 2D material used (BN, MoS<sub>2</sub> or graphene). In addition to these experiments, the elastic theory of membranes was used for theoretical calculation of nanobubble shape and mechanical properties. This theory validates the experimental observations and yields the expression for the ratio of the maximum nanobubble's height to the radius of its footprint (H/R) for round-type nanobubbles. In the experiments<sup>8</sup> the substance inside the nanobubbles was unknown. Therefore there was no possibility to estimate adhesion energy magnitude between trapped substance and 2D-crystal or substrate which was used as a parameter in the elastic theory of the membranes. Instead, the adhesion energy was fitted so that theoretically predicted H/R ratio matches with experimental measurements.

Another issue associated with application of the elastic theory of membranes to modeling of graphene nanobubbles is related to the fact that all material properties, such as Young's modulus and adhesion energies, are assumed to be constant. It is not obvious. In fact, one study<sup>18</sup> showed that to correctly apply this theory to

Center for Design, Manufacturing and Materials, Skolkovo Institute of Science and Technology, Moscow, Russia. Correspondence and requests for materials should be addressed to E.I. (email: [Evgeny.Iakovlev@skolkovotech.ru](mailto:Evgeny.Iakovlev@skolkovotech.ru))

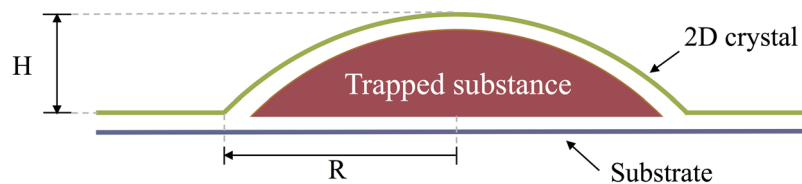


**Figure 1.** Schematic representation of a meridional 2D slice of the graphene nanobubble. Trapped substance: argon atoms; 2D crystal: curved graphene sheet; Substrate: graphene sheet frozen in the direction perpendicular to the substrate; H: maximum height, and R: radius of the nanobubble, both measured for the undisturbed 2D crystal.

LJ parameter	This study	Ref. <sup>36</sup>	Ref. <sup>37</sup>
$\sigma_{Ar-Ar}$ , Å	3.400	3.405	3.406
$\varepsilon_{Ar-Ar}$ , meV	10.400	10.340	10.330
$\sigma_{Ar-C}$ , Å	3.400	3.380	3.380
$\varepsilon_{Ar-C}$ , meV	5.438	4.998	6.749

**Table 1.** Lennard-Jones potential parameters used in this work and in previous studies. Cut-off radius  $r_{cut}$  for all cases in this study is 10.2 Å.

atomically thin and micron-sized membranes, the dependence of Young's modulus and bending rigidity on the size of the system should be accounted for. Therefore, verifying the elastic theory of membranes with the help of molecular dynamics (MD) will be useful. In atomistic modeling, all material parameters can be calculated, and the graphene nanobubble takes shape spontaneously. In general, MD simulations could play a valuable role in evaluating the assumptions of the elasticity theory of nanoscale membranes and in providing a benchmark system for validating analytic theories.

In this paper, the MD method is used to investigate graphene nanobubbles. Here we use a graphene sheet with graphite substrate. Together with the substance trapped inside, these two parts compose the graphene nanobubble. Nanobubbles with radii in the range of 7–34 nm are studied. The first goal of this paper is to study state of the matter inside graphene nanobubbles, and in particular, to show if solid state of the matter can be observed. The second goal is to study the nanobubbles shape and to see if it fits to the predictions of the standard theory of elastic membranes<sup>8</sup>.

It is shown that argon is in the solid state of the matter with a close-packed crystal structure in all the nanobubbles with various radii. The thermodynamic states of the observed crystal structures in the pressure-temperature (P-T) diagram are located considerably below the melting curve of the bulk argon. We attribute this behavior to the stabilizing role of the interface between the 2D crystal and the substrate. It is also shown that the results provided by theory of elastic membranes agree well with those obtained by atomistic modeling. We also report here the existence of so-called “pancake” nanobubbles, which have not been observed in heterostructures yet, and which contradicts the theory of elastic membranes, but have been found at the interface between highly oriented pyrolytic graphite and water<sup>19</sup>.

## Methods

The MD method is used to study the properties of graphene nanobubbles. The model of the graphene nanobubble is presented schematically in Fig. 1. The model consists of three parts: a 2D crystal, i.e., the graphene sheet, a trapped substance, i.e., the argon atoms, and a substrate, i.e., another graphene sheet.

The carbon-carbon interaction is described by the adaptive intermolecular reactive bond order potential (AIREBO)<sup>20</sup> which is known to describe well the mechanical properties of graphene and graphite<sup>21</sup>. The interaction between argon atoms is described by Lennard-Jones potential (see Table 1). The interaction between carbon-argon atoms is also described by the Lennard-Jones potential, the parameters of which are adjusted using Lorentz-Berthelot combining rules<sup>22</sup>:

$$\begin{aligned}\sigma_{ij} &= \frac{\sigma_i + \sigma_j}{2}, \\ \varepsilon_{ij} &= \sqrt{\varepsilon_i \varepsilon_j}\end{aligned}\quad (1)$$

Carbon-carbon parameters  $\sigma_{C-C} = 3.4$  Å,  $\varepsilon_{C-C} = 2.84$  meV, that are used in combining rules, are taken from Lennard-Jones part of AIREBO potential<sup>20</sup>. The resulting parameters agree with the previously used ones (see Table 1).

A typical calculation consists of three stages: (i) construction of initial configuration, (ii) relaxation and (iii) statistical acquisition.

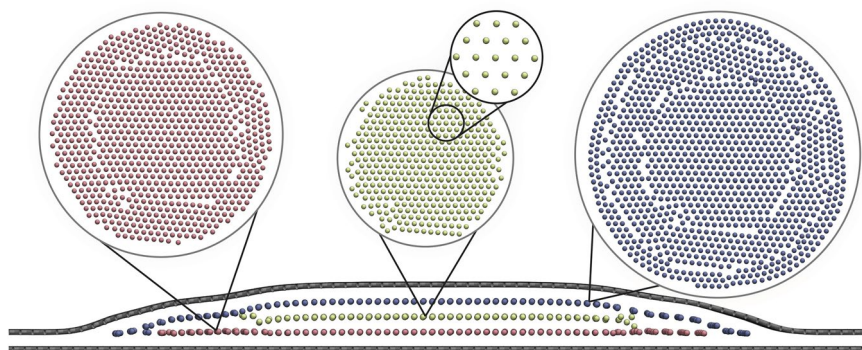


**Figure 2.** 2D slice of the simulated graphene nanobubble with a radius of 7.3 nm and 3 layers of argon inside. Insets show the top view of each layer of argon and its hexagonal structure.

- (i) The cubic box is used in the simulations. Firstly, two graphene layers are generated, they are stacked the same as in graphite: the bond length is 1.418 Å, the distance between layers is 3.35 Å. Then the upper graphene sheet is curved according to a previous experimental study<sup>8</sup>:

$$h/H = 1 - (r/R)^2 + 0.25[(r/R)^2 - (r/R)^4] \quad (2)$$

where  $h$  is the height at a particular point, and  $r$  is the radius at that point. The two graphene layers consist of the same number of carbon atoms, hence the bonds in the upper layer are stretched. The corresponding average strain is of order  $(H/R)^2 \approx 1 - 2\%$ . Finally, between the substrate and the 2D crystal, argon atoms in simple cubic lattice are inserted.

- (ii) Calculations are performed using the software package, LAMMPS<sup>23</sup>. Periodic boundary conditions are applied in the in-plane ( $xy$ ) directions. Non-periodic and fixed boundary conditions are applied in  $z$  direction, so that particles do not interact across the boundary and do not move from one side of the simulation box to the other. Two types of minimization were performed, MD and conjugate gradient descent, which yielded the same final results, except for the smallest nanobubble. In that case, the final results depend on the method of minimization, and we obtain two types of nanobubbles with the same number of argon atoms, regular and pancake. During the relaxation stage, the NPT ensemble is imposed on the substrate, and the force component perpendicular to the surface is set to zero. The target pressure for NPT ensemble is set to 0 bars, the target temperature for NPT ensemble is set to 300 K, which allows the relaxation of the stresses that occur in the substrate due to the initial artificial formation of the nanobubble. The 2D crystal and argon atoms are allowed to move in the NVT ensemble. All temperatures for NVT ensemble are set to 300 K. When the stresses in the substrate are removed, the substrate atoms are fixed, the 2D crystal and argon atoms continue to be set in the NVT ensemble. The MD time step for all calculations is set to 1 fs. The number of time steps to calculate one nanobubble varies from 5 to 20 million depending on the bubble size.

It should be noted, although the initial shape of the nanobubble is set to the experimental one eq. 2, in general case the initial and final shapes of the nanobubble can differ significantly. The final shape is controlled by the number of inserted argon atoms. Thus the 2D crystal experiences strong fluctuations during the relaxation stage if the number of argon atoms is not equal to the equilibrium one (see Supplementary video 1). The final period of relaxation stage is shown at Supplementary video 2, structuring of argon atoms can be seen.

- (iii) After the energy of the system stabilizes, we assume that equilibrium is achieved, and statistical information can be gathered. During the statistic acquisition stage, the NVT ensemble is imposed on the 2D crystal and argon atoms, the substrate atoms are fixed, and properties such as the shape of the nanobubble, structural properties of argon, and stresses in the 2D crystal are calculated. To evaluate the pressure inside the nanobubble, the volume is calculated using the Voronoi tessellation<sup>24</sup>. The per-atom stress tensor is evaluated according to ref.<sup>25</sup>. After averaging the per-atom stress tensor and obtaining the total stress tensor of the argon atoms, the pressure is calculated as a minus trace of the obtained stress tensor.

To analyze the obtained crystal structure of solid argon inside graphene nanobubbles, we use common neighbor analysis (CNA)<sup>26,27</sup>. The CNA uses a decomposition of the radial distribution function and provides direct interpretation of various features of the radial distribution function in terms of atomic structure. It can be used to identify atoms in particular environment, such as FCC, HCP, BCC or icosahedral.

Visualization is done by software package VMD<sup>28</sup>.

**Data Availability.** The datasets generated during the current study are available from the corresponding author on reasonable request.

#	R, nm	H, nm	H/R	N <sub>Ar</sub>	N <sub>layers</sub>	ρ, g/cm <sup>3</sup>	P, MPa	L <sub>x</sub> , nm	L <sub>y</sub> , nm	L <sub>z</sub> , nm
1	7.8	0.64	0.083	2463	2	1.962	417	43.51	43.60	100
2	7.3	0.95	0.130	2463	3	1.911	398	43.55	43.60	100
3	13.8	1.57	0.114	12952	5	1.859	257	43.43	43.54	100
4	16.9	2.16	0.128	26153	7	1.849	229	78.77	79.17	100
5	24.0	2.77	0.116	73624	9	1.841	197	98.67	98.85	100
6	33.3	3.70	0.111	196331	12	1.837	172	98.55	98.83	100

**Table 2.** Parameters of the simulated graphene nanobubbles. R: radius; H: maximum height; N<sub>Ar</sub>: number of argon atoms inside the nanobubble; N<sub>layers</sub>: number of argon layers inside the nanobubble; ρ: argon density; P: argon pressure; L<sub>x</sub>, L<sub>y</sub>, L<sub>z</sub>: final lengths of the simulation box.

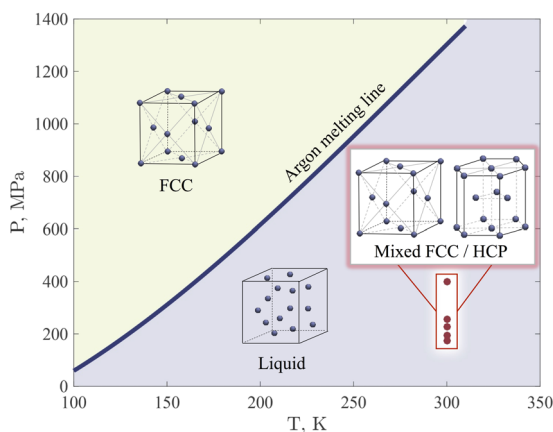


**Figure 3.** The melting line of bulk argon<sup>29,30</sup> and the thermodynamic state of argon inside the graphene nanobubbles (red dots).

## Results and Discussion

After relaxation, the argon inside all considered graphene nanobubbles with various radii is found to be in the solid state (see Fig. 2). For the largest bubble with a radius of 33.3 nm, CNA shows that 65% of the final crystal is face-centered cubic (FCC), 26% is hexagonal close-packed (HCP). Remaining 9% of undetermined atoms can be attributed to grain boundaries, defects and atoms that are in contact with 2D crystal or substrate. The argon atoms are layered perpendicular to the substrate. The spacing between argon layers for all simulated nanobubbles is approximately  $3.05 \pm 0.05$  Å, and the in-layer distance between neighboring atoms is  $3.7 \pm 0.5$  Å. These distances are directly calculated from atomic configurations during statistical acquisition stage of the modelling.

Table 2 shows the parameters of the simulated graphene nanobubbles. According to this table, all calculated pressures in the trapped substance are considerably lower than the melting pressure of bulk argon at 300 K, which is 1200 MPa<sup>29,30</sup> (see Fig. 3). Therefore, in the case of argon atoms trapped inside nanobubbles, we observed additional stabilization that prevents the solid-to-liquid phase transition. We predict that further increasing the graphene nanobubble radius and the concomitant decrease in the argon pressure will eventually lead to the solid-to-liquid phase transition in the confined argon system. Figure 3 clearly shows that the melting line of argon in the nanobubble confinement (if one exist) should be located significantly below the melting line of bulk argon on P-T diagram.

The decrease in the pressure at which the melting takes place becomes even more noticeable if we consider the HCP phase of argon. The phase transition from the FCC argon to HCP argon occurs at pressures of several tens of GPa<sup>31</sup> while calculated pressures inside graphen nanobubbles do not exceed 400 MPa. This can be explained by the fact that the specific free energy of HCP argon is very close to the specific free energy of FCC argon and metastable mixture of HCP/FCC could exist for very long time. HCP and FCC are close-packed structures and argon is inert atom without a designated direction of chemical bonding. Moreover, in solid argon in the graphene nanobubbles HCP structure is observed near surface of 2D crystal that could additionally lower its energy.

For the simulated nanobubbles, except for nanobubble 1, we observed a universal shape, i.e., a constant ratio between the maximum height and the radius. According to the elastic theory of membranes<sup>8</sup> of round nanobubbles, this H/R ratio depends only on the material constants:

$$\frac{H}{R} = \left[ \frac{\pi(\gamma_{GS} - \gamma_{GB} - \gamma_{SB})}{5cY} \right]^{\frac{1}{4}} \quad (3)$$

where  $H$  is the maximum height of the nanobubble,  $R$  is the radius of the nanobubble,  $\gamma_{GS}$ ,  $\gamma_{GB}$ ,  $\gamma_{SB}$  are the adhesion energies between the graphene and substrate, the graphene and the substance inside the nanobubble, and the

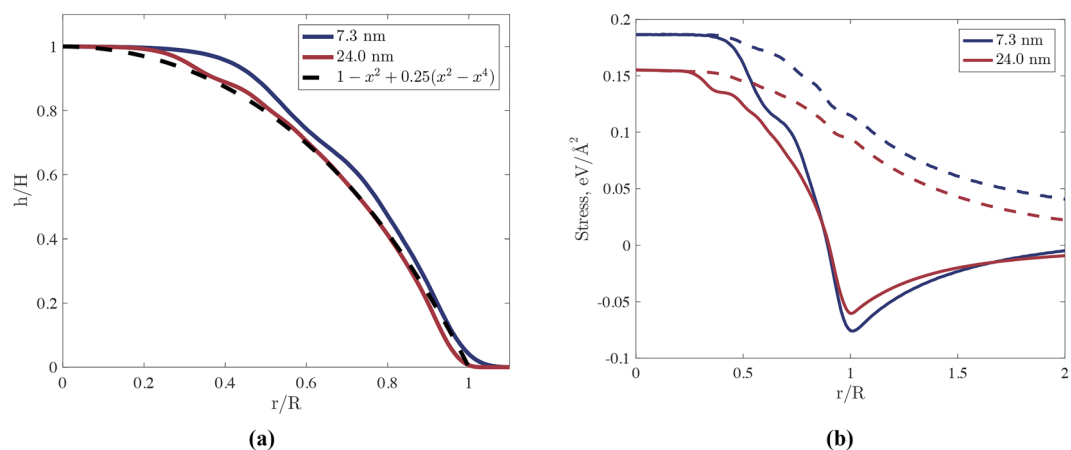


**Figure 4.** (a) Dashed black line: shape of the graphene nanobubble in dimensionless coordinates taken from<sup>8</sup>; blue line: shape of the graphene nanobubble with  $R = 7.3$  nm obtained from MD; red line: shape of the graphene nanobubble with  $R = 24.0$  nm obtained from MD. (b) Distribution of stress  $\sigma_{rr}$  (solid lines) and  $\sigma_{\theta\theta}$  (dashed lines) along the radial direction. Blue lines: graphene nanobubble with  $R = 7.3$  nm; red lines: graphene nanobubble with  $R = 24.0$  nm.

substrate and the substance, respectively,  $Y$  is Young's modulus of graphene; and  $c$  is a dimensionless coefficient, which is 0.7 in the case of round nanobubbles.

To validate equation (3), Young's modulus  $Y$  of graphene and the adhesion energies  $\gamma_{GS}$ ,  $\gamma_{GB}$ ,  $\gamma_{SB}$  are required. For consistency, all these parameters should be calculated from the potential used to model the nanobubble. Young's modulus  $Y$  for the AIREBO potential was previously calculated<sup>21</sup> to be  $21.12 \text{ eV}/\text{\AA}^2$  ( $1.01 \text{ TPa}$ ), which agrees well with *ab initio* calculations and experiments.

The adhesion energy between the graphene and the substrate is calculated as the work required to separate graphene from the substrate. For the AIREBO potential, we obtain a value of  $\gamma_{GS} = 0.017 \text{ eV}/\text{\AA}^2$ , which is the typical adhesion energy of graphene membranes<sup>32</sup>. In our case,  $\gamma_{GB} = \gamma_{SB}$  because the 2D crystal and substrate consist of the same material. This adhesion energy is also calculated in this work. Three layers of graphene in contact with argon atoms are considered. The potential energy  $U_{\text{composite}}$  of this system is also calculated. Then, only argon atoms are considered at the same pressure and the same temperature of  $T = 300 \text{ K}$ , and their potential energy  $U_{\text{argon}}$  is evaluated. Finally, the potential energy of the three layers of graphene,  $U_{\text{graphene}}$ , is computed. Adhesion energies  $\gamma_{GB}$  and  $\gamma_{SB}$  are evaluated as  $(U_{\text{composite}} - U_{\text{argon}} - U_{\text{graphene}})/S_{\text{area}}$ . For two different argon pressures,  $86 \text{ MPa}$  and  $291 \text{ MPa}$ , we calculate  $\gamma_{GB} = \gamma_{SB}$  to be  $0.0049 \text{ eV}/\text{\AA}^2$  and  $0.0052 \text{ eV}/\text{\AA}^2$ , respectively. Because these values are very similar, for estimation, we take the average of these two values,  $\gamma_{GB} = \gamma_{SB} = 0.0051 \text{ eV}/\text{\AA}^2$ . Thus, for values of  $Y = 22.12 \text{ eV}/\text{\AA}^2$ ,  $\gamma_{GS} = 0.017 \text{ eV}/\text{\AA}^2$ , and  $\gamma_{GB} = \gamma_{SB} = 0.0051 \text{ eV}/\text{\AA}^2$  that are obtained purely by MD, the elastic theory of membranes according to equation (3) gives  $H/R = 0.128$ .

The calculated values of the  $H/R$  ratio for nanobubbles 2–6 (see Table 2) are within 10% of 0.128, which is the value obtained using the elastic theory of membranes. This result confirms the applicability of this theory to interpreting atomic-force microscope measurements.

Figure (4a) shows the shape of the obtained graphene nanobubbles in dimensionless coordinates compared with the dimensionless shape given by the elastic theory of membranes. The results obtained using MD calculations agree with those obtained from the elastic theory of membranes. The slight difference is explained by the fact that the elastic theory of membranes has not considered that a solid structure inside the bubble can lead to a stepped morphology. In addition, in the elastic theory of membranes, bending rigidity is neglected. Therefore, the analytic curve is “stuck” at zero at  $r = R$ , whereas that calculated from the MD curve smoothly approaches zero. Additionally, the distribution of stress along the radial direction is calculated, and the radial and angular components of the stress are presented in Fig. (4b). The overall form of the curves coincides with the dimensionless form obtained via the elastic theory of membranes.

AFM studies<sup>8</sup> of graphene nanobubbles do not give information about structure of a trapped material. Combined scanning tunneling microscopy (STM), low energy electron microscopy (LEEM) and synchrotron-based photoemission electron microscopy (XPEEM) make possible to investigate both the shape of the nanobubbles and the structure of trapped material. Experimental research of graphene nanobubbles filled with argon on Ir<sup>14</sup> provides direct evidence of argon cluster formation at and above room temperature which supports the existence of solid argon inside graphene nanobubble. The direct comparison between results of this work and experimental study<sup>14</sup> can not be done due to fundamental difference in types of substrate. In our case the substrate is graphene and interaction between 2D crystal and substrate governed by Van der Waals forces. When substrate is metallic as in study<sup>14</sup> the interaction between the 2D crystal and the substrate has a complex nature related to the redistribution of the charge density between atoms<sup>10</sup>.

Argon is solid at room temperature at a pressure which is significantly lower than that shown by the P-T diagram (see Fig. 3) and than expected for the condensation of compressed argon. This fact could be interpreted from the point of view of well-known physical phenomenon of multilayer adsorption. If argon exist in gaseous or liquid

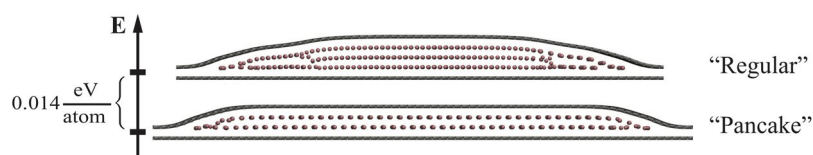


**Figure 5.** 2D slice of “regular” and “pancake” graphene nanobubbles on the energy scale.

state and is in contact with graphene sheet, structured layers of argon arise at the interface. Monte Carlo simulation of argon adsorption on graphite<sup>33</sup> shows that at pressure 100 MPa and temperature 260 K approximately three argon layers are constructed on the substrate. These pressure and temperature are close to the parameters in largest nanobubbles that is simulated (see Table 2). In case of the graphene nanobubbles there are two surfaces that can adsorb argon atoms and hence at least 6 layer have to arise at this conditions. Therefore it is not so unexpected that argon solidify inside the graphene nanobubbles at lower pressures in comparison with bulk argon.

Nanobubble 1 in Table 2 significantly differs from the others in terms of its small ratio of  $H/R = 0.083$ . Such a small ratio indicates that this type of nanobubble is flatter than others. We will refer to this exotically shaped graphene nanobubble as a “pancake” graphene nanobubble. A pancake nanobubble was obtained during the initial configuration setup (see Methods for more details) when a conjugate gradient minimization of energy was used instead of MD minimization. For a higher number of atoms inside the nanobubbles, both minimization algorithms lead to the same final “regular” form. The number of argon atoms in graphene nanobubbles 1 and 2 (see Table 2) is the same, but they exhibit different geometries, e.g., different numbers of layers of solid argon. Additionally, the pancake nanobubble has a lower energy than the regular nanobubble with the same number of argon atoms inside (see Fig. 5). To the best of our knowledge, this is the first report of the possible existence of a pancake nanobubble in heterostructures. Pancake nanobubbles have been observed in a completely different system at the interface between highly oriented pyrolytic graphite and water<sup>34,35</sup>. We assume that this suggests that these two systems are highly analogous. The emergence of the pancake shape is a manifestation of the complicated interplay between surface interactions and the inner state of trapped substances.

## Conclusions

Argon trapped in small graphene nanobubbles with a radius of less than 33 nm does exist in a solid close-packed phase with a mixture of FCC and HCP lattices. The pressure of argon in these nanobubbles is considerably lower than the pressure required for the ordinary crystallization to occur in a bulk system. Therefore, these objects present good examples of physical systems in which the phase state is highly affected by interface interactions. Compared with nanotubes, which can only accommodate a few dozen atoms inside, the heterostructured nanobubbles can accumulate millions of atoms and molecules, and therefore can be treated as true thermodynamic systems. In this work, we observed a layered structure of argon atoms inside graphene nanobubbles. The shape of the observed nanobubbles, except for the smallest one, obeyed a universal shape law, i.e., a constant ratio of height to radius, independent on the nanobubble radius. This is consistent with the elastic theory of membranes<sup>8</sup>, which was previously used to describe the morphology of graphene nanobubbles. The dimensionless shape and the stress distribution calculated from MD are in good agreement with the elastic theory of membranes. We also found very small nanobubbles with an exotic pancake shape that has not been reported so far in the case of heterostructured nanobubbles. However, this shape has been observed for nanobubbles at the interface between water and highly oriented pyrolytic graphite.

We expect that a subsequent increase in the nanobubble radius will lead to a pressure drop inside nanobubble and will eventually lead to the solid-liquid phase transition in the confined argon system. This research clearly demonstrates the possibility that nanobubbles in heterostructures can be used to investigate the fundamentally interesting phenomenon of phase transition in confined systems.

## References

- Geim, A. K. & Grigorieva, I. V. Van der Waals heterostructures. *Nature* **499**, 419–425 (2013).
- Novoselov, K., Mishchenko, A., Carvalho, A. & Neto, A. C. 2d materials and van der Waals heterostructures. *Science* **353**, aac9439 (2016).
- Mishchenko, A. *et al.* Twist-controlled resonant tunnelling in graphene/boron nitride/graphene heterostructures. *Nat Nano* **9**, 808–813 (2014).
- Withers, F. *et al.* Light-emitting diodes by band-structure engineering in van der Waals heterostructures. *Nat Mater* **14**, 301–306 (2015).
- Levy, N. *et al.* Strain-induced pseudo-magnetic fields greater than 300 tesla in graphene nanobubbles. *Science* **329**, 544–547 (2010).
- Qi, Z. *et al.* Pseudomagnetic fields in graphene nanobubbles of constrained geometry: A molecular dynamics study. *Physical Review B* **90**, 125419 (2014).
- Lim, C. H. Y. X. *et al.* A hydrothermal anvil made of graphene nanobubbles on diamond. *Nature communications* **4**, 1556 (2013).
- Khestanova, E., Guinea, F., Fumagalli, L., Geim, A. & Grigorieva, I. Universal shape and pressure inside bubbles appearing in van der Waals heterostructures. *Nature Communications* **7** (2016).
- Vasu, K. S. *et al.* Van der Waals pressure and its effect on trapped interlayer molecules. *Nature communications* **7**, 12168 (2016).
- Voloshina, E. & Dedkov, Y. Atomic force spectroscopy and density-functional study of graphene corrugation on ru (0001). *Physical Review B* **93**, 235418 (2016).
- Kim, H. W. *et al.* Nanoscale control of phonon excitations in graphene. *Nature communications* **6**, 7528 (2015).
- Sutter, P., Sadowski, J. T. & Sutter, E. A. Chemistry under cover: tuning metal-graphene interaction by reactive intercalation. *Journal of the American Chemical Society* **132**, 8175–8179 (2010).

13. Mu, R. *et al.* Visualizing chemical reactions confined under graphene. *Angewandte Chemie International Edition* **51**, 4856–4859 (2012).
14. Zamborlini, G. *et al.* Nanobubbles at gpa pressure under graphene. *Nano letters* **15**, 6162–6169 (2015).
15. Lanciprete, R. *et al.* Self-assembly of graphene nanoblister sealed to a bare metal surface. *Nano letters* **16**, 1808–1817 (2016).
16. Fan, X. *et al.* Atomic arrangement of iodine atoms inside single-walled carbon nanotubes. *Physical Review Letters* **84**, 4621 (2000).
17. Koga, K., Gao, G., Tanaka, H. & Zeng, X. C. Formation of ordered ice nanotubes inside carbon nanotubes. *Nature* **412**, 802 (2001).
18. Los, J., Fasolino, A. & Katsnelson, M. Mechanics of thermally fluctuating membranes. *arXiv preprint arXiv* **1703**, 08400 (2017).
19. Zhang, X. H. *et al.* Detection of novel gaseous states at the highly oriented pyrolytic graphite– water interface. *Langmuir* **23**, 1778–1783 (2007).
20. Stuart, S. J., Tutein, A. B. & Harrison, J. A. A reactive potential for hydrocarbons with intermolecular interactions. *The Journal of chemical physics* **112**, 6472–6486 (2000).
21. Zhao, H., Min, K. & Aluru, N. Size and chirality dependent elastic properties of graphene nanoribbons under uniaxial tension. *Nano letters* **9**, 3012–3015 (2009).
22. Hudson, G. & McCoubrey, J. Intermolecular forces between unlike molecules. a more complete form of the combining rules. *Transactions of the Faraday Society* **56**, 761–766 (1960).
23. Plimpton, S. Fast parallel algorithms for short-range molecular dynamics. *Journal of computational physics* **117**, 1–19 (1995).
24. Rycroft, C. Voro++: A three-dimensional voronoi cell library in c++. *Lawrence Berkeley National Laboratory* (2009).
25. Thompson, A. P., Plimpton, S. J. & Mattson, W. General formulation of pressure and stress tensor for arbitrary many-body interaction potentials under periodic boundary conditions. *The Journal of chemical physics* **131**, 154107 (2009).
26. Faken, D. & Jónsson, H. Systematic analysis of local atomic structure combined with 3d computer graphics. *Computational Materials Science* **2**, 279–286 (1994).
27. Tsuzuki, H., Branicio, P. S. & Rino, J. P. Structural characterization of deformed crystals by analysis of common atomic neighborhood. *Computer physics communications* **177**, 518–523 (2007).
28. Humphrey, W., Dalke, A. & Schulten, K. Vmd: visual molecular dynamics. *Journal of molecular graphics* **14**, 33–38 (1996).
29. de Koning, M., Antonelli, A. & Yip, S. Single-simulation determination of phase boundaries: A dynamic clausius–clapeyron integration method. *The Journal of Chemical Physics* **115**, 11025–11035 (2001).
30. Hardy, W., Crawford, R. & Daniels, W. Experimental determination of the p–t melting curve of argon. *The Journal of Chemical Physics* **54**, 1005–1010 (1971).
31. Errandonea, D., Boehler, R., Japel, S., Mezouar, M. & Benedetti, L. R. Structural transformation of compressed solid ar: An x-ray diffraction study to 114 GPa. *Phys. Rev. B* **73**, 092106, <https://doi.org/10.1103/PhysRevB.73.092106> (2006).
32. Koenig, S. P., Boddeti, N. G., Dunn, M. L. & Bunch, J. S. Ultra-strong adhesion of graphene membranes. *arXiv preprint arXiv* **1107**, 2174 (2011).
33. Fan, C., Do, D., Li, Z. & Nicholson, D. Computer simulation of argon adsorption on graphite surface from subcritical to supercritical conditions: the behavior of differential and integral molar enthalpies of adsorption. *Langmuir* **26**, 15852–15864 (2010).
34. Lohse, D. & Zhang, X. Surface nanobubbles and nanodroplets. *Rev. Mod. Phys.* **87**, 981–1035 (2015).
35. Belova, V. *et al.* Influence of adsorbed gas at liquid/solid interfaces on heterogeneous cavitation. *Chemical Science* **4**, 248–256 (2013).
36. Jain, S. K., Piskun, J. P., Pellenq, R. J.-M. & Gubbins, K. E. Effects of activation on the structure and adsorption properties of a nanoporous carbon using molecular simulation. *Adsorption* **11**, 355–360 (2005).
37. Jakubov, T. S. & Mainwaring, D. E. Direct calculations of the dispersion interaction between fullerenes and their equation for the potential energy. *Adsorption* **14**, 727–732 (2008).

## Author Contributions

P.Z. planned simulations. E.I. performed simulations. E.I. and P.Z. contributed to the data post-processing and analyzed the simulation results. P.Z. wrote the paper. I.A. supervised the project. All authors reviewed the manuscript.

## Additional Information

**Supplementary information** accompanies this paper at <https://doi.org/10.1038/s41598-017-18226-9>.

**Competing Interests:** The authors declare that they have no competing interests.

**Publisher's note:** Springer Nature remains neutral with regard to jurisdictional claims in published maps and institutional affiliations.

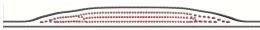
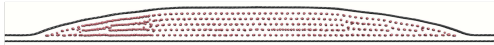
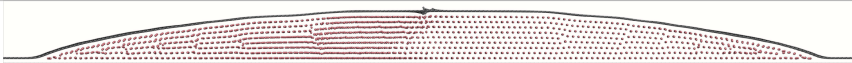
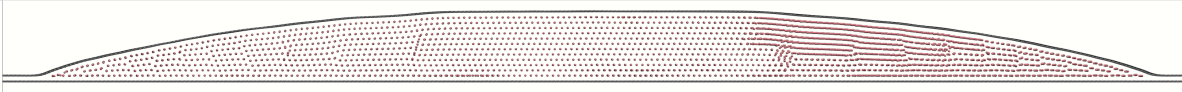


**Open Access** This article is licensed under a Creative Commons Attribution 4.0 International License, which permits use, sharing, adaptation, distribution and reproduction in any medium or format, as long as you give appropriate credit to the original author(s) and the source, provide a link to the Creative Commons license, and indicate if changes were made. The images or other third party material in this article are included in the article's Creative Commons license, unless indicated otherwise in a credit line to the material. If material is not included in the article's Creative Commons license and your intended use is not permitted by statutory regulation or exceeds the permitted use, you will need to obtain permission directly from the copyright holder. To view a copy of this license, visit <http://creativecommons.org/licenses/by/4.0/>.

© The Author(s) 2017

# Supplementary information for manuscript “Atomistic study of the solid state inside graphene nanobubbles”

Evgeny Iakovlev, Petr Zhilyaev, and Iskander Akhatov

	R, nm	H, nm	$N_{Ar}$
	7.8	0.64	2463
	7.3	0.95	2463
	13.8	1.57	12952
	16.9	2.16	26153
	24.0	2.77	73624
	33.3	3.70	196331

**Table 1.** Side view of considered graphene nanobubbles filled with argon at  $T=300$  K (in scale).

## **3.2 The shape of the bubble and the state of the trapped matter**

The first findings from the MD study made us think that there is a strong correlation between the shape of the bubble and the state of trapped matter. Also, it follows from theoretical calculations, which show that the height of the bubble to the radius ratio is proportional to the adhesion energy to the power of  $1/4$ . Next, the adhesion energy between argon and the graphite substrate is calculated. It is shown that the higher density, the more adhesion energy as more attracted argon atoms to the substrate. That means that bubbles with a higher  $H/R$  ratio correspond to the more sparse state of the trapped matter. Moreover, bubbles with a low  $H/R$  ratio most probably contain condense liquid or solid-state.

### **3.2.1 Contribution**

My contribution to this work: carried out all MD calculations and data analysis, took part in results discussion, and writing the manuscript.

# Obtaining the state of matter inside graphene nanobubble from its shape

E S Iakovlev, P A Zhilyaev and I Sh Akhatov

Skolkovo Institute of Science and Technology, Skolkovo Innovation Center Bldg 3, Moscow  
143026, Russia

E-mail: [evgeny.iakovlev@skolkovotech.ru](mailto:evgeny.iakovlev@skolkovotech.ru)

**Abstract.** Graphene nanobubble (GN) is a system consisting of the substrate, the graphene sheet and the substance trapped between them. Radius of GN regulates the pressure inside the bubble and for small GN with radius of several nanometers extreme pressures up to 1 GPa due to the van der Waals interaction can be observed. Therefore trapped substances inside GN can exist in a number of different states of matter. In this study we theoretically establish the connection between the shape of GN and the state of the trapped material inside. Both atomistic and continuum models are used to describe mechanical and thermodynamic properties of GN. Atomistic approach is applied to calculate the elastic constants and the adhesion energies. These parameters are used as inputs for the following analyses in terms of continuum media.

## 1. Introduction

Two-dimensional (2D) heterostructures allow to develop materials with adjustable properties [1]. Such structures are assembled by layer-by-layer stacking of 2D crystals, for example, graphene, hexagonal boron nitride, molybdenum disulphide ( $\text{MoS}_2$ ), other dichalcogenides and layered oxides.

While creating such structures some substance can be trapped between layers [2] that leads to formation of the surface bubbles [3]. It was shown that such bubbles possess number of interesting properties such as universal shape scaling [3], i.e. the ration of the height of the nanobubble ( $H$ ) to the radius of the footprint ( $R$ ) remains constant for various radii, giant pseudo magnetic field [4], extreme pressure insight [5]. In particular case when outer layer is graphene such nanobubbles are called graphene nanobubbles (GN). In this study we consider the graphene nanobubbles for which the substrate is the graphite and the trapped material is argon (figure 1).

Due to large graphene stiffness and strong van der Waals (vdW) interaction between the outer graphene sheet and the graphite substrate sufficiently large pressure is built inside GN. The smaller the radius of GN the larger the pressure is created by vdW interaction. Extreme pressures up to 1 GPa are experimentally observed for GN with radius of several nanometers [5]. Inside GN on the graphite substrate with radii of the order of 400 nm the experimental estimation of pressure is 2 MPa [3]. Therefore the state of matter inside the GN may exist in various phases: gas, liquid or solid depending on the type of molecules and size of the GN.

From the experimental perspective direct investigating of the state of matter inside GN is rather complex problem. One have to use cutting edge and expensive experimental techniques



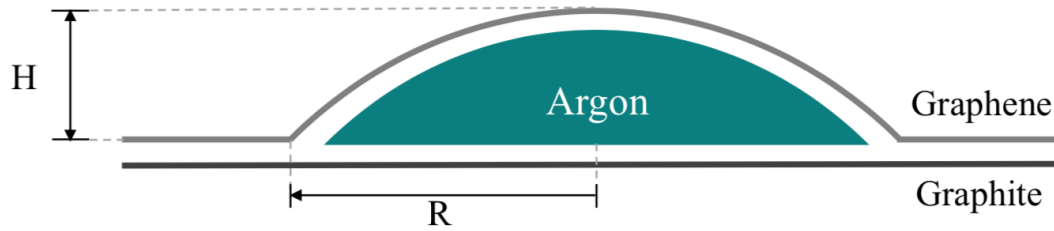


**Figure 1.** Schematic two-dimensional slice of the graphene nanobubble and its corresponding geometrical parameters.

such as transmitting electron microscopy (TEM) or synchronizing-based photoemission electron microscopy (XPEEM) [6]. On the other hand obtaining information about the shape of GNs is routine task done by atomic force microscopy (AFM). Thus it is of particular interest to establish the relation between the shape of the GN and the state of matter inside, so one can obtain information about the matter directly from AFM experiments.

In this study we theoretically establish the relation between the shape of the GN and the phase of the trapped material inside. Atomistic modelling is used to calculate the elastic constants and the adhesion energies. These parameters are used as inputs for the following analyses in terms of continuum media.

## 2. Methods

In our molecular dynamics part of this research software package LAMMPS [7] (the Large-scale Atomic/Molecular Massively Parallel Simulator) is used.

To calculate the elastic properties of graphene the adaptive intermolecular reactive bond order potential (AIREBO) [8] is used to describe the carbon–carbon interaction. It was shown that this potential describe well the mechanical properties of graphene [9].

Graphene layer is generated using software package VMD [10]. The boundary condition are set to periodic in order to model continuous graphene crystal. Then it is statically elongated in two different directions (zigzag and armchair) [9] and stresses are measured.

Lennard-Jones potential is used to evaluate the adhesion energy between argon and the graphite substrate. For argon–argon interaction the parameters are  $\sigma_{\text{Ar-Ar}} = 3.405 \text{ \AA}$ ,  $\varepsilon_{\text{Ar-Ar}} = 10.34 \text{ meV}$  [11]. Lorentz–Berthelot combining rules [12] are used to define carbon–argon interaction:  $\sigma_{\text{C-Ar}} = 3.4025 \text{ \AA}$ ,  $\varepsilon_{\text{C-Ar}} = 5.42 \text{ meV}$ . To apply these rules the carbon–carbon parameters are taken from Lennard-Jones part of AIREBO potential [8]:  $\sigma_{\text{C-C}} = 3.4 \text{ \AA}$ ,  $\varepsilon_{\text{C-C}} = 2.84 \text{ meV}$ .

To calculate the adhesion energy we modeled three cases: argon–graphite system, only argon system, only graphite system. To evaluate the adhesion energy we measure the potential energy per unit area difference between combined graphite–argon system and separated systems. Thus the adhesion energy can be calculated as  $\gamma_{\text{SB}} = (U_{\text{graphite+argon}} - (U_{\text{graphite}} + U_{\text{argon}}))/S$ .

In graphite–argon system three graphene layers represent substrate. They are generated using VMD. The size of graphene layer is  $L_x = 100.698 \text{ \AA}$ ,  $L_y = 102.098 \text{ \AA}$ , where  $L_x, L_y$  are lengths in  $x$  and  $y$  directions. The  $z$ -length of the simulation box is  $L_z = 107 \text{ \AA}$ , the substrate fills  $6.7 \text{ \AA}$ , the remaining space is filled by argon. Initially the argon atoms are inserted into the simulation box in simple cubic lattice. Different initial densities are set to study pressure dependence of the adhesion energy. Then the argon atoms are allowed to move in the  $NVT$

ensemble. The temperature is set to 300 K for all cases. The carbon atoms in graphite are fixed. After the energy of the system stabilizes, we assume that equilibrium is achieved, and statistical information can be gathered.

To simulate the argon system the separate calculations are performed. The number of argon atoms is the same as in corresponding case of the graphite–argon system. The size of the simulation box is  $L_x = 100.698 \text{ \AA}$ ,  $L_y = 102.098 \text{ \AA}$ ,  $L_z = 100 \text{ \AA}$ . Then argon atoms are allowed to move in the  $NVT$  ensemble. The temperature is set also to 300 K.

### 3. Results and discussion

All continuum studies use macroscopic parameters as input in their models. In the case of graphene nanobubbles they are Young's modulus of graphene and the adhesion energy between the bulk substance and the graphite. The precise values of these parameters allow to achieve better predictions of the shape of the nanobubble, the stresses of upper graphene sheet, the pressure inside the bubble. Also it gives more accurate value of the height to the footprint radius ratio, given by [3].

In theoretical part of the study [3] the free energy of the bubble is consist of tree parts: the elastic energy of the upper graphene sheet, vdW energy between the graphene, the substrate and trapped substance, and the free energy of trapped material. Minimizing the free energy with respect to the height and the radius, the  $H$  to  $R$  relation can be obtained:

$$\frac{H}{R} = \left[ \frac{\pi(\gamma_{GS} - \gamma_{GB} - \gamma_{SB})}{5cY} \right]^{\frac{1}{4}}, \quad (1)$$

where  $\gamma_{GS}$ ,  $\gamma_{GB}$ ,  $\gamma_{SB}$  are graphene–substrate, graphene–bulk and substrate–bulk adhesion energies respectively,  $Y$  is Young's modulus of graphene sheet,  $c$  is dimensionless coefficient depending only on the shape of the nanobubble, in the case of the round-shape bubbles  $c = 0.7$ . In our model  $\gamma_{GB} = \gamma_{SB}$  as substrate (graphite) consists of graphene layers. Usually it is unknown [3] what kind of substance is trapped inside the bubble. Therefore it is especially important to have the additional information from the atomistic study.

#### 3.1. Young's modulus

The Young's modulus of graphene is calculated from strain-stress curves (figure 2). The zigzag and armchair directions are slightly differs for the large strains. However for the small strains graphene is isotropic and linear elasticity is observed. For the case of graphene nanobubbles the average strain is of order 1–2% [3]. Therefore in the continuum model we can assume graphene as linearly elastic material. Calculating the slope of stress-strain curve at point (0,0) we can get the value for two-dimensional graphene Young's modulus  $Y = 21.19 \text{ eV/\AA}^2$ . Also we can divide this value by the average distance between layers in graphite  $3.35 \text{ \AA}$  and derive the three dimensional modulus 1.01 TPa that is in agreement with previous molecular dynamics study [9], experiments [13] and ab initio calculations [14].

#### 3.2. Adhesion energy

Calculated adhesion energies at different pressures are presented in figure 3. The strong dependence is observed at low pressures where argon is in a gas phase. Thus one should carefully use the continuum approach while modeling large nanobubbles with the low pressure of the trapped substance. For high pressures the adhesion energy can be treated as constant.

In theoretical part of [3] when applying equation (1) it is assumed that the adhesion energy is constant. This assumption leads to the conclusion that the ratio  $H/R$  is independent of the radius. But our results show that this conclusion is hold only if the trapped matter inside is in the condensed form such as incompressible liquid or solid. For gas phase inside the GN the adhesion energy strongly depend on the pressure (see figure 3) and as a consequence it is also

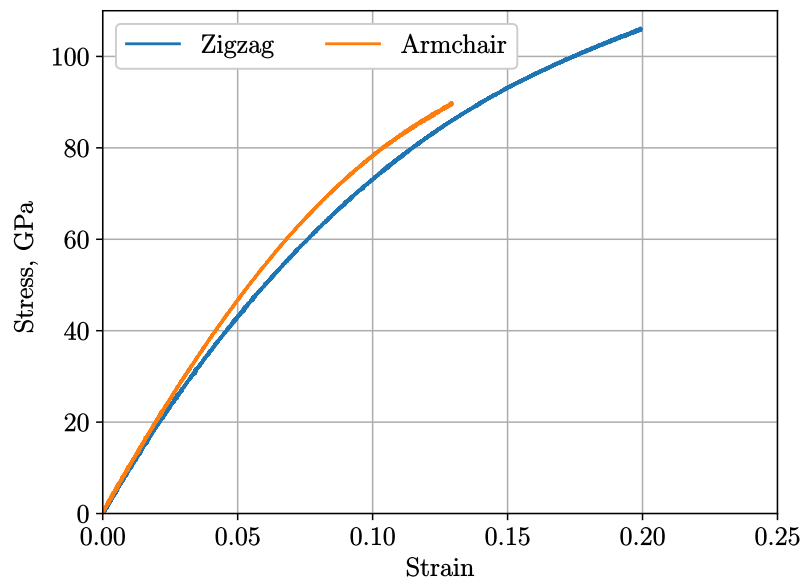


**Figure 2.** Stress-strain curve for single graphene layer modelled by AIREBO potential [8]. Both zigzag and armchair direction are presented. The Young's modulus obtained from the slope of the curve equals  $21.19 \text{ eV}/\text{\AA}^2$ .

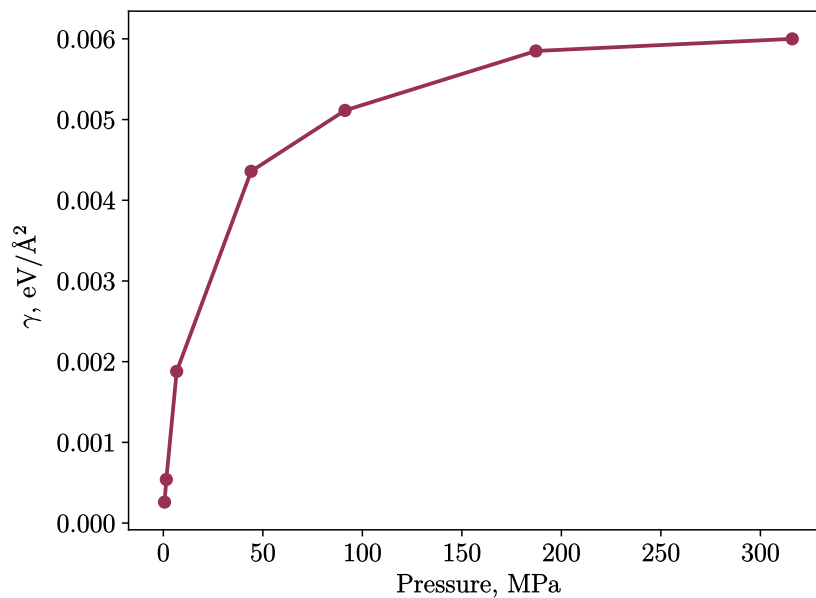


**Figure 3.** Dependence of argon pressure on the adhesion energy to graphite. The approximate boundary between gas phase and liquid phase of argon in terms of pressure is 100 MPa.

depend on the radius of the GN. Therefore the findings from [3] is not true and there is no universal shape for GN with gas phase if one exist.

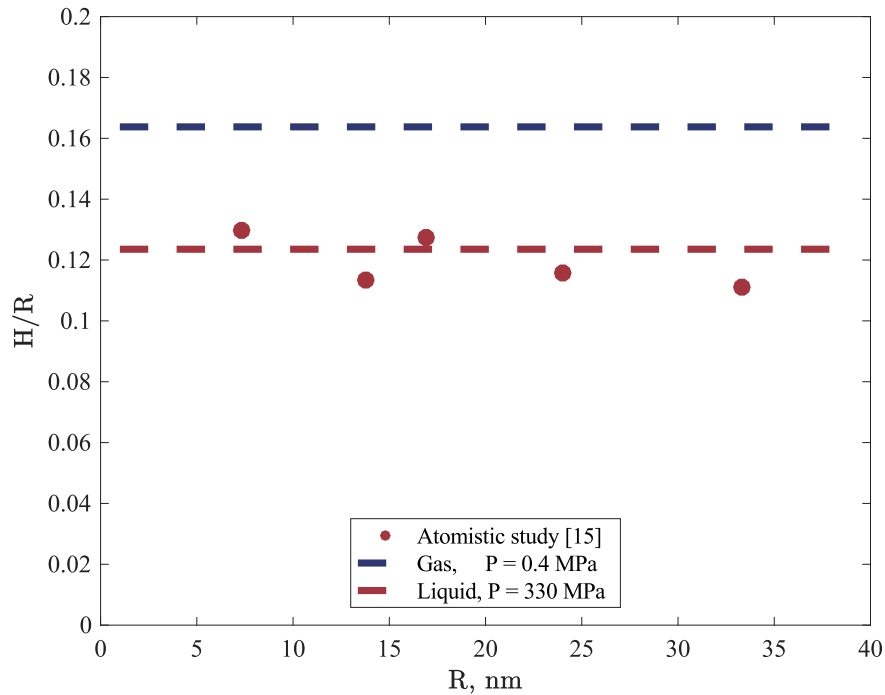


**Figure 4.** Prediction of the height to the radius ratio from continuum theory and from direct molecular dynamics study [15].

Adhesion energy for solid and liquid states typically has different values and, according to equation (1), the GNs with liquid or solid state inside should have also different  $H/R$  ratio. Unfortunately, if adhesion energies for liquid and solid states differ not significantly then root of the fourth degree in equation (1) will make this difference even more inconspicuous.

The figure 4 shows  $H/R$  ratio obtained with the help of equation (1) for two adhesion energies of gas and liquid phases of argon correspondingly. Dots in figure 4 present direct molecular dynamics modelling [15] of the GNs. In the study [15] argon inside the GN is in a solid state. Nevertheless the results of  $H/R$  value for both liquid and solid states of argon have very close values. We attribute this to the small differences in adhesion energies of liquid and solid argon.

#### 4. Conclusion

This research provides insight into the importance of the accurate determination of the constants used in the continuum approach while modeling the graphene nanobubbles. The precise two-dimensional Young's modulus of graphene is calculated. Also the strong dependence of the adhesion energy is detected at low pressures. Atomistic simulations can provide the crucial parameters for continuum approach particularly when it is impossible or problematic to measure them experimentally, for example, the adhesion energy.

Moreover this study shows that universal shape phenomenon [3] is only applicable in limited region of pressures and the dependence of adhesion energy on pressure should be taken into account when gas phase (if one exist) or liquid–solid phase transition is considered. The universal shape phenomenon is only valid in the thermodynamics regions where trapped material is either in liquid or solid state, and no phase transition occurs.

The result of this work can also be used as theoretical background for investigation of the phase state of the trapped material inside the graphene nanobubbles only using experimental information about their shape ( $H/R$  ratio).

## References

- [1] Geim A K and Grigorieva I V 2013 *Nature* **499** 419–25
- [2] Haigh S J, Gholinia A, Jalil R, Romani S, Britnell L, Elias D C, Novoselov K S, Ponomarenko L A, Geim A K and Gorbachev R 2012 *Nat. Mater.* **11** 764–7
- [3] Khestanova E, Guinea F, Fumagalli L, Geim A K and Grigorieva I V 2016 *Nat. Commun.* **7** 12587
- [4] Levy N, Burke S A, Meaker K L, Panlasigui M, Zettl A, Guinea F, Neto A H C and Crommie M F 2010 *Science* **329** 544–7
- [5] Vasu K S, Prestat E, Abraham J, Dix J, Kashtiban R J, Beheshtian J, Sloan J, Carbone P, Neek-Amal M, Haigh S J, Geim A K and Nair R R 2016 *Nat. Commun.* **7** 12168
- [6] Zamborlini G, Imam M, Patera L L, Menten T O, Stojic N, Africh C, Sala A, Binggeli N, Comelli G and Locatelli A 2015 *Nano Lett.* **15** 6162–9
- [7] Plimpton S 1995 *J. Comput. Phys.* **117** 1–19
- [8] Stuart S J, Tutein A B and Harrison J A 2000 *J. Chem. Phys.* **112** 6472–86
- [9] Zhao H, Min K and Aluru N R 2009 *Nano Lett.* **9** 3012–5
- [10] Humphrey W, Dalke A and Schulten K 1996 *J. Mol. Graphics* **14** 33–8
- [11] Jain S K, Pikunic J P, Pellenq R J M and Gubbins K E 2005 *Adsorption* **11** 355–60
- [12] Hudson G H and McCoubrey J C 1960 *Trans. Faraday Soc.* **56** 761–6
- [13] Lee Ch, Wei X, Kysar J W and Hone J 2008 *Science* **321** 385–8
- [14] Liu F, Ming P and Li J 2007 *Phys. Rev. B* **76** 064120
- [15] Iakovlev E, Zhilyaev P and Akhatov I 2017 *Sci. Rep.* **7** 17906

## 3.3 Prepare to continuum approach: adhesion energy

The continuum approach requires different input parameters, such as Young's modulus of graphene, equations of state for trapped matter, and adhesion energies of interaction between the substrate, the graphene sheet, and the substance. This chapter compiles our research in calculating adhesion energy between graphite and the matter (ethane in this article). Two approaches are proposed to calculate the adhesion energy. The first one is to use the MD method to calculate the difference of the energies between the combined system (solid surface and gas or liquid) and two isolated systems. The second approach is to interpolate heat adsorption from atomistic simulation data, and then, Langmuir isotherm gets the adhesion energy. We use in further calculations the first method as it is more accurate.

### 3.3.1 Contribution

My contribution to this work: carried out all MD calculations and data analysis, took part in results discussion, and writing the manuscript.

# Adhesion energy of ethane–graphite interface: Atomistic study

**E S Iakovlev, P A Zhilyaev and I Sh Akhatov**

Skolkovo Institute of Science and Technology, Skolkovo Innovation Center Bldg 3, Moscow  
143026, Russia

E-mail: [evgeny.iakovlev@skolkovotech.ru](mailto:evgeny.iakovlev@skolkovotech.ru)

**Abstract.** Adhesion energy is an important characteristic of interfacial interactions. Usually one apply notion of adhesion energy to solid–solid interfaces, but it also could be extended to gas–solid and liquid–solid interfaces. In later case phenomenon of adsorption is closely related to the adhesion energy. In this work we apply molecular dynamics method to calculate the specific adhesion energy for gas and liquid ethane on a graphite substrate. Influence of temperature and density on the value of the specific adhesion energy is investigated. Langmuir adsorption model is applied to interpret results and establish connection between notions of adsorption heat and specific adhesion energy. Appearance of multilayer adsorption is detected for higher densities. Developed model and numerical approach to calculate adhesion energy and surface coverage can be applied for different types of the adsorbate and the substrate.

## 1. Introduction

Adhesion energy is the main characteristic of the interaction between the interfaces. This is the energy that is released when one surface comes into contact with another surface. Computational studies using atomistic calculations [1, 2] provide valuable insights into structure and energetic changes that occurs between surfaces. The procedure to calculate the energy of adhesion between two solid surfaces is straightforward. The basic idea is to measure potential energy between two surfaces at different distances with relaxation [3]. The algorithm of evaluation the adhesion energy of gas–solid and liquid–solid interface is more complicated. There are a number of different ways to obtain value of adhesion energy from atomistic calculations: (method 1) difference of energies between combined system (solid surface + gas or liquid) and two isolated systems, (method 2) calculate heat adsorption from interpretation of atomistic data [4, 5] using one of the adsorption isotherms such as Langmuir isotherm.

In the present work, we use both methods to calculate the adhesion energy between ethane and graphite and show that they give comparable results. Molecular dynamics (MD) method is used to obtain atomistic data. Langmuir adsorption isotherm is applied to establish connection between adsorption and adhesion. Proposed approach is applicable both to liquid–solid and gas–solid interfaces. In this study we consider only plain surface. It should be noted, that the roughness of the surface [6, 7] and confinement [8] can also contribute to adhesion energy.

## 2. Methods

Software package LAMMPS [9] (large-scale atomic-molecular massively parallel simulator) is used to perform MD simulations. Graphene layers are generated with the use of the VMD

 Content from this work may be used under the terms of the [Creative Commons Attribution 3.0 licence](https://creativecommons.org/licenses/by/3.0/). Any further distribution of this work must maintain attribution to the author(s) and the title of the work, journal citation and DOI.

**Table 1.** Lennard-Jones potential parameters used in this work. Cut-off radius  $r_{\text{cut}}$  for all cases in this study is 14 Å.

LJ parameter	CH <sub>3</sub> -CH <sub>3</sub>	C-CH <sub>3</sub> (I)	C-C (I)	C-CH <sub>3</sub> (II)	C-C (II)
$\sigma$ , Å	3.750	3.575	3.400	3.575	3.400
$\epsilon$ , meV	8.450	4.900	2.840	4.510	2.410

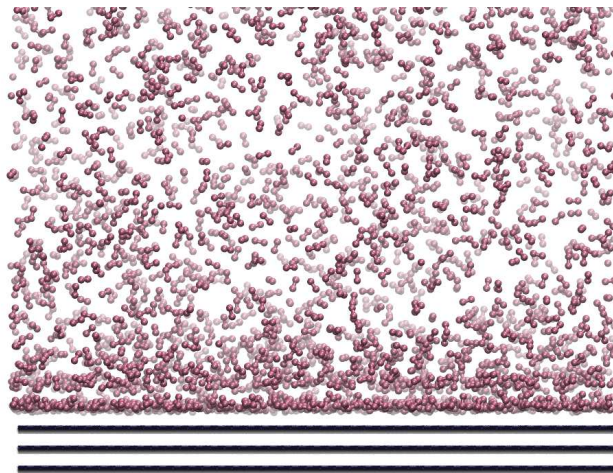


**Figure 1.** Side view of MD simulation. The density is set equal to 0.166 g/cm<sup>3</sup>. Temperature is 300 K. Formation of second layer can be seen.

software package [10]. The boundary condition is set to periodic in order to model continuous graphene crystal.

Lennard-Jones potential is used to estimate the energy of adhesion of ethane to a graphite substrate. The TraPPE (transferable potentials for phase equilibria) united atom [11] is used to describe ethane-ethane interaction. This coarse grain potential is more computationally efficient than full atomic potentials and it is known to describe thermodynamical properties with high level of accuracy [12]. This force field implies that CH<sub>3</sub> is pseudo-atom that makes calculations computationally efficient. The bond length between CH<sub>3</sub> sited is fixed and equal to 1.540 Å. For comparison we use two Lennard-Jones parameters for C-CH<sub>3</sub>. Both are derived from Lorentz-Berthelot combining rules [13]. In first case we take C-C from Lennard-Jones part of AIREBO potential [14] (I), which is known to describe carbon materials properties well [15], in second case parameters are taken from study [16] (II). The calculations with second parameterization are performed only for 310 K to check sensitivity of adhesion energy to potential parameters. All parameters are shown in table 1.

For method 1 to calculate the adhesion energy, we simulate 3 cases: ethane-graphite system, only ethane system, only graphite system. To evaluate the adhesion energy we measure the potential energy per unit area difference between combined graphite-ethane system and separated systems. Thus the adhesion energy can be calculated as  $\gamma_{\text{SB}} = (U_{\text{graphite+ethane}} - (U_{\text{graphite}} + U_{\text{ethane}}))/S$ . Carbon atoms do not interact during simulations in this study, therefore we used  $U_{\text{graphite}} = 0$  in this equation.

In graphite-ethane system 3 graphene layers represent substrate (figure 1), which is generated using VMD. The sizes of graphene layer are  $L_x = 100.698$  Å and  $L_y = 102.098$  Å, where  $L_x, L_y$

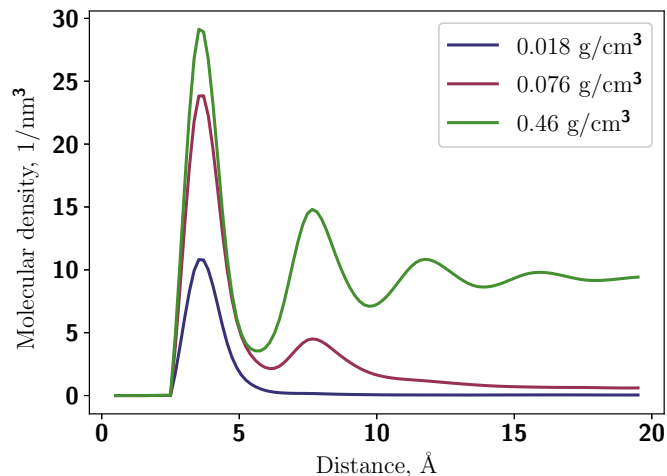


**Figure 2.** Molecular density distribution along  $z$  direction near substrate. Temperature is set to 310 K. Formation of 1, 2 and 3 layers adsorption can be seen.

are the lengths in  $x$  and  $y$  directions. The  $z$ -length of the simulation box is  $L_z = 107 \text{ \AA}$ , the substrate fills  $6.7 \text{ \AA}$ , the remaining space is filled by ethane. Initially the ethane molecules are inserted into the simulation box in simple cubic lattice. Different initial densities are set to study pressure dependence of the adhesion energy, also we consider different temperatures. Then the ethane molecules are allowed to move in the  $NVT$  ensemble. The temperature is set to 280, 290, 300, 310 K to study ethane below and above critical temperature. The carbon atoms in graphite are fixed. After the energy of the system stabilizes, we assume that equilibrium is achieved, and statistical information can be gathered.

To simulate the ethane system, the separate calculations are performed. The number of ethane molecules is the same as in corresponding case of the graphite–ethane system. The size of the simulation box is  $L_x = 100.698 \text{ \AA}$ ,  $L_y = 102.098 \text{ \AA}$ ,  $L_z = 100 \text{ \AA}$ . Then ethane molecules are allowed to move in the  $NVT$  ensemble. The temperature is set to corresponding calculations of graphite–ethane system.

To apply method 2, one needs to obtain surface coverage of the graphite. To evaluate surface coverage we calculate averaged number density of ethane molecules near substrate in  $z$  direction. Example of this density distribution is shown in figure 2. Then we obtain the number of molecules in the first layer by integrating this function from 0 to the first minimum of density distribution.

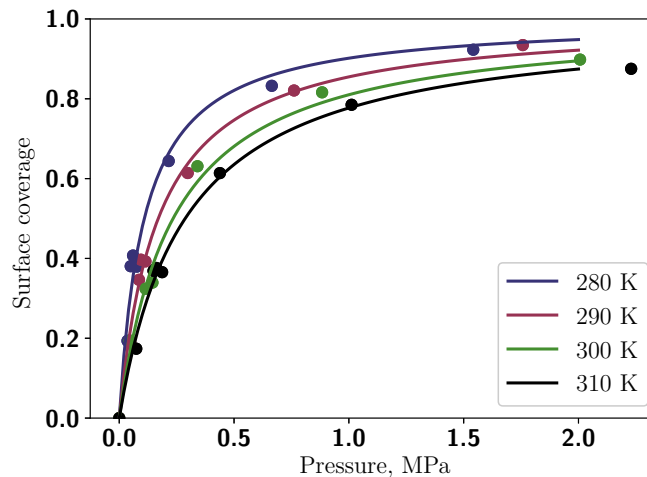
To calculate pressure of ethane in case of graphite–ethane system, we select molecules located in the gap between  $z$  coordinates:  $25 \text{ \AA}$  and  $75 \text{ \AA}$ . Then the per-atom stress tensor is evaluated according to [17]. After averaging the per-atom stress tensor and obtaining the total stress tensor of the ethane atoms, the pressure is calculated as a minus trace of the obtained stress tensor.

### 3. Results and discussion

Langmuir adsorption model is used to evaluate specific adhesion energy according to method 2. We compare results of such prediction with direct MD calculation of adhesion energy. To apply Langmuir adsorption model we have to deal only with low densities because one of the basic assumptions is mono-layer coverage. Thus we select cases with only one layer adsorption, it is indicated by one maximum in figure 2. The pressure of ethane in this case is calculated using method described in previous section. Then we fit MD points to the Langmuir isotherm

**Table 2.** Table of equilibrium constants  $K$  for different temperatures.

Temperature, K	280	290	300	310
$K$ , 1/MPa	9.2	5.9	4.3	3.5

**Figure 3.** Surface coverage as a function of gas pressure at different temperatures: markers represent MD results; lines are Langmuir isotherm approximation.

$\theta = \rho/\rho_m = Kp/[1 + Kp]$ , where  $\theta$  is the fractional occupancy of the adsorption sites;  $\rho$  is the specific density per unit area;  $\rho_m$ —the specific density per unit area for the fully filled adsorption layer;  $p$  is pressure of ethane gas under the adsorbed layer;  $K$  is equilibrium constant of the reaction between the adsorbate molecule  $A$  and an empty site  $S$ ,



where  $A_{ad}$  is an adsorbed complex.

We use the method of least squares to adjust parameters: equilibrium constant  $K$  is adjusted for every temperature, density of the fully filled adsorption layer  $\rho_m$  is the same for all cases because physical number of available sites are constant and depend only on the geometry and material of the substrate. We obtain  $\rho_m = 4.3$  molecules/nm<sup>2</sup>. Fitting equilibrium constants can be found in table 2. Plotted points of MD calculation of surface coverage and corresponding Langmuir isotherm are shown in figure 3.

The results given in table 2 allow to calculate the heat of adsorption  $\Delta H$ :

$$K = K_0 e^{-\frac{\Delta H}{kT}}. \quad (2)$$

We take the log of both sides of 2 and fit the data using the method of least squares, which gives us  $\Delta H = -0.242$  eV. Then we multiply the heat of adsorption by number of molecules in the adsorbed layer and divide it by area of surface to obtain the specific adhesion energy:  $\gamma = -\Delta H N/S$ . We take negative as we treat  $\gamma$  as the gain in energy due to adsorption. On the other hand the specific adhesion energy is calculated directly from MD as energy difference between graphite–ethane and ethane systems. Both estimations are shown in figure 4. For low

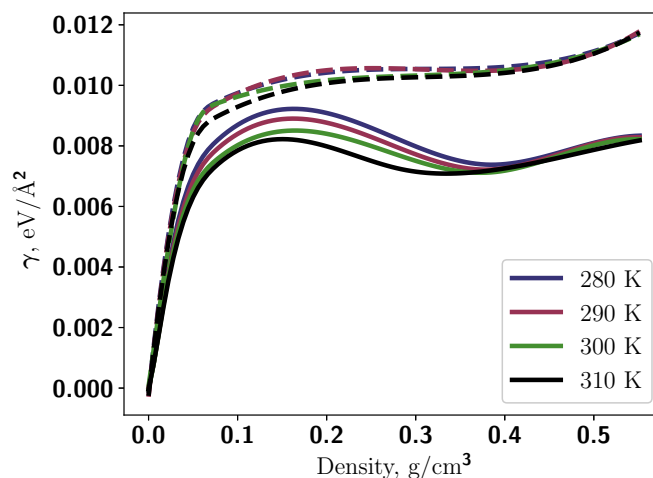


**Figure 4.** Specific adhesion energy at different temperatures: solid lines are calculated directly from MD; dotted lines are evaluated from the Langmuir isotherm.

densities Langmuir model gives good match with direct MD calculations, while for high densities the assumption of mono-layer adsorption is not satisfied that is why the divergence is observed.

#### 4. Conclusion

We perform MD simulations to calculate the surface coverage and the specific adhesion energy for different densities and temperatures of the graphite–ethane system. We use Langmuir adsorption model to interpret the results for low densities and predict from them the specific adhesion energy. One should use advanced adsorption models, such as Brunauer–Emmett–Teller theory, to get more precise estimation. Nevertheless, the benchmark shown in this work shows the possibility of prediction of specific adhesion energy from adsorption models.

#### References

- [1] Frenkel D and Smit B 2001 *Understanding Molecular Simulation: From Algorithms to Applications* vol 1 (Elsevier)
- [2] Kuksin A Yu, Morozov I, Norman G, Stegailov V and Valuev I 2005 *Mol. Simul.* **31** 1005–17
- [3] Gao W, Xiao P, Henkelman G, Liechti K M and Huang R 2014 *J. Phys. D: Appl. Phys.* **47** 255301
- [4] Tsukanov A and Psakhie S 2017 *Physical Mesomechanics* **20** 43–54
- [5] Tsukanov A and Psakhie S 2016 *Facta Universitatis, Series: Mechanical Engineering* **14** 269–80
- [6] Aslyamov T and Khlyupin A 2017 *J. Chem. Phys.* **147** 154703
- [7] Aslyamov T, Pletneva V and Khlyupin A 2019 *J. Chem. Phys.* **150** 054703
- [8] Derjaguin B V, Churaev N V, Muller V M and Kisin V 1987 *Surface Forces* (Springer)
- [9] Plimpton S 1995 *J. Comput. Phys.* **117** 1–19
- [10] Humphrey W, Dalke A and Schulten K 1996 *J. Mol. Graphics* **14** 33–8
- [11] Martin M G and Siepmann J I 1998 *J. Phys. Chem. B* **102** 2569–77
- [12] Kondratyuk N D, Norman G E and Stegailov V V 2016 *J. Chem. Phys.* **145** 204504
- [13] Hudson G and McCoubrey J 1960 *Trans. Faraday Soc.* **56** 761–6
- [14] Stuart S J, Tutein A B and Harrison J A 2000 *J. Chem. Phys.* **112** 6472–86
- [15] Orekhov N and Stegailov V 2015 *Carbon* **87** 358–64
- [16] Ackerman D M, Skoulidas A I, Sholl D S and Karl Johnson J 2003 *Mol. Simul.* **29** 677–84
- [17] Thompson A P, Plimpton S J and Mattson W 2009 *J. Chem. Phys.* **131** 154107

## 3.4 Continuum approach: argon case

The continuum approach allows the calculation of the properties of the graphene nanobubbles with any radius and any amount of the trapped matter. In this chapter, we develop the model that uses the principle of minimization of the energy to describe the equilibrium system. The total energy of the graphene nanobubble consists of the elastic energy of graphene, the adhesion energy between the substrate, the trapped matter, the graphene sheet, and the bulk energy of the substance. We use numerical optimization in order to find the minimum of the energy functional. Then, we describe the final state of the matter, the shape of the graphene nanobubble, and compare the results qualitatively with previous MD calculations and experimental studies. Also, a new phenomenon is discovered. We called it the "forbidden region" - the range of radii where no stable bubbles can be found and separate the bubbles with the trapped liquid and gas phases. Still, there is a gap between atomistic simulations which study tiny bubbles with solid-state inside, and continuum approach, which allows studying bigger bubbles with trapped not solid substance.

### 3.4.1 Contribution

My contribution to this work: took part in model development, carried out all MD calculations and implemented continuum model in Python, took part in results discussion, and writing the manuscript.

# Liquid–gas phase transition of Ar inside graphene nanobubbles on the graphite substrate

Petr Zhilyaev<sup>1</sup>, Evgeny Iakovlev  and Iskander Akhatov

Center for Design, Manufacturing and Materials, Skolkovo Institute of Science and Technology, Skolkovo Innovation Center, Building 3, Moscow, 143026, Russia

E-mail: [P.Zhilyaev@skoltech.ru](mailto:P.Zhilyaev@skoltech.ru), [Evgeny.Iakovlev@skolkovotech.ru](mailto:Evgeny.Iakovlev@skolkovotech.ru) and [I.Akhatov@skoltech.ru](mailto:I.Akhatov@skoltech.ru)

Received 18 December 2018, revised 4 February 2019

Accepted for publication 11 February 2019

Published 14 March 2019



CrossMark

## Abstract

Graphene nanobubbles (GNBs) are formed when a substance is trapped between a graphene sheet (a 2D crystal) and an atomically flat substrate. The physical state of the substance inside GNBs can vary from the gas phase to crystal clusters. In this paper, we present a theoretical description of the gas–liquid phase transition of argon inside GNBs. The energy minimization concept is used to calculate the equilibrium properties of the bubble at constant temperature for a given mass of captured substance. We consider the total energy as a sum of the elastic energy of the graphene sheet, the bulk energy of the inner substance and the energy of adhesion between this substance, the substrate and graphene. The developed model allows us to reveal a correlation between the size of the bubble and the physical state of the substance inside it. A special case of a GNB that consists of argon trapped between a graphene sheet and a graphite substrate is considered. We predict the ‘forbidden range’ of radii, within which no stable GNBs exist, that separates bubble sizes with liquid argon inside from bubble sizes with gaseous argon. The height-to-radius ratio of the bubble is found to be constant for radii greater than 200 nm, which is consistent with experimental observations. The proposed model can be extended to various types of trapped substances and 2D crystals.

Supplementary material for this article is available [online](#)

Keywords: graphene, graphene nanobubbles, molecular dynamics, phase transition, multiscale modeling, theory of elasticity

(Some figures may appear in colour only in the online journal)

## 1. Introduction

A graphene nanobubble (GNB) is a system that consists of an atomically flat substrate, a sheet of graphene (a 2D crystal) and a trapped substance between them (figure 1(a)). GNBs produce a giant pseudomagnetic field [1, 2] and can be used as field-effect devices [3], and their presence can alter phonon-electron interactions [4]. In some cases, the trapped substance experiences extreme pressure inside the GNB and consequently acquires special properties. For example, the dielectric constant of water between a graphene sheet and a

diamond substrate increases to such an extent that etching of the diamond substrate occurs [5]. In addition, GNBs are considered a prospective container that can aid in observing chemical reactions in real time [6].

Little information about the physical state of the substance inside GNBs is available. Experiments using combined low energy electron microscopy and synchrotron-based photoemission electron microscopy (XPEEM) show that for small GNBs (radii on the order of 1 nm) on metal substrates, the substance inside is presented in the form of structured clusters [7]. Experiments using real time x-ray photoelectron spectroscopy show that argon atoms aggregate into multilayer clusters inside GNBs on a Ni substrate [8]. From indirect

<sup>1</sup> Author to whom any correspondence should be addressed.

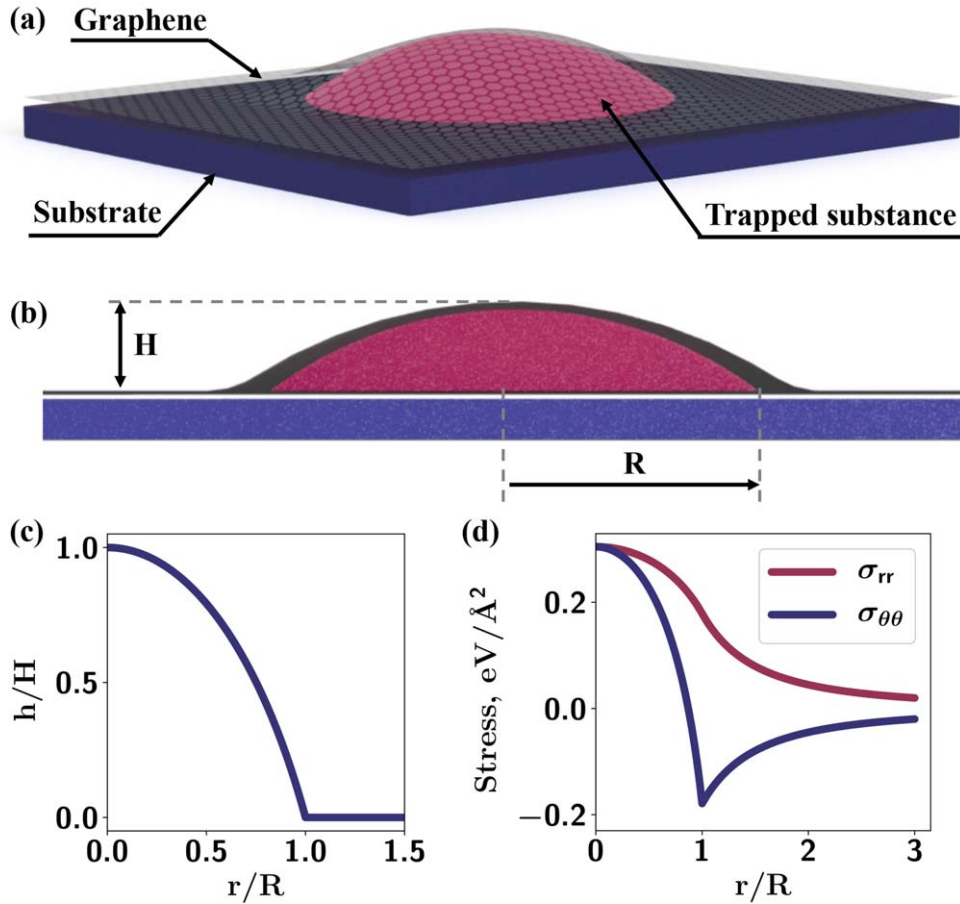


**Figure 1.** (a) Schematic representation of a graphene nanobubble (GNB). (b) Meridional slice of a GNB. The height ( $H$ ) of a GNB is the distance between the top point of the bubble and the surface of the undisturbed graphene sheet. (c) Height profile of a GNB in dimensionless coordinates ( $r/R$ ,  $h/H$ ). The calculated profiles for all trapped masses and both temperatures coincide. (d) Distribution of stress  $\sigma_{rr}$  (red line) and  $\sigma_{\theta\theta}$  (blue line) along the radial direction.

atomic force microscopy (AFM) measurements and theoretical speculations, the substance inside larger GNBs (radii on the order of 100 nm) on a graphite substrate is predicted to be in the liquid phase [9]. Molecular dynamics (MD) calculations of GNBs on a graphite substrate with argon inside indicate that the trapped substance is in a solid state [10]. A similar phenomenon of crystallization is experimentally observed in carbon nanotubes [11] and graphene nanocapillaries [12], where crystal water is detected at room temperature.

Although experimental evidence that condensation of trapped substances occurs inside GNBs exists, theoretical models describing the physical state of the substance and its correlation with the GNB shape are still lacking. Furthermore, solid, liquid and gas phases are detected in separate experiments; hence, a phase transition between them is expected to exist. However, no theoretical or experimental studies describing or observing such a phenomenon exist.

In this paper, we present a multiscale approach to model the liquid–gas phase transition inside a GNB. In our study, we consider a GNB that consists of argon trapped between a graphene sheet and a graphite substrate. Although we study particular materials, the proposed model can be easily extended to other types of trapped substances, 2D crystals and

substrates. The developed theory enables the establishment of a relationship between the GNB shape and the physical state of the trapped substance.

## 2. Methods

In our approach, all calculated mechanical and thermodynamic properties of the GNB are derived from the minimization of the total energy of the system:

$$E_{\text{total}} = E_{\text{elastic}} + E_{\text{bulk}} + E_{\text{adhesion}}, \quad (1)$$

where  $E_{\text{elastic}}$  is the elastic energy of the graphene sheet,  $E_{\text{bulk}}$  is the energy of the trapped substance, and  $E_{\text{adhesion}}$  is the energy that includes the surface interaction among the substrate, the graphene sheet and the trapped substance.

The elastic energy of the graphene sheet is evaluated in the framework of elasticity theory [13]. The total elastic energy is given as the sum of the stretching and bending parts:

$$E_{\text{elastic}} = \int_0^\infty [\Psi_s(u_{\alpha\beta}, h) + \Psi_b(h)] 2\pi r dr, \quad (2)$$

where  $\Psi_s$  and  $\Psi_b$  are the stretching and bending energies per unit area,  $u_{\alpha\beta}$  is the strain tensor,  $h$  is the height profile, and  $r$  is the radius.

The functional relation of the strain tensor components with the radial displacement ( $u_r$ ) and height profile ( $h$ ) is

$$u_{rr} = \frac{\partial u_r}{\partial r} + \frac{1}{2} \left( \frac{\partial h}{\partial r} \right)^2, \quad u_{\theta\theta} = \frac{u_r}{r}. \quad (3)$$

For the following discussion, we assume that Poisson's ratio is equal to zero. In this case, the stress tensor components are

$$\sigma_{rr} = Y u_{rr}, \quad \sigma_{\theta\theta} = Y u_{\theta\theta}, \quad (4)$$

where  $Y$  is the Young's modulus of the graphene sheet with dimensions of energy per unit area.

Then, the specific stretching and bending elastic energies can be expressed as

$$\Psi_s = \frac{1}{2} u_{\alpha\beta} \sigma_{\alpha\beta} = \frac{Y}{2} \left[ \left( \frac{\partial u_r}{\partial r} \right)^2 + \frac{\partial u_r}{\partial r} \left( \frac{\partial h}{\partial r} \right)^2 + \frac{1}{4} \left( \frac{\partial h}{\partial r} \right)^4 + \left( \frac{u_r}{r} \right)^2 \right], \quad (5)$$

$$\Psi_b = \frac{\kappa}{2} \left[ \left( \frac{\partial^2 h}{\partial r^2} \right)^2 + \frac{1}{r^2} \left( \frac{\partial h}{\partial r} \right)^2 \right]. \quad (6)$$

The part of the energy associated with the trapped substance ( $E_{\text{bulk}}$ ) at given temperature, volume and density is the work required to assemble the trapped substance from particles located at infinity. Let us assume that assembling is performed particle-by-particle at a fixed volume. This means that the density changes gradually from zero to the desired value. At any given moment, the pressure and temperature during assembly are constant. The addition of a unit mass of particles changes  $E_{\text{bulk}}$  by the value of the chemical potential ( $\mu$ ). Thus, integrating the chemical potential from zero density to the given density yields the bulk energy:

$$E_{\text{bulk}} = V \int_0^\rho \mu(\rho') d\rho'. \quad (7)$$

The part of the energy related to adhesion ( $E_{\text{adhesion}}$ ) is the change in the energy of the system due to detachment of the graphene sheet from the substrate and adhesion of the trapped substance to both the graphene sheet and substrate. It can be expressed via the area of the GNB footprint and the specific adhesion energies:

$$E_{\text{adhesion}} = \gamma \pi R^2, \quad (8)$$

$$\gamma = \gamma_{GS} - \gamma_{GT} - \gamma_{ST}, \quad (9)$$

where  $\gamma_{GS}$ ,  $\gamma_{GT}$  and  $\gamma_{ST}$  are the specific adhesion energies between the graphene sheet and the substrate, the graphene sheet and the trapped substance, and the substrate and the trapped substance, respectively.

To find the equilibrium GNB at a given mass ( $M$ ), the following procedure is utilized (figure 2). We vary the radius of the GNB, and for each particular radius, the total energy is evaluated (outer cycle). The GNB with the lowest energy is assumed to be the equilibrium one. For each GNB radius, we vary the pressure created by the graphene sheet (inner cycle on figure 2). If the pressure and radius are known, one can calculate  $E_{\text{elastic}}$ , the height profile and the radial displacement

distribution. This part of the procedure is iterated until  $M = \rho V$ , where  $\rho$  is determined by the equation of state (EOS) of the trapped substance and the volume  $V$  is obtained from the height profile. The EOS of argon is taken from tabulated NIST data [14, 15].

Boundary conditions are imposed based on the following assumptions. The bubble is assumed to be symmetric, which leads to boundary conditions for radial displacement  $u_r(0) = 0$  and derivative of the height profile  $h'(0) = 0$  at the zero radial coordinate. Since the elastic energy is bounded, the natural boundary condition for the displacement at infinity is  $u_r(\infty) = 0$ . The additional constraint  $h(r \geq R) = 0$  arises due to bubble localization in space.

To resolve the boundary conditions and other constraints numerically, the computational domain is subdivided into two regions. The first region, where the trapped substance is located, is the interval from 0 to  $R$ , and the second region is the interval from  $R$  to infinity, where no trapped substance is present. In the first region, the height profile and displacement are represented as a series expansion of Chebyshev polynomials. The height profile is zero in the second region; therefore, the problem is significantly simplified, and one can derive an analytic solution for the elastic energy ( $Y u_r^2(R)$ ). The Chebyshev polynomial coefficients are calculated by minimizing the following function:

$$\min_{u_r(r), h(r)} \int_0^R [\Psi_s(u_r(r), h(r)) + \Psi_b(h(r))] 2\pi r dr + Y u_r^2(R) - PV. \quad (10)$$

Ones  $R$  and  $P$  are known the adhesion energy is evaluated via equation (8). In this study, specific adhesion energies  $\gamma_{GS}$ ,  $\gamma_{GT}$ ,  $\gamma_{ST}$  are obtained from MD calculations using the LAMMPS software package [16]. The specific adhesion energy between the graphene and the substrate is calculated as the work per unit area required to separate the graphene sheet from graphite. For the AIREBO potential [17], we obtain a value of  $\gamma_{GS} = 0.017 \text{ eV } \text{\AA}^{-2}$ , which is the typical adhesion energy of graphene membranes [18]. The adhesion energies  $\gamma_{GT}$  and  $\gamma_{ST}$  are assumed to be equal. The specific adhesion energy  $\gamma_{ST}$  is calculated as the combination of the potential energies of three systems: graphite, argon, and combined argon and graphite (figures 3(c)–(d)):

$$\gamma_{ST} = U_{\text{graphite}} + U_{\text{argon}} - U_{\text{argon+graphite}}, \quad (11)$$

where  $U_{\text{graphite}}$ ,  $U_{\text{argon}}$  and  $U_{\text{argon+graphite}}$  are the specific potential energies calculated from MD simulations. The explicit dependence on the density and temperature of argon is also taken into consideration (figure 3(a)). Details of MD simulation can be found in the supplementary material available online at [stacks.iop.org/NANO/30/215701/mmedia](https://stacks.iop.org/NANO/30/215701/mmedia).

To evaluate  $E_{\text{bulk}}$  using equation (8), data on the chemical potential of argon are taken from NIST [15]. In cases where the final density is in the liquid or mixed gas–liquid regions, the linear interpolation of the chemical potential between gas and liquid is used (figure 3(b)).

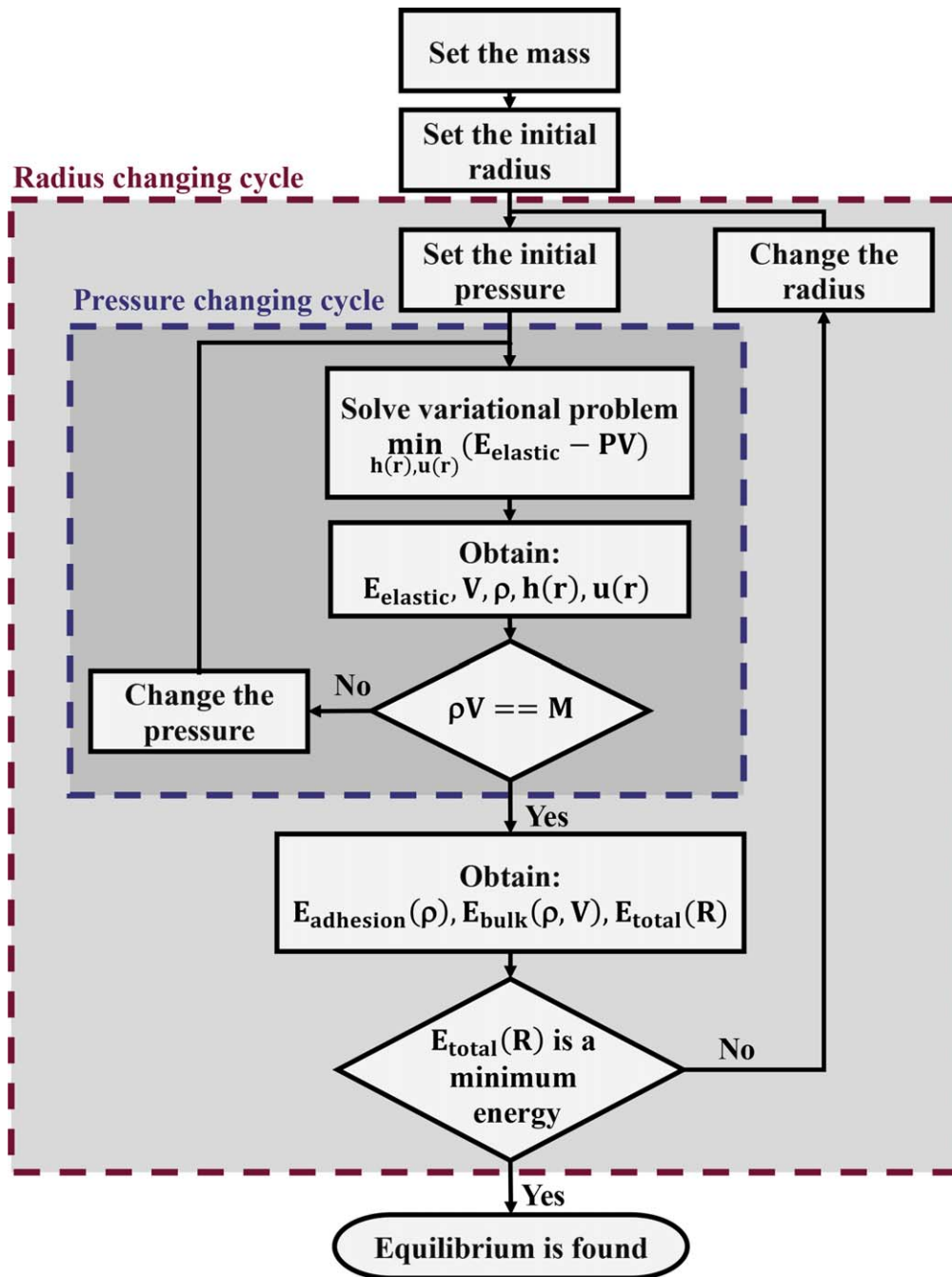


**Figure 2.** Algorithm used to find the equilibrium GNB shape and calculate its physical properties. The mass of the trapped substance and the temperature of the system are given and fixed. There are two nested cycles: the inner cycle, in which the pressure is changing, and the outer cycle, in which the radius is changing. The ‘pressure changing cycle’ ends when the calculated pressure is such that the corresponding density multiplied by the volume of the bubble equals the given mass of the trapped substance. The ‘radius changing cycle’ ends when the energy of the system reaches its global minimum.

### 3. Results and discussion

In this work, we consider a GNB at two temperatures —  $T_1 = 140$  K and  $T_2 = 300$  K. Argon at 140 K has a distinct gas-to-liquid phase transition, while at 300 K, no gas-to-liquid phase transition exists, and at higher densities, argon becomes supercritical. The application of the multiscale model described above gives self-similar profiles (figure 1(c)) for all phase states of the trapped material (gas, liquid, and supercritical fluid) inside the GNB. By self-similar profiles,

we mean that the height profile for all GNBs along the dimensionless  $(r/R, h/H)$  axes are the same.

Characteristic radial and angular components of the stress are presented in figure 1(d). The angular component of the stress has a distinct minimum at the GNB radius. For GNBs with the same  $H/R$  ratio, self-similar profiles of stress components are obtained along the  $(r/R, \sigma)$  axes.

The height-to-radius ratio is found to be almost constant for GNBs at 140 K and equal to 0.11 (figure 4(a)). GNBs at 300 K have constant  $H/R = 0.17$  only for radii greater than

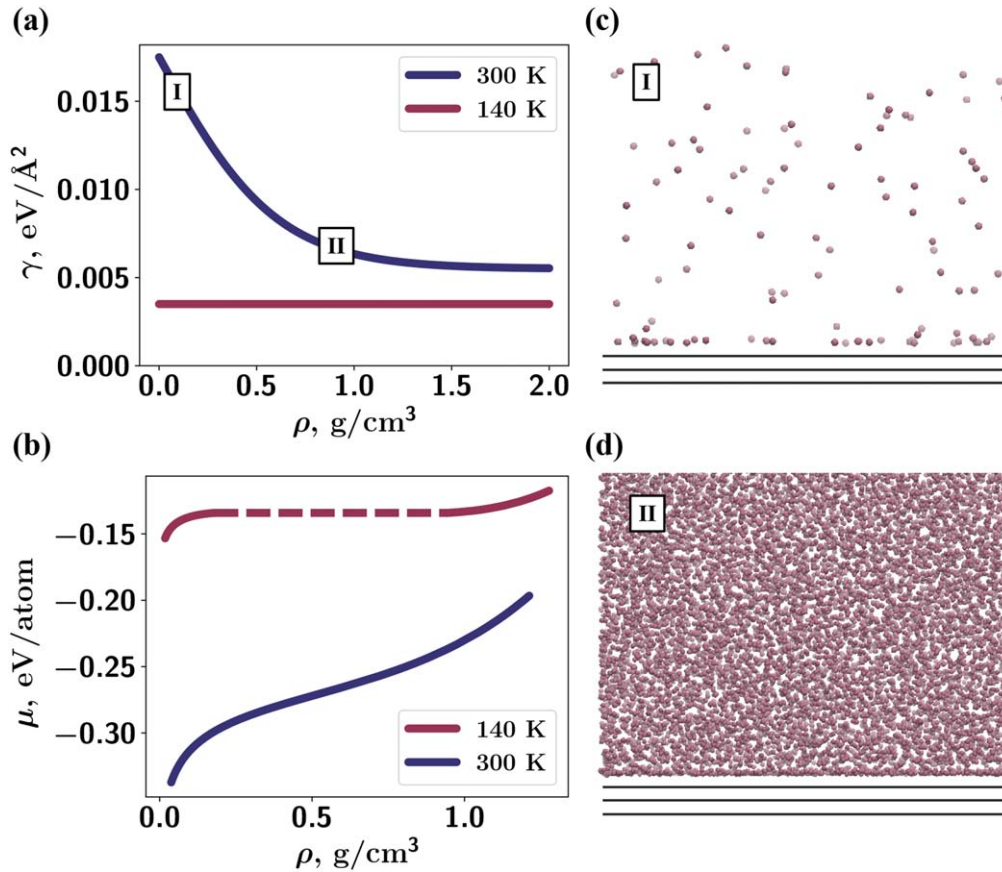


**Figure 3.** (a) Dependence of  $\gamma = \gamma_{GS} - \gamma_{GT} - \gamma_{ST}$  on the density of the substance at 140 and 300 K. Strong condensation results in a constant adhesion energy at 140 K. At 300 K, a larger density gives a stronger interaction of the substance and the substrate that yields a lower energy of the system. (b) Chemical potential at 140 and 300 K used in the proposed model [15]. (c)–(d) Atomistic calculation of the specific adhesion energy (snapshots of MD simulations at 300 K and different densities). Drawn with visual molecular dynamics [20].

200 nm. A similar phenomenon of a constant  $H/R$  ratio is experimentally observed in work [9], although the trapped material in that study is unknown, and only a qualitative comparison can be performed.

In contrast, ‘small’ GNBs at 300 K with radii less than 200 nm have  $H/R$  ratios that depend on the radius. The  $H/R$  ratio changes because the specific adhesion energy depends on the density of the trapped substance at 300 K. Figure 3(a) shows the dependence of the adhesion energy (equation (9)) obtained from atomistic simulations at both temperatures on argon density. At 140 K ‘strong’ argon condensation is observed, leading to a constant adhesion energy. Therefore, based on the numerical results, we can assume that a constant adhesion energy leads to a constant  $H/R$  ratio. This result is consistent with the analytic approach proposed in [9].

The developed model predicts the existence of a ‘forbidden region’ for argon at 140 K—a range of radii within which no stable GNBs can be found. The lower bound of the ‘forbidden region’ is 160 nm, and the obtained upper bound is 330 nm. The explanation for this effect is given by the dependence of the total energy on the bubble radius calculated during the ‘radius changing cycle’ (figure 4(b)). The  $E_{\text{total}}(R)$  function at some masses clearly has two local minima. The equilibrium GNB corresponds to the deeper minimum. There is a GNB mass that gives equally deep minima, and a small

increase or decrease in this mass changes the equilibrium radius discontinuously (abruptly). Hence, the existence of two local minima and the switch between them is the reason for the ‘forbidden region’.

The proposed model can be developed further if one replaces the bulk EOS of the trapped substance by the EOS of confined matter. This is important specifically for small GNBs where surface interactions begin to dominate volume interactions and the use of the bulk EOS is inappropriate. One example of such a surface effect is the premature crystallization of argon in GNBs that was observed in MD simulations [10]. However, the development of the EOS of confined matter and incorporation into the theory of GNBs is beyond the scope of this paper.

Experimental verification of proposed theoretical model could be done using different complementary techniques. With AFM measurements one could obtain statistics on GNBs sizes. In case of controllable temperature and known type of trapped substance one should observe ‘forbidden region’ of sizes and its shrinkage with increase of temperature. There is a number of experimental studies where AFM is successfully used to investigate shape of GN at different thermodynamic conditions [9, 19]. Another opportunity is to use XPEEM to get atoms arrangement of trapped substance from its electronic structure. For example, in [7] this experimental

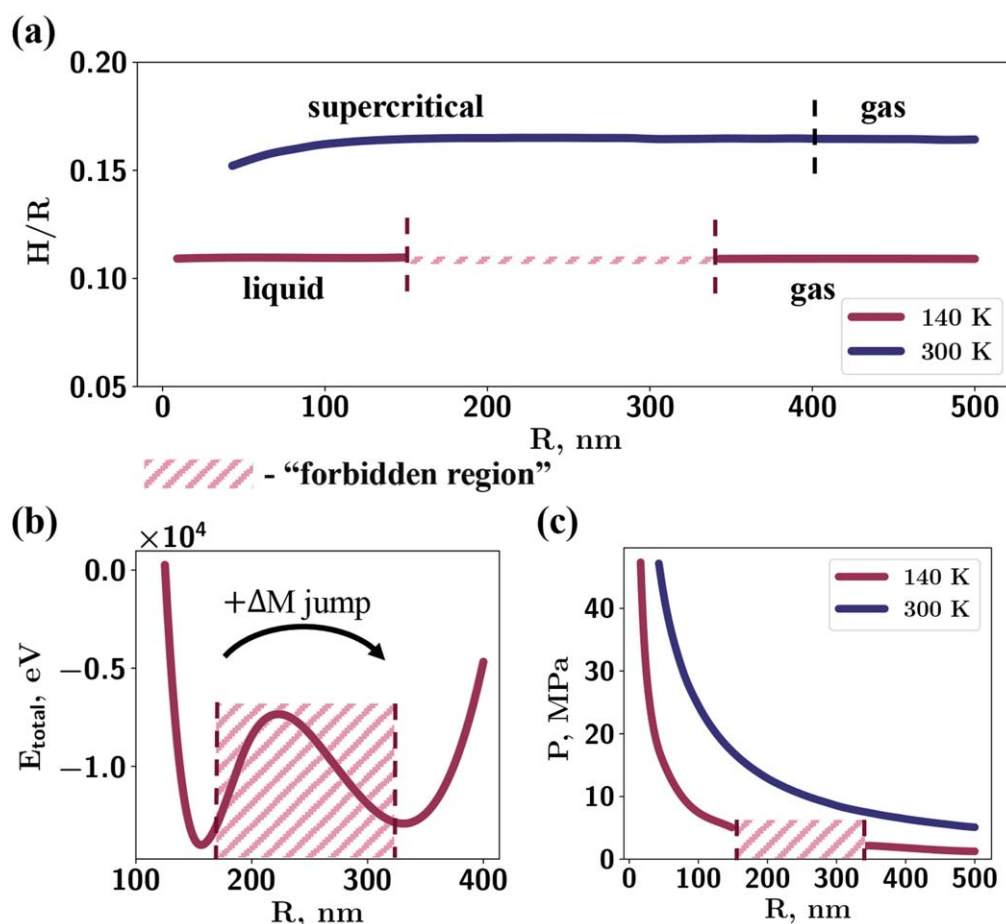


**Figure 4.** (a)  $H/R$  ratio dependence on the radius for two temperatures. A ‘forbidden region’ is found for the 140 K temperature, in which no stable GNBs are presented. This region separates the liquid and gas phases. (b) The total energy profile for a GNB with a fixed mass at 140 K. The global minimum in the ‘left’ well corresponds to the equilibrium GNB with radius 160 nm. The energy profile of a GNB with a slightly larger mass has a global minimum in the ‘right’ well. This phenomenon is the reason for the ‘forbidden region’. (c) Pressure inside a GNB at 140 and 300 K. The ‘forbidden region’ is shown in all figures.

technique allows to make a conclusion about crystal structure of argon atoms inside GNs. If trapped matter is a molecular system, Fourier-transform infrared spectroscopy could be applied to investigate condensation of trapped matter due to bond formation [5]. Therefore there is a number of experimental opportunities to verify proposed model of phase transition in GNs.

To conclude, we have presented a multiscale model to describe GNBs and, in particular, the liquid phase transition of the substance trapped inside them. The developed model combines both continuum and atomistic approaches. In the framework of the continuum approach, the elastic energy of the membrane and bulk energy of the trapped substance are calculated. MD simulations are used for evaluation of adhesion energies. The proposed model provides information on the shape of the bubble, stress distributions, pressure inside the bubble and, most importantly, physical state of the substance trapped inside. It also gives a connection between all the listed characteristics and the size of the bubble. In the case of argon as the trapped substance at 140 K, the model reveals the presence of a ‘forbidden region’, a range of radii within which stable GNBs cannot be found. This region appears to be a general feature of all GNBs regardless of the type of

trapped substance due to the presence of two local minima in the  $E_{\text{total}}(R)$  function of the bubble with a fixed mass.

## Acknowledgments

The research was carried out using supercomputers at Joint Supercomputer Center of the Russian Academy of Sciences (JSCC RAS). The Authors also acknowledge the usage of the Skoltech CDISE HPC cluster ARKUDA for obtaining the results presented in this paper.

## ORCID iDs

Evgeny Iakovlev  <https://orcid.org/0000-0003-0642-7315>

## References

- [1] Levy N, Burke S, Meaker K, Panlasigui M, Zettl A, Guinea F, Neto A C and Crommie M 2010 *Science* **329** 544–7

- [2] Qi Z, Kitt A L, Park H S, Pereira V M, Campbell D K and Neto A C 2014 *Phys. Rev. B* **90** 125419
- [3] Settnes M, Power S R, Brandbyge M and Jauho A P 2016 *Phys. Rev. Lett.* **117** 276801
- [4] Kim H W et al 2015 *Nat. Commun.* **6** 7528
- [5] Lim C H Y X, Sorkin A, Bao Q, Li A, Zhang K, Nesladek M and Loh K P 2013 *Nat. Commun.* **4** 1556
- [6] Mu R, Fu Q, Jin L, Yu L, Fang G, Tan D and Bao X 2012 *Angew. Chem., Int. Ed.* **51** 4856–9
- [7] Zamborlini G, Imam M, Patera L L, Menten T O, Stojić N, Africh C, Sala A, Binggeli N, Comelli G and Locatelli A 2015 *Nano Lett.* **15** 6162–9
- [8] Larciprete R, Colonna S, Ronci F, Flammini R, Lacovig P, Apostol N, Politano A, Feulner P, Menzel D and Lizzit S 2016 *Nano Lett.* **16** 1808–17
- [9] Khestanova E, Guinea F, Fumagalli L, Geim A and Grigorieva I 2016 *Nat. Commun.* **7** 12587
- [10] Iakovlev E, Zhilyaev P and Akhatov I 2017 *Sci. Rep.* **7** 17906
- [11] Koga K, Gao G, Tanaka H and Zeng X C 2001 *Nature* **412** 802
- [12] Algara-Siller G, Lehtinen O, Wang F, Nair R, Kaiser U, Wu H, Geim A and Grigorieva I 2015 *Nature* **519** 443
- [13] Landau L D and Lifshitz E M 1959 *Course of Theoretical Physics Vol 7: Theory and Elasticity* (Oxford: Pergamon)
- [14] Linstrom P J and Mallard W G 2001 *J. Chem. Eng. Data* **46** 1059–63
- [15] Tegeler C, Span R and Wagner W 1999 *J. Phys. Chem. Ref. Data* **28** 779–850
- [16] Plimpton S 1995 *J. Comput. Phys.* **117** 1–19
- [17] Stuart S J, Tutein A B and Harrison J A 2000 *J. Chem. Phys.* **112** 6472–86
- [18] Koenig S P, Boddeti N G, Dunn M L and Bunch J S 2011 *Nat. Nanotechnol.* **6** 543
- [19] Boddeti N G, Liu X, Long R, Xiao J, Bunch J S and Dunn M L 2013 *Nano Lett.* **13** 6216–21
- [20] Humphrey W, Dalke A and Schulten K 1996 *J. Mol. Graph.* **14** 33–8

# Supplementary materials

## 1. MD calculation of the specific adhesion energy between argon and graphite

In our molecular dynamics part of this research software package LAMMPS [1] (Large-scale Atomic/Molecular Massively Parallel Simulator) is used.

Lennard-Jones potential is used to evaluate the adhesion energy between argon and the graphite substrate. For argon–argon interaction the parameters are  $\sigma_{\text{Ar–Ar}} = 3.405 \text{ \AA}$ ,  $\epsilon_{\text{Ar–Ar}} = 10.34 \text{ meV}$  [2]. Lorentz–Berthelot combining rules [3] are used to define carbon–argon interaction:  $\sigma_{\text{C–Ar}} = 3.4025 \text{ \AA}$ ,  $\epsilon_{\text{C–Ar}} = 5.42 \text{ meV}$ . To apply these rules the carbon–carbon parameters are taken from Lennard-Jones part of AIREBO potential [4]:  $\sigma_{\text{C–C}} = 3.4 \text{ \AA}$ ,  $\epsilon_{\text{C–C}} = 2.84 \text{ meV}$ .

To calculate the adhesion energy we modeled three cases: argon–graphite system, only argon system, only graphite system. To evaluate the adhesion energy we measure the potential energy per unit area difference between combined graphite–argon system and separated systems. Thus the adhesion energy can be calculated as  $\gamma_{SB} = (U_{\text{graphite+argon}} - (U_{\text{graphite}} + U_{\text{argon}}))/S$ .

In graphite–argon system three graphene layers represent substrate. They are generated using VMD. The size of graphene layer is  $L_x = 100.698 \text{ \AA}$ ,  $L_y = 102.098 \text{ \AA}$ , where  $L_x, L_y$  are lengths in  $x$  and  $y$  directions. The  $z$ -length of the simulation box is  $L_z = 107 \text{ \AA}$ , the substrate fills  $6.7 \text{ \AA}$ , the remaining space is filled by argon. Initially the argon atoms are inserted into the simulation box in simple cubic lattice. Different initial densities are set to study pressure dependence of the adhesion energy. Then the argon atoms are allowed to move in the  $NVT$  ensemble. The temperature is set to 140 K and 300 K. The carbon atoms in graphite are fixed. After the energy of the system stabilizes, we assume that equilibrium is achieved, and statistical information can be gathered.

To simulate the argon system the separate calculations are performed. The number of argon atoms is the same as in corresponding case of the graphite–argon system. The size of the simulation box is  $L_x = 100.698 \text{ \AA}$ ,  $L_y = 102.098 \text{ \AA}$ ,  $L_z = 100 \text{ \AA}$ . Then argon atoms are allowed to move in the  $NVT$  ensemble. The temperature is set also to 140 K and 300 K.

## References

- [1] Plimpton S 1995 *J. Comput. Phys.* **117** 1–19
- [2] Jain S K, Pikunic J P, Pellenq R J M and Gubbins K E 2005 *Adsorption* **11** 355–360
- [3] Hudson G and McCoubrey J 1960 *Trans. Faraday Soc.* **56** 761–766
- [4] Stuart S J, Tutein A B and Harrison J A 2000 *J. Chem. Phys.* **112** 6472–6486

## 3.5 Continuum approach: ethane case

In this chapter, we use the model developed in the previous section and applies it to the nanobubbles with trapped ethane at near room temperature. We decided to perform this calculation since hydrocarbons are used in the process of the experiments of creating 2D heterostructures. So it is likely that some hydrocarbon mixture appears to be trapped in the bubble. Thus the more realistic system is studied. The "forbidden region" below critical temperature is observed, which separates two different phases: liquid and gas.

### 3.5.1 Contribution

My contribution to this work: took part in model development, carried out all MD calculations and implemented continuum model in Python, took part in results discussion, and writing the manuscript.



Cite this: *Phys. Chem. Chem. Phys.*,  
2019, 21, 18099

## Modeling of the phase transition inside graphene nanobubbles filled with ethane

Evgeny Iakovlev,<sup>1</sup> Petr Zhilyaev<sup>2</sup> and Iskander Akhatov<sup>3</sup>

Graphene nanobubbles consist of a substance that is trapped between graphene sheets and atomically flat substrates. This substance is an example of confinement in which both the bulk and surface interactions and the tension of the graphene determine the mechanical and thermodynamic properties of the system. The van der Waals pressure build up due to the graphene–substrate attraction and surface influence facilitates the advanced condensation of trapped substances. Different phases of the trapped substance are assumed to be found inside the graphene nanobubbles depending on their radii. Smaller radii are attributed to the crystal and liquid phases, and larger radii correspond to the gas phase. In this study, graphene nanobubbles filled with ethane on a graphite substrate are investigated. The choice of trapped substance is inspired by typical experiments in which graphene nanobubbles are obtained with a mixture of hydrocarbons inside. We apply a multiscale model based on both molecular dynamics simulations and a continuum 1D model to obtain the shape of the bubble, stress distribution and phase state of the trapped substance. Calculations are performed for a set of temperatures below and above the critical temperature of ethane. A liquid–gas phase transition below the critical temperature leads to a ‘forbidden range’ of radii, in which no stable bubbles exist.

Received 19th June 2019,  
Accepted 31st July 2019

DOI: 10.1039/c9cp03461g

rsc.li/pccp

### 1 Introduction

Graphene nanobubbles (GNBs) are a system consisting of a substrate, a graphene layer placed on top of the substrate and a substance trapped between them (see Fig. 1). Initially, these nanobubbles were treated as undesirable defects during the process of van der Waals (vdW) heterostructure manufacturing (stacking together 2D crystals). However, after a more detailed investigation, many GNBs with interesting and unique features have been discovered. The strained sheet of the outer graphene layer in GNBs is shown to generate a large pseudo-magnetic field.<sup>1,2</sup> GNBs can be used to visualize reactions of CO on Pt catalysts.<sup>3</sup> Confining water in GNBs on a diamond substrate drastically changes its dielectric constant, which results in the etching of a hard surface.<sup>4</sup> In addition, GNBs are places of intense photoluminescence emission due to strained-induced changes in the band structure.<sup>5</sup>

Although GNBs are not currently used in industrial applications, there are many potential opportunities. For example, the ability to capture a large amount of hydrocarbons inside GNBs makes it possible to use them for novel gas storage technologies. Also curved graphene changes how light is refracted through nanobubbles and creates different colors.<sup>6</sup> These ‘mechanical pixels’ can be used in

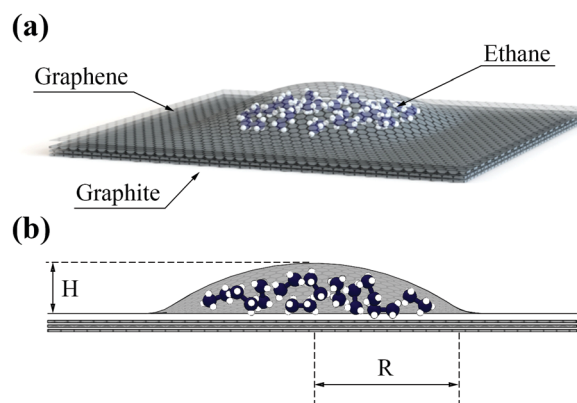


Fig. 1 (a) Schematic representation of a graphene nanobubble (GNB). (b) Meridional slice of a GNB. The height ( $H$ ) of a GNB is the distance between the top point of the bubble and the surface of the undisturbed graphene sheet.

flexible, durable and energy efficient displays. Moreover, deformations caused by GNBs alter the local electronic structure. This property could have many applications in strain- and valleytronics devices.<sup>7</sup>

Little is known about the type of trapped substances inside GNBs. There have been only a few studies<sup>8,9</sup> in which the type of trapped substance is controlled by direct ion implantation. However, in these studies, only small bubbles are obtained with radii on the order of nanometers. When GNBs are spontaneously

Center for Design, Manufacturing and Materials, Skolkovo Institute of Science and Technology, Skolkovo Innovation Center, Building 3, Moscow, 143026, Russia.  
E-mail: Evgeny.Iakovlev@skolkovotech.ru

formed during vdW heterostructure production, the type of trapped substance is still uncertain. Another study<sup>10</sup> advocates a mixture of hydrocarbons to be inside the GNBs. Other researchers<sup>11</sup> believe that water is the trapped substance with a small amount of hydrocarbon contaminants. These investigators confirm their assumptions that bubble formation is strongly dependent on temperature (particularly beyond 100 °C) and humidity.<sup>12</sup>

The next important question arises when considering the phase state of matter in GNBs. Previously, it was universally assumed that GNBs are filled with gas.<sup>13–16</sup> However, mechanical models based on this assumption result in small adhesion values for the graphene interfaces compared with the experimental data.<sup>13</sup> On the other hand, atomic force microscopy (AFM) measurements and further theoretical considerations predict that the substance inside GNBs (radii in the range from 100–1000 nm) on a graphite substrate is in the liquid phase.<sup>10,11</sup> Trapped substances in GNBs with small radii (on the order of 1 nm) on metal substrates are known to exist in the form of structural clusters.<sup>8,9</sup> The type of trapped substance in these studies is controlled by the irradiation of a graphene membrane with argon ions, and an explicit investigation of the inner phase is performed.

Theoretical studies have also shown that both solid and liquid phases could be found inside GNBs. Molecular dynamics (MD) simulations also predict the condensation of trapped matter. For example, in an MD study,<sup>17</sup> solid-state argon was observed in GNBs (radii less than 30 nm) on a graphite substrate. In other MD research,<sup>18</sup> helium, water and ethanol were considered trapped substances, and all of them were found to be in a liquid state at room temperature.

Although there are experimental observations indicating that different condensation phases exist inside GNBs depending on their radii, there is a demand for theoretical models that consider the phase state of the trapped substance. Furthermore, different types of phases (gas, liquid and solid) can be found in various experiments. Obviously, one can assume that the transition between phases can occur, either with a temperature change (*e.g.*, in particular, in bubbles filled with liquid, as the temperature increases, the trapped substance can become a gas) or with a radius change (*e.g.*, in the assembly of bubbles, one can find small bubbles filled with liquid and larger bubbles filled with gas). However, no experiments have consistently studied the phase transition of trapped substances inside GNBs. Additionally, there is no theoretical description of this phenomenon to promote and guide further experiments. Only recently, the authors have proposed a model that considers the presence of phase transitions.<sup>19</sup>

In this paper, we apply a previously developed approach<sup>19</sup> to study the mechanical properties, shape and phase state of GNBs filled with ethane on a graphite substrate. The basic approach involves the minimization of the energy of the whole system, namely, the elastic energy of graphene stretching, the adhesion energy between the substrate, graphene and ethane and the bulk energy of ethane. Specific adhesion energies are calculated using MD simulations. A set of temperatures in the range 260–320 K is considered, which includes the critical point

of ethane  $T_c = 305$  K. The radii of the obtained GNBs are found in the range 50–600 nm. Liquid and gas phases of ethane are observed for selected ranges of temperatures and radii. Temperatures less than  $T_c$  result in a ‘forbidden region’, where no energetically stable GNBs exist.

## 2 Methods

In the applied model, all computed mechanical and thermodynamic properties of the GNBs are obtained as a result of the total energy minimization of the system:

$$E_{\text{total}} = E_{\text{elastic}} + E_{\text{bulk}} + E_{\text{adhesion}}, \quad (1)$$

where  $E_{\text{elastic}}$  is the elastic energy of the graphene sheet,  $E_{\text{bulk}}$  is the energy of the trapped substance, and  $E_{\text{adhesion}}$  is the energy that includes the surface interaction among the substrate, the graphene sheet and the trapped substance.

The elastic energy  $E_{\text{elastic}}$  of the graphene sheet is calculated by means of elasticity theory.<sup>20</sup> The bulk energy of ethane  $E_{\text{bulk}}$  is obtained by integrating the chemical potential as a function of the density while keeping the volume of the system fixed. The adhesion energy  $E_{\text{adhesion}}$  can be represented as the specific adhesion energies multiplied by the corresponding surface areas. For more details of the applied model, please see ref. 19.

In this work, the MD method<sup>21,22</sup> is used to verify the mechanical properties of graphene sheets and calculate the adhesion energy between the ethane and graphite substrates. All presented MD simulations are performed using the large-scale atomic/molecular massively parallel simulator (LAMMPS) software package.<sup>23</sup>

To calculate the elastic energy of the graphene sheet, two parameters are needed: the Young's modulus and Poisson's ratio. The Poisson's ratio of the graphene sheet is assumed to be zero. To verify the Young's modulus, the adaptive intermolecular reactive empirical bond order (AIREBO) potential is used,<sup>24</sup> which is known to describe the properties of carbon structures.<sup>25</sup> In this work, the calculated Young's modulus is equal to 21.12 eV Å<sup>-2</sup> (1.01 TPa), which is in agreement with other simulation<sup>26</sup> and experimental data.

The MD approach provides a general framework to evaluate specific adhesion energies, reveals the elemental stages of the adsorption mechanisms, takes into account surface structure reconstruction and allows the introduction of surface defects.<sup>27–30</sup> The specific adhesion energy between graphene and graphite is calculated using the AIREBO potential. The adhesion energy is found to be equal to 0.017 eV Å<sup>-2</sup>, which is the typical adhesion energy of graphene membranes.<sup>31</sup>

The specific adhesion energy between ethane and graphene at given temperatures and densities is obtained using the ethane transferable potentials for phase equilibria (TraPPE) potential.<sup>32</sup> This potential is more computationally efficient than the AIREBO potential, and it is known to describe the thermodynamic properties with a high level of accuracy.<sup>33</sup> TraPPE exploits a united atom approach, *i.e.*, CH<sub>3</sub> is considered as one particle. Carbon–carbon interactions are described by

**Table 1** Lennard-Jones potential parameters used in this work. The cut-off radius  $r_{\text{cut}}$  for all cases in this study is 14 Å

LJ parameter	CH <sub>3</sub> -CH <sub>3</sub>	C-CH <sub>3</sub>	C-C
$\sigma$ , Å	3.750	3.575	3.400
$\epsilon$ , meV	8.450	4.900	2.840

the Lennard-Jones (LJ) potential, a parameter taken from the LJ part of the AIREBO potential. The Lorentz–Berthelot combining rules<sup>34</sup> are applied to obtain the carbon-CH<sub>3</sub> parameters. A summary of all potential parameters used for calculating the specific adhesion energy between ethane and graphene is presented in Table 1. In the MD simulations graphite is represented by 3 graphene layers. All MD calculations are performed in the *NVT* ensemble.

To evaluate the ethane bulk energy, NIST data<sup>35,36</sup> with respect to the chemical potential and equation of state (EOS) are used.

The total energy is a function of the radial displacement  $u(r)$  in the outer graphene sheet and the height profile  $h(r)$  of the GNB. The minimization of the total energy is performed for a GNB with a particular mass. We vary the radius of the GNB, and for each particular radius, the total energy is evaluated. Comparing GNBs with equal mass and different radii, we find the GNB with the lowest energy and assume that this is the equilibrium case. When minimizing the GNB at a particular radius, self-consistency with the ethane EOS is achieved, *i.e.*, the pressure produced by the graphene sheets should be equal to the bulk pressure from the EOS if the density and temperature are known.

The radial displacement and height profiles are determined at specific radii and pressures by minimizing the elastic energy. The computational domain is divided into two parts: (i) from zero to the radius and (ii) from the radius to infinity (see Fig. 2). In the first part of the computational domain, numerical minimization is performed, and functions  $u(r)$  and  $h(r)$  are represented on the basis of Chebyshev's polynomials of the first kind. In the second part, *i.e.*,  $h(r) = 0$ , it is possible to obtain an analytical solution of  $u(r)$ , which is  $u(r) = (R/r)u(R)$ . The algorithm presented above is implemented in Python code and is available online.<sup>37</sup>

### 3 Results and discussion

All material parameters used in the model of the GNBs are obtained from elsewhere, except for the specific surface energy between ethane and graphene. This value and its dependence on the density and temperature are calculated by the MD method at 260, 280, 310 and 330 K (see Fig. 3a). At low densities ( $\rho \lesssim 0.05 \text{ g cm}^{-3}$ ) in the gas phase for all temperatures, the specific adhesion energy linearly increases. In the region of intermediate densities ( $0.05 \lesssim \rho \lesssim 0.5 \text{ g cm}^{-3}$ ) that corresponds to the mixed gas-liquid phase (260, 280 K) or supercritical fluid (310, 330 K), a fluctuation of the specific adhesion energy is observed. These fluctuations result from multilayer absorption. Each completed layer of adsorbed molecules

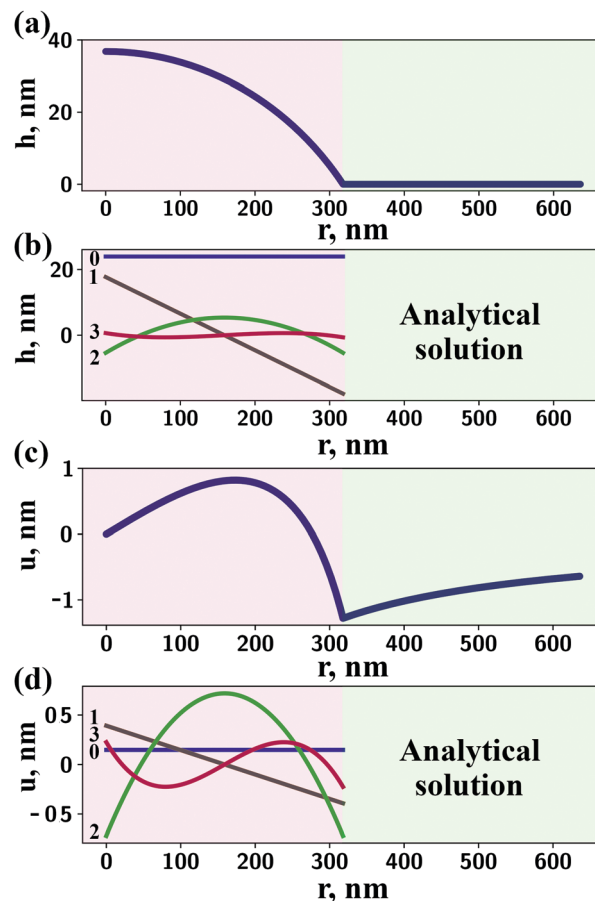


**Fig. 2** (a) Calculated height profile for a GNB with  $R = 31.8 \text{ nm}$ ; (b) left side – representation of the first 4 members of Chebyshev's polynomial decomposition for  $h(r)$  (in this work, the total number of members is 20), right side – trivial analytical solution  $h(r) = 0$ ; (c) radial displacement in the graphene sheet for the same bubble; (d) left side – representation of the first 4 members of Chebyshev's polynomial decomposition for  $u(r)$ , right side – analytical solution  $u(r) = (R/r)u(R)$ .

provides an increase in the specific surface energy. A successive increase in density for an incomplete layer does not necessarily lead to better adhesion to the substrate due to bulk attraction. At high densities ( $\rho \gtrsim 0.5 \text{ g cm}^{-3}$ ), when several adsorption layers are formed, the influence of the bulk is negligible, and the specific surface energy becomes constant.

In the applied model, we use a simplified approximation for the dependence of the specific surface energy on density, which does not take into account the fluctuation described above. This model is fitted by a hyperbolic tangent using MD simulation results (see Fig. 3b).

The typical height profile  $h(r)$  of the GNB obtained by the model is presented in Fig. 2a. All the obtained height profiles match each other in dimensionless coordinates ( $r/R$ ,  $h/H$ ), where  $R$  is the radius of the GNB and  $H$  is its height. These data are in agreement with analytical results from membrane elastic theory.<sup>10</sup> The typical radial displacement profile  $u(r)$  is also shown in Fig. 2c.

If  $h(r)$  and  $u(r)$  are known, then the algorithm allows the calculation of the radial  $\sigma_{rr}$  and angular stress  $\sigma_{\theta\theta}$  distributions

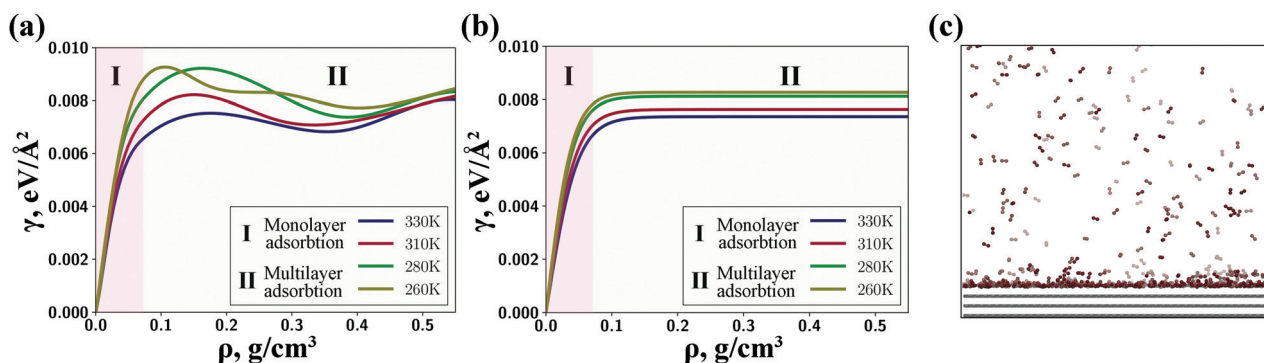


Fig. 3 (a) The dependence of the adhesion energy between ethane and the graphite substrate on the density for each temperature calculated by MD. Two regions are highlighted: region I corresponds to the linear growth of monolayer adsorption and in region II the adhesion energy stabilizes due to multilayer adsorption. (b) Adhesion energy curve used in the model. Hyperbolic tangent approximation  $A \tanh(B\rho)$  is used to fit the data. (c) Snapshot of the MD calculation of the adhesion energy between graphene and ethane at  $T = 280$  K and  $\rho = 0.05$  g cm<sup>-3</sup>. Drawn with visual molecular dynamics software.<sup>58</sup>

in the membrane of the GNB (see Fig. 4b). An additional check of the numerical model is to reproduce the pressure from  $\sigma_{rr}$  and  $\sigma_{\theta\theta}$  at each point of the membrane. Due to the equilibrium condition:

$$P = \frac{\sigma_{rr}}{r_r} + \frac{\sigma_{\theta\theta}}{r_\theta} \quad (2)$$

where  $r_r$  and  $r_\theta$  represent the principal radii of curvature at a particular point. The results of the proposed check are presented in Fig. 4c. There is good agreement between the initial fixed pressure inside the GNB and the pressure obtained from eqn (2).

The  $H/R$  ratio is a geometrical characteristic of a GNB that can be measured experimentally and shows how “flat” the bubble is. The  $H/R$  ratio dependence on temperature for the equilibrium GNB is presented in Fig. 5a. We observe a general trend in which the  $H/R$  ratio increases with temperature growth. For temperatures 260, 280, and 310 K, the  $H/R$  ratio curves exhibit a discontinuity due to the ‘forbidden region’ of the radii with no equilibrium GNBs inside.

The ‘forbidden region’ formation is explained by the existence of two local minima in the isomass energy curve  $E_M(R)$  for certain masses and temperatures (Fig. 5b). Away from the

‘forbidden region’ border, one local minimum in  $E_M(R)$  is usually observed. In the case of two local minima, one of them is also the global minimum. At a particular mass a switch of the global minimum to another local minimum occurs and hence the equilibrium radius of the GNB changes discontinuously. The width of the ‘forbidden region’ decreases with increasing temperature and completely disappears at temperatures slightly higher than the critical temperature of ethane (305 K).

The  $H/R$  ratio curves for temperatures of 330 and 310 K are located above the critical point (see Fig. 5a). Hence, the trapped substance inside the corresponding GNBs is in the supercritical or gas phase. For temperatures of 260 and 280 K, the ‘forbidden region’ separates the  $H/R$  ratio curves into left and right branches. The equilibrium GNBs located on the left branch are filled with the liquid phase of ethane. In this part of the curve, the  $H/R$  ratio is constant due to the small compressibility of the liquid phase. These results are in agreement with the analytical model, which also predicts an incompressible fluid inside the bubble provided that the  $H/R$  ratio is constant.<sup>10,39</sup> Equilibrium GNBs located on the right branch are filled with a mixture of gas and liquid phases, *i.e.* the bubbles are not large enough to transfer all of the trapped substance to the gas phase.

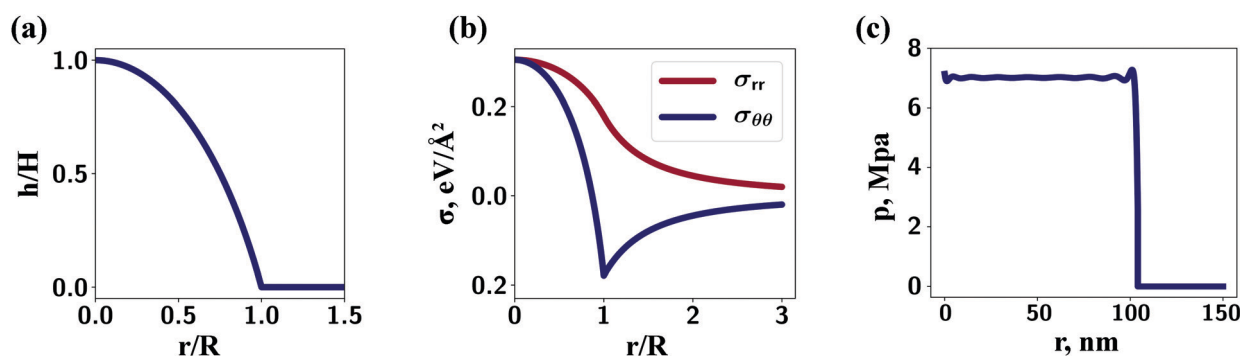


Fig. 4 (a) Height profile of a GNB in dimensionless coordinates. The profiles coincide for all bubbles. (b) Radial and angular stress profiles with a dimensionless  $x$  axis. (c) Pressure profile along the GNB's radius generated by the graphene membrane as a solution of the elastic problem. Calculated from eqn (2).

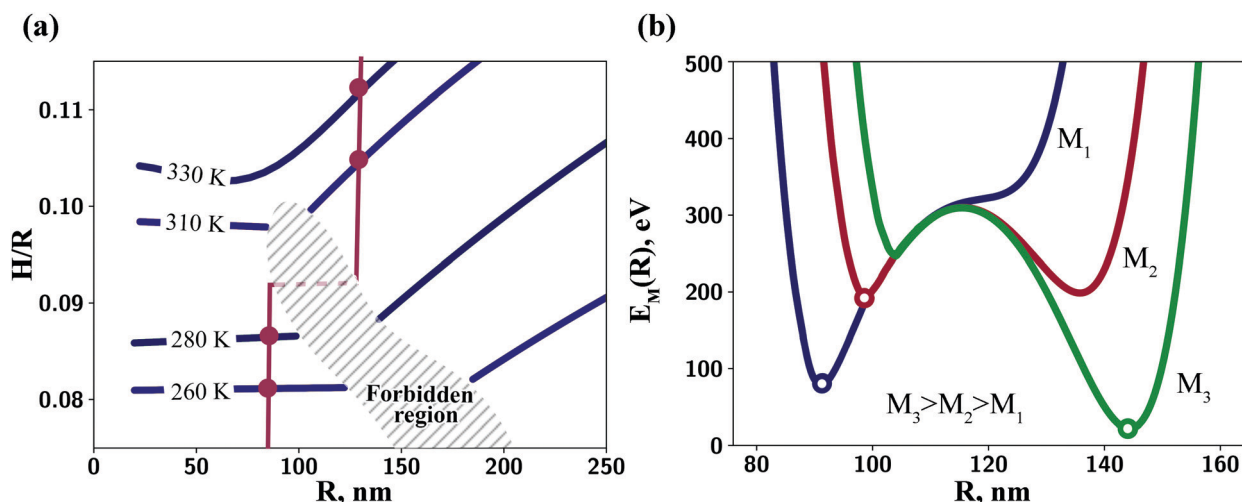


Fig. 5 (a) Calculated  $H/R$  ratio at 260, 280, 310 and 330 K. The 'forbidden region' width decreases with temperature growth. The red line with dots represents the hypothetical evolution of the bubble with a fixed mass of trapped ethane. The equilibrium GNB radius changes abruptly, then the bubble reaches the 'forbidden region'. (b) Energy profiles for GNBs with 3 different masses. When the mass increases, the equilibrium radius (marked with a circle) shifts to the right. Thus, bubbles with masses  $M_1$  and  $M_2$  have a minimum in the left well, and bubbles with mass  $M_3$  have a minimum in the right well. This shift from the left well to the right well causes the 'forbidden region'.

The calculated  $H/R$  ratio curve can be used to observe the path of the hypothetical heating of one bubble with a fixed mass. One can monitor the evolution of its form and migration from the left to the right branch during the temperature increase (red line in Fig. 5a). If the bubble is initially situated at the edge of the left branch, a small increase in temperature results in a discontinuous jump in the radius. This result of the proposed model could be used in an experimental setup in which an ensemble of GNBs is heated and their radii are monitored. Some of the GNBs that are located near the 'forbidden region' will have jumps in their radius-temperature dependence.

Additionally, one can investigate ensembles of GNBs statically without heating of the sample. If enough bubbles for good statistics are observed and the temperature is below  $T_c$ , then the proposed model predicts two effects: (1) an interval of radii where no bubbles are detected (the 'forbidden region'), where (2) bubbles with radii less than the left boundary of the 'forbidden region' have a constant  $H/R$  ratio, and bubbles with radii above the right boundary have an increasing  $H/R$  ratio.

## 4 Conclusion

In this work, a multiscale model is used to investigate GNBs with ethane inside. Ethane is chosen because hydrocarbons are substances that are typically trapped in most experiments. The main focus is to observe and study the liquid-gas phase transition of the trapped substances. The morphology and mechanical and thermodynamic properties of GNBs with ethane are obtained from the proposed model. GNBs at temperatures of 260, 280, 310, and 330 K and for radii up to 250 nm were studied.

For temperatures below the approximate critical point of ethane (305 K), a 'forbidden region' of radii with no stable GNBs emerges, and its width grows as the temperature decreases. We assume that this decrease is a general phenomenon for all

GNBs regardless of the type of trapped substance because of the existence of two local minima in the  $E_M(R)$  function of a bubble with a fixed mass.

We expect that for hydrocarbons of a higher molecular weight and a higher critical point, the 'forbidden region' must be wider at room temperature. Therefore, the effect of the 'forbidden region' should be more pronounced in typical experiments in which hydrocarbons of higher molecular weight are assumed to be trapped.

The considered problem is closely connected to phase transitions in confined systems, such as thin films, pores, and nanochannels.<sup>40</sup> In these systems, the effects of disjoining pressure,<sup>41</sup> orientational ordering,<sup>42</sup> electronic screening,<sup>43</sup> and surface roughness<sup>44–46</sup> can lead to a distortion of the phase diagram. The effect of condensation and "exotic" structuring is also observed in nanoscale systems, such as nanotubes, graphene cells and slit nanopores. For example, water, benzene and cyclohexane molecules inside graphene nanotubes and carbon slit nanopores exhibit various structured forms.<sup>47–49</sup> Additionally, water trapped between two graphene sheets exists in the previously unknown 'square ice' solid phase.<sup>50</sup> The considered example of a phase transition in confinement differs from that described above because the walls are not rigid and can deform and change their shape due to the inner pressure of the trapped substance. Taking into account the changing shape of the walls, it is possible to look from a different perspective on the problem of phase transitions in confinement systems and even predict new previously unknown physical phenomena such as the 'forbidden region'.

## Conflicts of interest

There are no conflicts to declare.

## Acknowledgements

The research was carried out using supercomputers at the Joint Supercomputer Center of the Russian Academy of Sciences (JSCC RAS). The authors also acknowledge the usage of the Skoltech CDISE HPC cluster ARKUDA for obtaining the results presented in this paper.

## References

- N. Levy, S. Burke, K. Meaker, M. Panlasigui, A. Zettl, F. Guinea, A. C. Neto and M. Crommie, *Science*, 2010, **329**, 544–547.
- Z. Qi, A. L. Kitt, H. S. Park, V. M. Pereira, D. K. Campbell and A. C. Neto, *Phys. Rev. B: Condens. Matter Mater. Phys.*, 2014, **90**, 125419.
- R. Mu, Q. Fu, L. Jin, L. Yu, G. Fang, D. Tan and X. Bao, *Angew. Chem., Int. Ed.*, 2012, **51**, 4856–4859.
- C. H. Y. X. Lim, A. Sorokin, Q. Bao, A. Li, K. Zhang, M. Nesladek and K. P. Loh, *Nat. Commun.*, 2013, **4**, 1556.
- A. V. Tyurnina, D. A. Bandurin, E. Khestanova, V. G. Kravets, M. Koperski, F. Guinea, A. N. Grigorenko, A. K. Geim and I. V. Grigorieva, *ACS Photonics*, 2019, **6**(2), 516–524.
- S. J. Cartamil-Bueno, P. G. Steeneken, A. Centeno, A. Zurutuza, H. S. van der Zant and S. Hourri, *Nano Lett.*, 2016, **16**, 6792–6796.
- T. Low and F. Guinea, *Nano Lett.*, 2010, **10**, 3551–3554.
- G. Zamborlini, M. Imam, L. L. Patera, T. O. Mentes, N. Stojic, C. Africh, A. Sala, N. Binggeli, G. Comelli and A. Locatelli, *Nano Lett.*, 2015, **15**, 6162–6169.
- R. Larciprete, S. Colonna, F. Ronci, R. Flammini, P. Lacovig, N. Apostol, A. Politano, P. Feulner, D. Menzel and S. Lizzit, *Nano Lett.*, 2016, **16**, 1808–1817.
- E. Khestanova, F. Guinea, L. Fumagalli, A. Geim and I. Grigorieva, *Nat. Commun.*, 2016, **7**, 12587.
- D. A. Sanchez, Z. Dai, P. Wang, A. Cantu-Chavez, C. J. Brennan, R. Huang and N. Lu, *Proc. Natl. Acad. Sci. U. S. A.*, 2018, **115**, 7884–7889.
- F. Pizzocchero, L. Gammelgaard, B. S. Jessen, J. M. Caridad, L. Wang, J. Hone, P. Bøggild and T. J. Booth, *Nat. Commun.*, 2016, **7**, 11894.
- P. Bampoulis, V. J. Teernstra, D. Lohse, H. J. Zandvliet and B. Poelsema, *J. Phys. Chem. C*, 2016, **120**, 27079–27084.
- K. Yue, W. Gao, R. Huang and K. M. Liechti, *J. Appl. Phys.*, 2012, **112**, 083512.
- H. An, B. H. Tan, J. G. S. Moo, S. Liu, M. Pumera and C.-D. Ohl, *Nano Lett.*, 2017, **17**, 2833–2838.
- A. Falin, Q. Cai, E. J. Santos, D. Scullion, D. Qian, R. Zhang, Z. Yang, S. Huang, K. Watanabe and T. Taniguchi, *et al.*, *Nat. Commun.*, 2017, **8**, 15815.
- E. Iakovlev, P. Zhilyaev and I. Akhatov, *Sci. Rep.*, 2017, **7**, 17906.
- H. Ghorbanfekr-Kalashami, K. Vasu, R. Nair, F. M. Peeters and M. Neek-Amal, *Nat. Commun.*, 2017, **8**, 15844.
- P. Zhilyaev, E. Iakovlev and I. Akhatov, *Nanotechnology*, 2019, **30**(21), 215701.
- L. D. Landau and E. M. Lifshitz, *Course of Theoretical Physics Vol. 7: Theory and Elasticity*, Pergamon Press, 1959.
- D. Frenkel and B. Smit, *Understanding molecular simulation: from algorithms to applications*, Elsevier, 2001, vol. 1.
- A. Y. Kuksin, I. Morozov, G. Norman, V. Stegailov and I. Valuev, *Mol. Simul.*, 2005, **31**, 1005–1017.
- S. Plimpton, *J. Comput. Phys.*, 1995, **117**, 1–19.
- S. J. Stuart, A. B. Tutein and J. A. Harrison, *J. Chem. Phys.*, 2000, **112**, 6472–6486.
- N. Orekhov and V. Stegailov, *Carbon*, 2015, **87**, 358–364.
- H. Zhao, K. Min and N. Aluru, *Nano Lett.*, 2009, **9**, 3012–3015.
- S. H. Ganjiani and A. H. Nezhad, *Phys. Chem. Chem. Phys.*, 2018, **20**, 5140–5148.
- J. A. Greathouse and R. T. Cygan, *Phys. Chem. Chem. Phys.*, 2005, **7**, 3580–3586.
- A. Tsukanov and S. Psakhie, *Phys. Mesomech.*, 2017, **20**, 43–54.
- A. Tsukanov and S. Psakhie, *Facta Univ., Ser. Mech. Eng.*, 2016, **14**, 269–280.
- S. P. Koenig, N. G. Boddetti, M. L. Dunn and J. S. Bunch, *Nat. Nanotechnol.*, 2011, **6**, 543.
- M. G. Martin and J. I. Siepmann, *J. Phys. Chem. B*, 1998, **102**, 2569–2577.
- N. D. Kondratyuk, G. E. Norman and V. V. Stegailov, *J. Chem. Phys.*, 2016, **145**, 204504.
- G. Hudson and J. McCoubrey, *Trans. Faraday Soc.*, 1960, **56**, 761–766.
- D. G. Friend, H. Ingham and J. F. Fly, *J. Phys. Chem. Ref. Data*, 1991, **20**, 275–347.
- P. J. Linstrom and W. G. Mallard, *J. Chem. Eng. Data*, 2001, **46**(5), 1059–1063.
- <https://github.com/evyak/nanobubbles>.
- W. Humphrey, A. Dalke and K. Schulten, *J. Mol. Graphics*, 1996, **14**, 33–38.
- E. Iakovlev, P. Zhilyaev and I. S. Akhatov, *J. Phys.: Conf. Ser.*, 2019, 012006.
- P. Huber, *J. Phys.: Condens. Matter*, 2015, **27**, 103102.
- B. V. Derjaguin, N. V. Churaev, V. M. Muller and V. Kisin, *Surface forces*, Springer, 1987.
- L. Harnau and S. Dietrich, *Phys. Rev. E: Stat., Nonlinear, Soft Matter Phys.*, 2002, **65**, 021505.
- J. Comtet, A. Niguès, V. Kaiser, B. Coasne, L. Bocquet and A. Siria, *Nat. Mater.*, 2017, **16**, 634.
- K. A. Terrón-Meja, R. López-Rendón and A. G. Goicochea, *Phys. Chem. Chem. Phys.*, 2015, **17**, 26403–26416.
- T. Aslyamov and A. Khlyupin, *J. Chem. Phys.*, 2017, **147**, 154703.
- T. Aslyamov, V. Pletneva and A. Khlyupin, *J. Chem. Phys.*, 2019, **150**, 054703.
- K. Koga, G. Gao, H. Tanaka and X. C. Zeng, *Nature*, 2001, **412**, 802.
- Y. D. Fomin, E. N. Tsiok and V. N. Ryzhov, *J. Comput. Chem.*, 2015, **36**, 901–906.
- Y. D. Fomin, V. Ryzhov and E. Tsiok, *J. Chem. Phys.*, 2015, **143**, 184702.
- G. Algara-Siller, O. Lehtinen, F. Wang, R. Nair, U. Kaiser, H. Wu, A. Geim and I. Grigorieva, *Nature*, 2015, **519**, 443.

## 3.6 Continuum approach: DFT implementation

Finally, the previous model is improved by including into consideration the inhomogeneity of the trapped fluid. This is a step to the model, which is capable of describing any type of the captured substance. This approach is implemented using classical density functional theory (c-DFT). Using the new model, we can derive profiles of the bubble, mechanical and thermodynamical properties and the density distribution of the matter inside. In this chapter, we analyze the results of the calculations with the new model. As a result, the same universal shape scaling rule is approved. Also, we find that the excess density becomes negative for nanobubbles with a radius less than 50 nm that can be attributed to the onset of the liquid-solid phase transition.

### 3.6.1 Contribution

My contribution to this work: carried out calculations of the bubbles profiles with respect to pressure and data analysis, took part in results discussion, and writing the manuscript.

# Model of graphene nanobubble: Combining classical density functional and elasticity theories

Cite as: J. Chem. Phys. 152, 054705 (2020); doi: 10.1063/1.5138687

Submitted: 15 November 2019 • Accepted: 14 January 2020 •

Published Online: 3 February 2020



T. F. Aslyamov,  E. S. Iakovlev,  I. Sh. Akhatov,  and P. A. Zhilyaev<sup>a)</sup> 

## AFFILIATIONS

Center for Design, Manufacturing and Materials, Skolkovo Institute of Science and Technology, Bolshoy Boulevard 30, bld. 1, Moscow 121205, Russia

<sup>a)</sup> Author to whom correspondence should be addressed: [p.zhilyaev@skoltech.ru](mailto:p.zhilyaev@skoltech.ru)

## ABSTRACT

A graphene nanobubble consists of a graphene sheet, an atomically flat substrate, and a substance enclosed between them. Unlike conventional confinement with rigid walls and a fixed volume, the graphene nanobubble has one stretchable wall, which is the graphene sheet, and its volume can be adjusted by changing the shape. In this study, we developed a model of a graphene nanobubble based on classical density functional theory and the elastic theory of membranes. The proposed model takes into account the inhomogeneity of the enclosed substance, the nonrigidity of the wall, and the alternating volume. As an example application, we utilize the developed model to investigate fluid argon inside graphene nanobubbles at room temperature. We observed a constant height-to-radius ratio over the whole range of radii considered, which is in agreement with the results from experiments and molecular dynamics simulations. The developed model provides a theoretical tool to study both the inner structure of the confined substance and the shape of the graphene nanobubble. The model can be easily extended to other types of nonrigid confinement.

Published under license by AIP Publishing. <https://doi.org/10.1063/1.5138687>

## I. INTRODUCTION

There is much evidence of the occurrence of exotic metamorphoses of trapped substances under nanoscopic confinement: square ice emerging inside graphene nanocapillaries,<sup>1</sup> the structuring of molecules inside carbon nanotubes and nanopores,<sup>2–5</sup> the considerable decrease in the dielectric constant of water trapped between a diamond surface and graphene,<sup>6</sup> gases ordering into a crystalline array inside nanopores,<sup>7</sup> the transition of simple liquids to the solid state caused by volume limitation,<sup>8</sup> and many others. In contrast, in some cases, the confinement itself can be highly influenced by the enclosed substance.<sup>9</sup> For example, it is known that adsorbed molecules in nanopores induce considerable stresses of approximately several GPa.<sup>10</sup> These stresses result in deformation<sup>11</sup> that can lead to dramatic changes in the confinement structure.<sup>12</sup> Therefore, in a general case, one has to consider a mutual influence of the confinement and the trapped substance in a self-consistent manner.

One appealing example in which an enclosed substance significantly affects confinement and vice versa is a graphene nanobubble (GNB). It consists of a graphene sheet attached to an atomically

flat substrate with a trapped substance between them. Originally, GNBs were treated as manufacturing defects during the assembly of van der Waals (vdW) heterostructures (different types of 2D crystals stacked together). However, subsequently, many intriguing and special features of GNBs have been discovered. For instance, the outer graphene sheet of GNBs under strain creates gigantic pseudomagnetic fields.<sup>13,14</sup> GNBs can be utilized as a container to visualize chemical reactions.<sup>15</sup> In addition, GNBs are spots of intense photoluminescence emission caused by strained-induced variations in the band structure.<sup>16</sup>

Of particular interest is the structure of the substance inside a GNB and its connection with the shape of the bubble. By probing the shape of the GNB, one can implicitly determine the phase state of trapped matter and adhesion energies.<sup>17–19</sup> The structure of matter inside GNBs ranges from crystal clusters for GNBs with radii on the order of nanometers<sup>20,21</sup> to incompressible fluids for GNBs with radii larger than 100 nm.<sup>17,22</sup> The shape of GNBs is closely related to the structure and properties of the substance trapped inside them. For spherical GNBs, the phenomenon of the “universal shape” (constant height-to-radius ratio) was experimentally found.<sup>17</sup> Subsequent theoretical studies<sup>18,19,23</sup> led to the conclusion that the

“universal shape” is a consequence of the constant adhesion energies in the considered range of GNB radii. Another intriguing phenomenon is the existence of exotic “pancake” GNBs,<sup>18,24</sup> which have flat forms with low height-to-radius ratios. Presumably, molecules or atoms of the substance trapped in such bubbles are highly ordered and arranged in a layered structure.<sup>24</sup>

Although a number of experimental studies have shown that various condensation phases can exist inside GNBs and that their structure and phase state are mainly determined by the radius of the bubble, there are still many unresolved questions and a great demand for advanced theoretical models that could provide more insights into the structure of the substance enclosed inside GNBs and its connections with the bubble’s shape. To address this issue, we develop a GNB model based on classical density functional theory (c-DFT) and the elastic theory of membranes. The c-DFT approach provides an inside structure of GNBs accounting for molecular interaction with both the graphite substrate and the graphene membrane. In our model, calculated substance density distribution allows us to define the pressure, which acts on the graphene membrane. The equilibrium GNBs correspond to the minimum energy, where the substance contribution to the total energy expression is also calculated using c-DFT. Therefore, c-DFT describes the spatial, mechanical, and energy properties of the trapped substances, which makes c-DFT one of the most appropriate approaches among various fluid theory methods. As an example, we investigate argon fluid inside GNBs with various radii at room temperature. All modeled equilibrium GNBs exhibit a constant height-to-radius ratio, which is consistent with published results of experiments and molecular dynamics simulations.

## II. METHODS

The c-DFT method is applied to obtain the density distribution of the confined substance and evaluate its Helmholtz free energy ( $E_{cf}$ ). The confined substance is assumed to have a noncrystalline structure, and in the following discussion, we will refer to it as the “confined fluid.” The mechanical properties of the membrane (graphene sheet) are described by the conventional theory of elasticity.<sup>25</sup> This theory is used to calculate the elastic energy ( $E_{el}$ ) of the graphene sheet and determine the height profile of the bubble and the distribution of in-plane deformations. In this model, the footprint radius of the bubble  $R$  [see Fig. 1(a)] may vary, and the change in the corresponding adhesion energy ( $E_{ad}$ ) is calculated as

$$E_{ad} = \gamma_{gs} S = \gamma_{gs} \pi R^2, \quad (1)$$

where  $\gamma_{gs}$  is the specific adhesion energy between the graphene sheet and the substrate,  $S$  is the footprint area, and  $R$  is the GNB footprint radius.

The total energy  $E_{total}$  of the system consists of three parts: the energy of the confined fluid, the elastic energy of the graphene sheet and the adhesion energy,

$$E_{total} = E_{cf} + E_{el} + E_{ad}. \quad (2)$$

To obtain an equilibrium nanobubble with a certain mass of the confined fluid, the total energy is minimized according to “the shape” of the GNB and the density profile of the confined fluid  $\rho(z)$ .

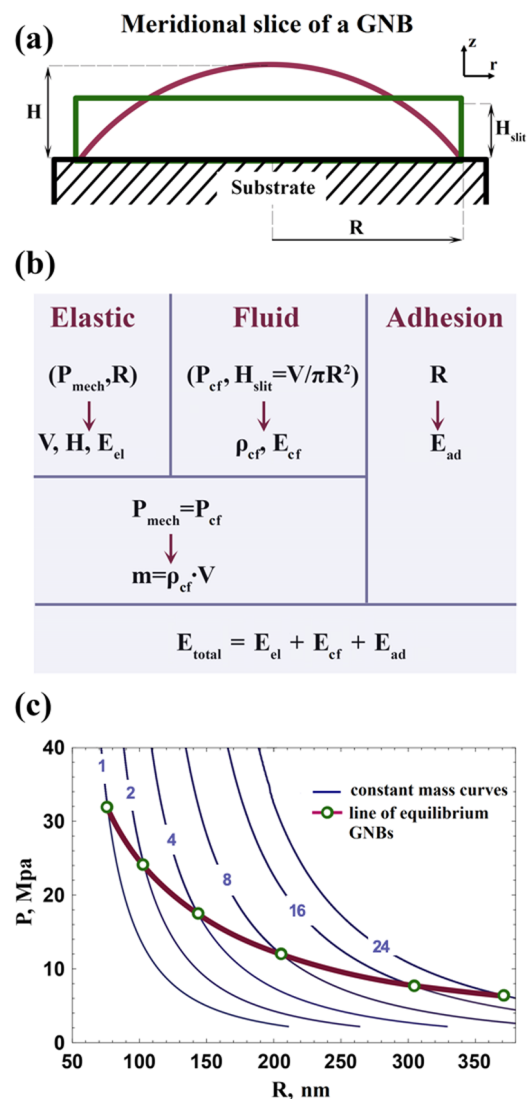


**FIG. 1.** (a) Schematic representation of a GNB. The height  $H$  of a GNB is the distance between the top point of the bubble and the surface of the undisturbed graphene sheet. The rectangle with a height  $H_{slit}$  represents the transformed geometry that is used in c-DFT calculations. (b) Visual diagram of the model, which describes the algorithm of the total energy calculation and (c) constant mass curves and a line of equilibrium GNBs filled with argon in  $(P, R)$  coordinates. Constant mass curves are calculated for a fixed mass and specified range of radii, and then, an equilibrium GNB with minimum energy is located. The numbers denote the isomass curves containing  $1, 2, 4, 8, 16, 24 \times 10^6$  of argon molecules inside GNBs.

“The shape” concept of the GNB includes the footprint radius, the height profile  $h(r)$ , and the displacement profile  $u(r)$ . In addition to the mass constraint imposed on the total energy minimization, there is an extra condition of mechanical equilibrium between the graphene sheet and the confined fluid, which implies that the pressure applied to the confined fluid is equal to the pressure developed by the graphene membrane [Fig. 1(b)].

The elastic energy of the graphene sheet is defined in terms of elasticity theory (see paragraph 14 in the book<sup>25</sup>). The energy expression from the theory of equilibrium of plates applied in cylindrical coordinates yields the following expression:

$$E_{el} = \int_0^\infty [\Psi_s(u_{\alpha\beta}, h) + \Psi_b(h)] 2\pi r dr, \quad (3)$$

where  $\Psi_s$  and  $\Psi_b$  are the stretching and bending energies per unit area, respectively;  $u_{\alpha\beta}$  is the strain tensor;  $h$  is the height profile; and  $r$  is the radius. The detailed expressions for specific stretching and bending elastic energies are provided in the [supplementary material](#) (see Sec. S1). Additionally, from the theory of elasticity, the pressure developed by the graphene sheet deformation is calculated as follows:

$$P_{mech} = \frac{\sigma_{rr}}{r_r} + \frac{\sigma_{\theta\theta}}{r_\theta}, \quad (4)$$

where  $r_r$  and  $r_\theta$  represent the principal radii of the curvature of the graphene membrane at a particular point and  $\sigma_{rr}$  and  $\sigma_{\theta\theta}$  are the radial and angular stress distributions in the graphene membrane, respectively.

To evaluate the internal energy of the confined fluid by using c-DFT, the bubble profile is reduced to the slit geometry representation [Fig. 1(a)]. The height of the slit geometry is evaluated as

$$H_{slit} = V/\pi R^2, \quad (5)$$

where  $V$  is the volume of the GNB.

Fundamental measure theory<sup>26</sup> (FMT), which is a version of c-DFT, is employed to calculate the specific Helmholtz free energy  $f$  and the density profile  $\rho(z)$  in the direction normal to the surface. The density fluid distribution  $\rho(z)$  can be found from the minimization of the grand potential  $\Omega[\rho(z)]$  as follows:

$$\frac{\delta\Omega[\rho]}{\delta\rho(z)} = 0. \quad (6)$$

The  $\Omega[\rho(z)]$  takes into account the ideal gas term, the fluid–fluid interactions, and surface–fluid interactions with both the substrate and graphene membrane,

$$\begin{aligned} \Omega/A = & k_B T \int_0^{H_{slit}} dz \rho(z) [\ln \rho(z) - 1] + f_{exc}(H_{slit}, \mu, T) \\ & + \int_0^{H_{slit}} dz \rho(z) (U_{ext}(z) - \mu), \end{aligned} \quad (7)$$

where  $A = \pi R^2$  is the footprint area;  $\mu$  is the bulk chemical potential;  $T$  is the temperature;  $f_{exc} = F_{exc}/A$  is the inhomogeneous excess specific free energies containing the terms of fluid attraction and repulsion; the term  $U_{ext}(z) = U_{substr}(z) + U_{membr}(H - z)$  is the external potential describing fluid interaction with the substrate  $U_{substr}(z)$ , and the membrane  $U_{membr}(H - z)$  at the distance  $H_{slit}$  from each other. The detailed expressions for the density functional and the external potentials are provided in the [supplementary material](#) (see Sec. S2). Then, the energy of the confined fluid is given by

$$\begin{aligned} E_{cf} = & \pi R^2 \left\{ k_B T \int_0^{H_{slit}} dz \rho(z) [\ln \rho(z) - 1] + f_{exc}(H_{slit}, \mu, T) \right. \\ & \left. + \int_0^{H_{slit}} dz \rho(z) U_{ext}(z) \right\}. \end{aligned} \quad (8)$$

The pressure  $P_{cf}$  inside the confined fluid is calculated according to the procedure described in this work as follows:<sup>27</sup>

$$P_{cf} = -\frac{\partial\Omega}{\partial V} = -\frac{1}{\pi R^2} \frac{\partial\Omega}{\partial H_{slit}}, \quad (9)$$

where  $\Omega[\rho]$  is the grand canonical potential that corresponds to the equilibrium confined fluid state  $\rho(z)$  and  $V = \pi R^2 H_{slit}$  is the volume of the GNBs.

The algorithm of the total energy evaluation of a GNB consists of two steps [see Fig. 1(b)]. In the first step, extensive tabulated data are generated for the elastic, confined fluid and adhesion parts of the total energy. Input parameters for every contribution are taken in a specified range, and corresponding meshes are built. The mesh of the elastic energy contribution is built in  $(P_{mech}, R)$  coordinates, the mesh of the confined fluid contribution is generated in  $(P_{cf}, H_{slit})$  coordinates, and the 1D mesh of the adhesion contribution is constructed in an  $(R)$  mesh. After the meshes are generated for every point, the output parameters of each energy contribution are calculated.

In the second step of the algorithm, the points of the obtained meshes are joined together. The procedure is as follows: A particular point in  $(P_{mech}, R)$  is chosen because the calculation of  $E_{el}$  is already performed. The volume  $V$  of the system is also known. Then, the point in  $(P_{cf}, H_{slit})$  that meets the following two conditions is found:  $P_{mech} = P_{cf}$  and  $H_{slit} = V/\pi R^2$ . At this stage, the density profile  $\rho(z)$  is obtained from c-DFT and the average density of the confined fluid is evaluated in the  $z$  direction as follows:

$$\rho_{cf} = \frac{1}{H_{slit}} \int \rho(z) dz. \quad (10)$$

The mass  $M$  of the bubble is simply evaluated as  $\rho_{cf} V$ . The joining with the remaining 1D  $R$ -mesh of adhesion is performed by choosing the point with the corresponding radius.

The procedure described above leads to numerous GNBs with the same mass but different radii, internal pressures, and total energies. They can be depicted as isomass curves in  $(P, R)$  coordinates [see Figs. 1(c) and 2(b)]. The equilibrium GNB on the isomass curve is determined as the bubble with the lowest total energy. As one can see from Fig. 1(c), the footprint radius decreases and the equilibrium pressure increases as the number of the trapped molecules becomes larger.

The developed model is applied to GNBs on a graphite substrate with trapped argon atoms. The temperature is fixed in all calculations and equals 300 K. The resulting equilibrium GNBs in  $(P, R)$  coordinates are shown in Fig. 1(c) and with additional details in Fig. 2(a). In accordance with our algorithm, the equilibrium GNB corresponds to the minimum of the isomass total energy, as shown in the inset in Fig. 2(a). GNBs in the range of 50–350 nm correspond to pressures in the range from 60 MPa to 8 MPa. This pressure range is way below crystallization pressure (1300 MPa) of argon at room temperature. It allows us to assume that argon inside the bubbles

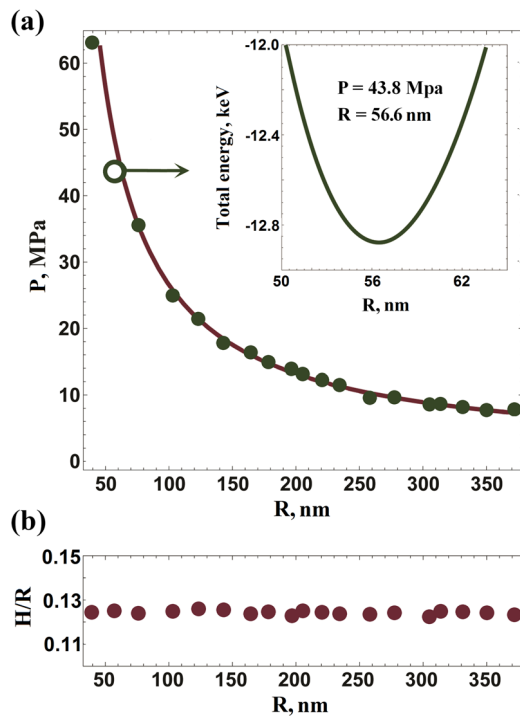


**FIG. 2.** (a) Line of equilibrium GNBs filled with argon in  $(P, R)$  coordinates. Calculations are performed for masses that correspond to a number of Ar atoms ranging from  $0.2 \times 10^6$  to  $24 \times 10^6$ . Inset: characteristic example of the total energy profile for the isomass curve of a GNB storing  $0.5 \times 10^6$  atoms. (b) Calculated height-to-radius ratio  $H/R$ . It is almost constant in the considered range of radii and equal to 0.125.

either in gas or liquid phases and the proposed model is applicable to GNBs considered. A significant increase in the pressure is observed for small GNBs ( $R < 100$  nm), which is in accordance with previous multiscale modeling<sup>28</sup> and MD simulations.<sup>24</sup>

The standard approach to characterize GNB profiles in AFM experiments is to measure the height-to-radius ( $H/R$ ) ratio. The study<sup>17</sup> shows that the  $H/R$  ratio is universal, i.e., independent of the bubbles' radius or volume. Our algorithm provides a geometric profile of the equilibrium GNBs that also allows the calculation of the height and radius. The constant ratio  $H/R = 0.125$  is observed for all considered equilibrium GNBs [see Fig. 2(b)] from our calculations. This result is in agreement with experimental data<sup>17</sup> and previous theoretical studies.<sup>24,28</sup> A semi-analytical expression for the  $H/R$  ratio could be derived from the theory of elastic membranes coupled with the assumption that the trapped substance is an incompressible liquid as follows:<sup>17</sup>

$$\frac{H}{R} = \left( \frac{\gamma_{gs} - \gamma_{gf} - \gamma_{sf}}{cY} \right)^{1/4}, \quad (11)$$

where  $\gamma_{gf}$  and  $\gamma_{sf}$  are the parameters of the graphene–fluid and substrate–fluid adhesion interactions, respectively,  $Y$  is Young's modulus of the 2D crystal,  $c$  is the geometrical parameter, obtained numerically, for a spherical bubble, which equals approximately 0.7.

Thus, the universal shape of a GNB can be assumed if adhesion properties and  $Y$  modulus do not significantly depend on the bubble's radius.

### III. RESULTS AND DISCUSSION

The developed model describes both the external equilibrium GNB properties ( $P, R$ ) and the corresponding inner structure. The confined fluid structure is characterized by the density distribution obtained from the c-DFT part of the model. The c-DFT approach calculations allow us to evaluate  $\rho_{cf}$  for a given height of the slit geometry and pressure. The typical density distributions are shown in Fig. 3 for various GNBs. Confined liquid structures can also be characterized in terms of excess density,

$$\rho_{exc} = \rho_{cf} - \rho_0, \quad (12)$$

where  $\rho_0$  is the bulk fluid density for the corresponding pressure. In Fig. 3, the inset shows the nonmonotonic behavior of  $\rho_{exc}$  for different equilibrium GNB pressures. All considered GNBs exhibit a positive excess density that corresponds to the presence of a dense layer near the surface. Nevertheless, if one extrapolates the excess density graph in the region of high pressures, which corresponds to GNBs with radii less than 50 nm, the excess density becomes negative. We assume that negative excess density could be the precursor to the liquid–solid phase transition. This prediction agrees well with recent molecular dynamics simulations<sup>24</sup> in which solid argon at room temperature was observed in GNBs with radii less than 35 nm.

We also considered trapped He at 300 K inside a GNB (see Sec. S3). The difference between the properties of He and Ar trapped inside a GNB at room temperature is insignificant. Computed density distributions exhibit only one prominent peak that

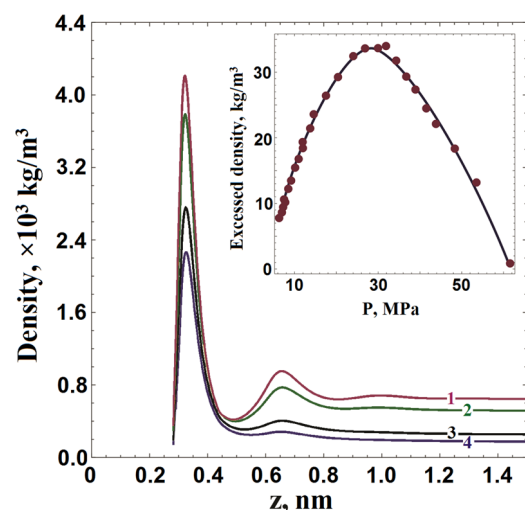


**FIG. 3.** Density distribution along the  $z$  axis obtained from c-DFT. Curves from 1 to 4 correspond to the following slit geometry parameters ( $H_{slit}, P$ ): (4.38 nm, 43.79 MPa), (6.7 nm, 31.74 MPa), (14.4 nm, 14.57 MPa), and (20.5 nm, 10.17 MPa), respectively. Inset: excess density at different pressures.

corresponds to the one well structured molecular layer near the surface and homogeneous fluid inside the GNB. These profiles qualitatively agree with the ones observed in the MD simulation.<sup>23</sup> Direct comparison with MD results<sup>23</sup> could not be done because of the extremely small bubble's height 0.83 nm considered in MD simulation.

One of the limitations of the developed model is that it cannot consider crystal structures that presumably arise for GNBs with radii less than 50 nm. There are two reasons for this limitation. First, an assumption about the isotropic pressure that is produced by the confined fluid is built into the model. Once the trapped substance is solid, this is not the case and one has to consider the anisotropic pressure tensor. As a result, the elastic problem for the graphene membrane became significantly harder to solve. Second, c-DFT itself is still a limited method for considering both confined liquid and solid phases simultaneously. The currently available liquid/solid-state c-DFT frameworks are still in the beginning stage of development.<sup>29</sup>

Nevertheless, the case of the solidification of the substance trapped inside GNBs is quite interesting. It is known both experimentally<sup>20,21</sup> and from MD simulations<sup>24</sup> that solid structures could emerge inside small GNBs with radii of less than approximately 50 nm. Additionally, small GNBs could exist in different morphological forms, for example, experimentally and MD observed "pancake" or "flat island" forms.<sup>18,24</sup> Thus, the development of a comprehensive GNB model that should be able to describe gas-, liquid- and solid-phase states of a trapped substance simultaneously is in demand and would be the objective of future research.

#### IV. CONCLUSION

We developed a model of GNBs that takes into account the inhomogeneous structure of the confined fluid and the mechanical stretching of the graphene membrane. The c-DFT approach is used to describe confined fluid properties. It provides information on the inner structure in terms of density profiles. The graphene sheet mechanics with a constant pressure profile are described by the theory of elasticity of membranes. Unlike the confined fluid theory in a solid porous medium, a GNB is an example of nonrigid confinement that requires an additional condition of mechanical equilibrium. We develop an algorithm that calculates GNB characteristics by taking into account the equilibrium of the graphene membrane and trapped fluid in a self-consistent manner. As an example application, we consider GNBs filled with argon at room temperature in the radii range of 50–350 nm. Our calculations present the universal shape of equilibrium GNBs for the whole range of radii, i.e., the constant  $H/R$  ratio, which is consistent with previous experimental measurements and MD simulations. Additionally, the density profiles and excess density of the GNBs in the considered range of radii are evaluated. It is shown that the extrapolation of the obtained results to the region of radii smaller than 50 nm leads to negative excess densities, which can presumably be attributed to the onset of the liquid–solid phase transition.

#### SUPPLEMENTARY MATERIAL

See the [supplementary material](#) for details about calculations of elastic energy, formulation of the DFT approach, and results of helium filled GNBs.

#### ACKNOWLEDGMENTS

The research was partially carried out using supercomputers at the Joint Supercomputer Center of the Russian Academy of Sciences (JSCC RAS). The authors also acknowledge the usage of the Skoltech CDISE HPC cluster "ARKUDA" for partly obtaining the results presented in this paper.

#### REFERENCES

- G. Algara-Siller, O. Lehtinen, F. Wang, R. Nair, U. Kaiser, H. Wu, A. Geim, and I. Grigorieva, "Square ice in graphene nanocapillaries," *Nature* **519**, 443 (2015).
- K. Koga, G. Gao, H. Tanaka, and X. C. Zeng, "Formation of ordered ice nanotubes inside carbon nanotubes," *Nature* **412**, 802 (2001).
- Y. D. Fomin, "Molecular dynamics simulation of benzene in graphite and amorphous carbon slit pores," *J. Comput. Chem.* **34**, 2615–2624 (2013).
- Y. D. Fomin, E. N. Tsiok, and V. N. Ryzhov, "The behavior of benzene confined in a single wall carbon nanotube," *J. Comput. Chem.* **36**, 901–906 (2015).
- Y. D. Fomin, V. Ryzhov, and E. Tsiok, "The behavior of cyclohexane confined in slit carbon nanopore," *J. Chem. Phys.* **143**, 184702 (2015).
- C. H. Y. X. Lim, A. Sorkin, Q. Bao, A. Li, K. Zhang, M. Nesladek, and K. P. Loh, "A hydrothermal anvil made of graphene nanobubbles on diamond," *Nat. Commun.* **4**, 1556 (2013).
- A. Vom Felde, J. Fink, T. Müller-Heinzerling, J. Pflüger, B. Scheerer, G. Linker, and D. Kaletta, "Pressure of neon, argon, and xenon bubbles in aluminum," *Phys. Rev. Lett.* **53**, 922 (1984).
- J. Klein and E. Kumacheva, "Confinement-induced phase transitions in simple liquids," *Science* **269**, 816–819 (1995).
- G. Y. Gor, P. Huber, and J. Weissmüller, "Elastocapillarity in nanopores: Sorption strain from the actions of surface tension and surface stress," *Phys. Rev. Mater.* **2**, 086002 (2018).
- Y. Long, J. C. Palmer, B. Coasne, M. Śliwiska-Bartkowiak, and K. E. Gubbins, "Pressure enhancement in carbon nanopores: A major confinement effect," *Phys. Chem. Chem. Phys.* **13**, 17163–17170 (2011).
- P. I. Ravikovitch and A. V. Neimark, "Density functional theory model of adsorption deformation," *Langmuir* **22**, 10864–10868 (2006).
- F.-X. Coudert, A. H. Fuchs, and A. V. Neimark, "Adsorption deformation of microporous composites," *Dalton Trans.* **45**, 4136–4140 (2016).
- N. Levy, S. Burke, K. Meaker, M. Panlasigui, A. Zettl, F. Guinea, A. C. Neto, and M. Crommie, "Strain-induced pseudo-magnetic fields greater than 300 tesla in graphene nanobubbles," *Science* **329**, 544–547 (2010).
- Z. Qi, A. L. Kitt, H. S. Park, V. M. Pereira, D. K. Campbell, and A. C. Neto, "Pseudomagnetic fields in graphene nanobubbles of constrained geometry: A molecular dynamics study," *Phys. Rev. B* **90**, 125419 (2014).
- R. Mu, Q. Fu, L. Jin, L. Yu, G. Fang, D. Tan, and X. Bao, "Visualizing chemical reactions confined under graphene," *Angew. Chem., Int. Ed.* **51**, 4856–4859 (2012).
- A. Tyurnina, D. Bandurin, E. Khestanova, V. G. Kravets, M. Koperski, F. Guinea, A. N. Grigorenko, A. K. Geim, and I. V. Grigorieva, "Strained bubbles in van der Waals heterostructures as local emitters of photoluminescence with adjustable wavelength," *ACS Photonics* **6**, 516 (2019).
- E. Khestanova, F. Guinea, L. Fumagalli, A. Geim, and I. Grigorieva, "Universal shape and pressure inside bubbles appearing in van der Waals heterostructures," *Nat. Commun.* **7**, 12587 (2016).
- E. Khestanova, "Van der Waals heterostructures: Fabrication, mechanical and electronic properties," Ph.D. thesis, The University of Manchester, United Kingdom, 2018.
- E. Iakovlev, P. Zhilyaev, and I. S. Akhatov, "Obtaining the state of matter inside graphene nanobubble from its shape," *J. Phys.: Conf. Ser.* **1147**, 012006 (2019).
- G. Zamborlini, M. Imam, L. L. Patera, T. O. Menten, N. Stojić, C. Africh, A. Sala, N. Binggeli, G. Comelli, and A. Locatelli, "Nanobubbles at GPa pressure under graphene," *Nano Lett.* **15**, 6162–6169 (2015).
- R. Larciprete, S. Colonna, F. Ronci, R. Flammini, P. Lacovig, N. Apostol, A. Politano, P. Feulner, D. Menzel, and S. Lizzit, "Self-assembly of graphene nanoblisters sealed to a bare metal surface," *Nano Lett.* **16**, 1808–1817 (2016).

- <sup>22</sup>D. A. Sanchez, Z. Dai, P. Wang, A. Cantu-Chavez, C. J. Brennan, R. Huang, and N. Lu, "Mechanics of spontaneously formed nanoblisters trapped by transferred 2D crystals," *Proc. Natl. Acad. Sci. USA* **115**, 7884–7889 (2018).
- <sup>23</sup>H. Ghorbanfekr-Kalashami, K. Vasu, R. Nair, F. M. Peeters, and M. Neek-Amal, "Dependence of the shape of graphene nanobubbles on trapped substance," *Nat. Commun.* **8**, 15844 (2017).
- <sup>24</sup>E. Iakovlev, P. Zhilyaev, and I. Akhatov, "Atomistic study of the solid state inside graphene nanobubbles," *Sci. Rep.* **7**, 17906 (2017).
- <sup>25</sup>L. D. Landau and E. M. Lifshitz, *Theory and Elasticity*, Course of Theoretical Physics Vol. 7 (Pergamon Press, 1959).
- <sup>26</sup>R. Roth, R. Evans, A. Lang, and G. Kahl, "Fundamental measure theory for hard-sphere mixtures revisited: The white bear version," *J. Phys.: Condens. Matter* **14**, 12063 (2002).
- <sup>27</sup>D. Grégoire, C. Malheiro, and C. Miqueu, "Estimation of adsorption-induced pore pressure and confinement in a nanoscopic slit pore by a density functional theory," *Continuum Mech. Thermodyn.* **30**, 347–363 (2018).
- <sup>28</sup>P. Zhilyaev, E. Iakovlev, and I. Akhatov, "Liquid–gas phase transition of Ar inside graphene nanobubbles on the graphite substrate," *Nanotechnology* **30**, 215701 (2019).
- <sup>29</sup>G. Kocher and N. Provatas, "New density functional approach for solid-liquid-vapor transitions in pure materials," *Phys. Rev. Lett.* **114**, 155501 (2015).

# Supplementary materials

## 1. S1

The functional relation of the strain tensor components with the radial displacement ( $u_r$ ) and height profile ( $h$ ) is

$$u_{rr} = \frac{\partial u_r}{\partial r} + \frac{1}{2} \left( \frac{\partial h}{\partial r} \right)^2, \quad u_{\theta\theta} = \frac{u_r}{r}. \quad (1)$$

We assume that Poisson's ratio is equal to zero. In this case, the stress tensor components are

$$\sigma_{rr} = Y u_{rr}, \quad \sigma_{\theta\theta} = Y u_{\theta\theta}, \quad (2)$$

where  $Y$  is the Young's modulus of the graphene sheet with dimensions of energy per unit area.

Then, the specific stretching and bending elastic energies can be expressed as

$$\begin{aligned} \Psi_s = \frac{1}{2} u_{\alpha\beta} \sigma_{\alpha\beta} = \frac{Y}{2} & \left[ \left( \frac{\partial u_r}{\partial r} \right)^2 + \frac{\partial u_r}{\partial r} \left( \frac{\partial h}{\partial r} \right)^2 \right. \\ & \left. + \frac{1}{4} \left( \frac{\partial h}{\partial r} \right)^4 + \left( \frac{u_r}{r} \right)^2 \right], \end{aligned} \quad (3)$$

$$\Psi_b = \frac{\kappa}{2} \left[ \left( \frac{\partial^2 h}{\partial r^2} \right)^2 + \frac{1}{r^2} \left( \frac{\partial h}{\partial r} \right)^2 \right]. \quad (4)$$

## 2. S2

In order to consider fluid properties inside GNBs we use slit pores as the geometrical model of the confinement. The grand potential accounting for inhomogeneous fluid distribution inside slit confinement can be written as follows:

$$\Omega[\rho(z)] = F[\rho(z)] + A \int_0^H dz \rho(z) (U_{\text{ext}}(z) - \mu) \quad (5)$$

where z-axis is directed perpendicularly to the surface into the fluid phase,  $F[\rho]$  is the Helmholtz free energy,  $U_{\text{ext}}$  is the external potential,  $\mu$  is the chemical potential,  $A$  and  $H$  are the surface area and the width of the slit pore. The equilibrium density distribution  $\rho$  is satisfied to the following condition:

$$\frac{\delta \Omega[\rho]}{\delta \rho} = 0 \quad (6)$$

The Helmholtz free energy can be split into two parts: the ideal term  $F_{id}$  and the excess term  $F_{exc}$  describing contributions of intermolecular repulsion and attraction. Henceforth Boltzmann and Plank constants are assumed to be equal to one:  $k_B = h = 1$ . Thus, Helmholtz free energy can be expressed as

$$F[\rho] = F_{id}[\rho] + F_{exc}[\rho] \quad (7)$$

For an ideal system without any interactions, the Helmholtz free energy is known exactly :

$$F_{id}[\rho] = k_B T A \int_0^H dz \rho(z) [\ln(\Lambda^3 \rho(z)) - 1] \quad (8)$$

where  $T$  is the temperature,  $\Lambda = (2\pi m T)^{1/2}$  is de Broglie wavelength,  $m$  is the mass of molecule. Expression (8) contains three-dimensional integration which can be reduced to one-dimensional integral using spatial symmetry.

Molecules are considered as not ideal system which is represented by spherical molecules with diameter  $d$  interacting via Lennard-Jones (LJ) potential  $U_{LJ}$

$$U_{LJ}(r) = 4\epsilon_{ff} \left[ \left(\frac{d}{r}\right)^{12} - \left(\frac{d}{r}\right)^6 \right] \quad (9)$$

where  $\epsilon_{ff}$  is the characteristic intermolecular energy. The excess term contains the repulsion contribution, which can be described by reference system – the system of hard sphere, and attraction contribution. Thus, the excess Helmholtz free energy can be written as

$$F_{exc}[\rho] = F_{HS}[\rho] + F_{att}[\rho] \quad (10)$$

Here for perturbed attraction part we use Weeks-Chandler-Andersen (WCA) scheme with the following representation of attraction potential:  $U_{att} = -\epsilon_{ff}$  if the distance  $r < \lambda$  and  $U_{att} = U_{LJ}(r)$  if  $r > \lambda$ , where  $\lambda = 2^{1/6}d$  corresponds to the minimum of LJ potential. The mean-field approximation for attraction part is

$$F_{att} = \frac{1}{2} \int \int d\vec{r}' d\vec{r} \rho(\vec{r}) \rho(\vec{r}') U_{att}(|\vec{r} - \vec{r}'|) \quad (11)$$

General expression for Helmholtz free energy of hard spheres has the following form

$$F_{HS} = T \int \Phi_{HS}[n_\alpha(r)] d\vec{r} \quad (12)$$

In current research we apply Rosenfeld-Schmidt-Lowen-Tarazona (RLST) version of FMT

$$\begin{aligned} \Phi_{HS}[n_\alpha] = & -n_0 \ln(1 - n_3) + \frac{n_1 n_2 - \vec{n}_{v1} \cdot \vec{n}_{v2}}{1 - n_3} + \\ & + \frac{n_2^3}{24\pi(1 - n_3)^2} \left( 1 - 3 \left(\frac{\vec{n}_{v2}}{n_2}\right)^2 + 2 \left(\frac{\vec{n}_{v2}}{n_2}\right)^3 \right) \end{aligned} \quad (13)$$

where  $n_\alpha$ ,  $\alpha = 0, 1, 2, 3$  and  $\vec{n}_\alpha$ ,  $\alpha = V1, V2$  are scalar and vector averaged functions respectively. These new variables have the following definition:

$$\begin{aligned} n_\alpha = & \int d\vec{r}' \rho(z') \omega_\alpha(\vec{r} - \vec{r}'), \\ \omega_0(r) = & \frac{\omega_2(r)}{4\pi R^2}, \quad \omega_1(r) = \frac{\omega_2(r)}{4\pi R}, \\ \omega_2(r) = & \delta(R - r), \quad \omega_3(r) = \Theta(R - r), \\ \omega_{V1}(\vec{r}) = & \frac{\omega_{V2}\vec{r}}{4\pi R}, \quad \omega_{V2}\vec{r} = \frac{\vec{r}}{r} \delta(R - r) \end{aligned} \quad (14)$$

where  $R$  is radius of molecule. As one can see in (14) the region of integration for  $n_\alpha$  corresponds to the size of molecule. Situation when a fluid molecule and solid surface has non empty crossover is impossible due to repulsion part of external potential.

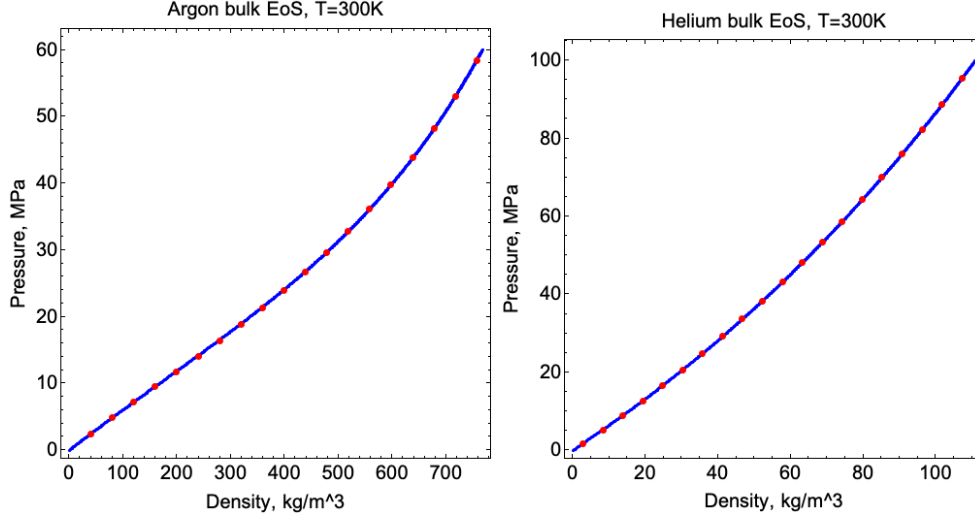


**Figure 1.** The comparison of bulk c-DFT EOS (blue curve) and NIST data of Argon and Helium at 300K (red dots) using corresponding parameters from Table 1.

The last term in (5) is external potential describing interaction between a fluid molecule and solid media  $F_{ext}$ . This potential has to take into account geometrical properties of solid surface:

$$F_{ext} = A \int dz \rho(z) U_{ext}(z) \quad (15)$$

In the expression of external potential we take into account the impact of two walls corresponding to graphene membrane and substrate:

$$U_{ext} = U_{substr} + U_{membr}(H - z) \quad (16)$$

In our study we considered symmetrical case using the same potential for both the membrane and the substrate, which is determined by 10-4 expression:

$$u_{ext}(z) = 2\pi\rho_s\epsilon_{sf}d_{sf}^2\Delta \left[ \frac{2}{5} \left( \frac{d_{sf}}{z} \right)^{10} - \left( \frac{d_{sf}}{z} \right)^4 \right] \quad (17)$$

where  $\rho_s = 0.114A^{-3}$  is the number density of carbon atoms in graphite,  $\Delta = 3.35A$  is the interlayer spacing in graphite,  $\epsilon_{sf}$  and  $d_{sf}$  are the characteristic energetic and scale parameters of the solid-fluid LJ potential. These solid-fluid interaction parameters are defined by the Lorentz-Berthelot rules

$$\epsilon_{sf} = (\epsilon_{ff}\epsilon_{ss})^{1/2}, \quad d_{sf} = \frac{1}{2}(d_{ff} + d_{ss}),$$

The comparison of the used DFT bulk equation of state with the NIST data is shown in Fig. 1.

The slit height  $H_{slit} = \frac{V}{\pi R^2}$  is defined from the volume corresponding to the realistic profile  $c_V R^2 H$ , where  $c_V$  is approximately equal to 1.7 [1]. Therefore the approximated height is linearly proportional to the real one  $H_{slit} = c_V/\pi H$  that correctly reflects the dependence on  $H$ . This approximation is not applicable in the case of extremely small GNBS when the height is comparable with the molecular diameter. Indeed slit geometry at  $H_{slit} \sim 2$  nm accounts for various confined fluids effects such as disjoining pressure, which are almost neglected for real GNB profile with  $H = \pi/c_V H_{slit} \sim 4$  nm.

**Table 1.** Parameters of fluid-fluid interaction for argon, and parameters of solid-solid interaction for carbon.

Trapped substance	$\epsilon_{ff}/k_B$ , K	$d_{ff}$ , Å	$\epsilon_{ss}/k_B$ , K	$d_{ss}$ , Å
Argon	110.6	3.17	28.0	3.4
Helium	15.5	2.26	28.0	3.4

Another type of the errors due to the slit pore approximation is related to the lack of the curvature in the expression of effective fluid-solid potential corresponding to graphene membrane. However the radius of curvature for the considered in our work GNBs can be estimated using the following expression:

$$R_{\text{curv}} = \left| \frac{(1 + h'(r)^2)^{3/2}}{h''(r)} \right| = \frac{(1 + (2Hr/R^2)^2)^{3/2}}{2H/R^2} \simeq \frac{R^2}{2H}$$

As we demonstrated for all considered GNB the ratio  $H/R$  is almost constant around 0.125, then  $R_{\text{curv}} = 4R \geq 200$  nm. Therefore the ratio  $R_{\text{curv}}/d \gg 1$  allows to neglect the curvature influence in the effective potential. Thus, the potential of the flat graphene sheet is reasonable approximation at considered GNB radii.

### 3. Helium GNB

To qualitatively compare the results of our approach with published MD simulations [2] we considered helium filled GNB at the temperature 300 K. The density fluid distributions of two equilibrium GNBs are shown in Fig. 2. The GNB containing  $0.1 \times 10^6$  of helium molecules can be considered as the smallest volume and the largest pressures, which can be described by our approach. Similar to argon filled GNB and MD results [2] even at largest pressure we observed only one adsorbed layer. Therefore, these calculations confirm our assumption that the difference between helium and argon is insignificant. The ratio  $H/R$  calculated for equilibrium helium GNBs is shown in Fig. 3

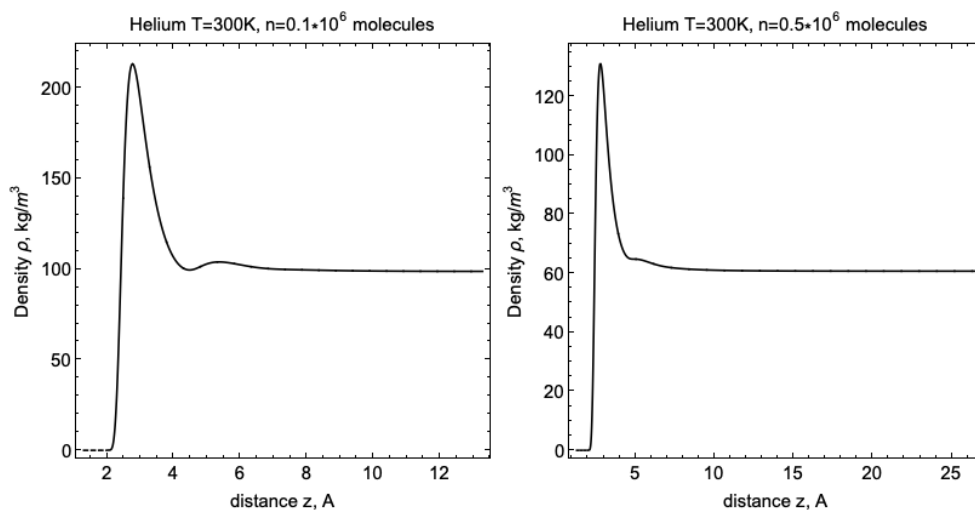


**Figure 2.** The inner density distributions of the helium GNBs stored  $0.5 \times 10^6$  and  $1 \times 10^6$  of the molecules at  $T = 300K$ . The equilibrium parameters are the following: (left)  $H = 38$  Å,  $R = 298$  Å,  $P = 85$  MPa and (right)  $H = 75$  Å,  $R = 585$  Å,  $P = 46$  MPa

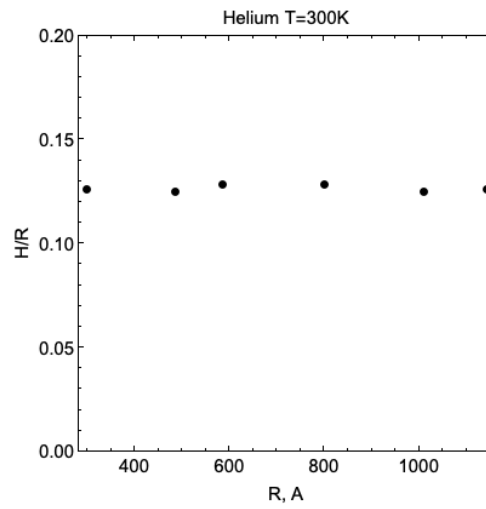


**Figure 3.** The ration  $H/R$  calculated for helium GNB at 300K filed with 0.1, 0.3, 0.5, 1, 1.5 and 2 millions of the molecules (from left to right).

### References

- [1] Khestanova E, Guinea F, Fumagalli L, Geim A and Grigorieva I 2016 *Nat. Commun.* **7** 12587
- [2] Ghorbanfekr-Kalashami H, Vasu K, Nair R, Peeters F M and Neek-Amal M 2017 *Nat. Commun.* **8** 15844

"Prediction is very difficult, especially if it's about the future."

Niels Bohr

## Chapter 4

# Conclusion

### 4.1 Summary

The work presented in this thesis is aimed to explore the properties of the graphene nanobubbles, which are good examples of the van der Waals nanobubbles family. Graphene is a well-studied two-dimensional crystal. That is why its properties are well described by different models.

Graphene nanobubbles were first discovered while creating two-dimensional heterostructures as undesired defects. However, further graphene nanobubbles are found to possess a large number of interesting properties, making a lot of researches work in this area. For example, there is a giant pressure inside graphene nanobubbles up to 1 GPa. Such great pressure makes it possible to use this type of matter confinement as hydrothermal reactors and surface modifiers. Although a large number of experimental studies are done, the behavior of the trapped matter was still not studied enough. Thus, for example, there are still disputes about the state of the trapped matter. The opinions vary from gas to solid states. Also, a lot of studies where it is even not defined what type of substance is captured by the bubble.

That is why comprehensive theoretical research is needed to understand the physics of the formation of the nanobubbles and the behavior of the trapped matter under such an unusual type of confinement. Firstly, the molecular dynamics simulations for small nanobubbles up to 33 nm are performed. The upper layer of the nanobubble is graphene, the trapped matter is argon, simulations are performed at

room temperature. These calculations reveal that argon exists in the solid phase at such conditions, despite the fact that pressure is not high enough and temperature is not low enough to crystallize argon in bulk. This phenomenon is a manifestation of the strong confinement effect created by the substrate and attracted 2D crystal.

Further investigation is aimed at the development of a model which is capable of studying the bigger nanobubbles. That is why the continuum approach is chosen. It combines the theory of elasticity of membranes, the equations of state of matter. This energy approach allows the calculation of the profiles of the nanobubbles, the strains and stresses of the upper graphene sheet, and the state of trapped matter. We performed simulations for graphene nanobubbles with trapped argon and ethane for various temperatures. We found that substances inside graphene nanobubble can undergo a phase transition and that different states of trapped matter affect the shape of the nanobubble. Thus the  $H/R$  ratio for nanobubbles with trapped liquid must be less than the trapped gas phase. Also, we predict the 'forbidden region', i.e., the range of radii where no stable bubble can be found at some temperature. This region separates the bubble with the matter of different phase states.

Finally, we implement the classical density functional theory into the last model. This improvement allows us to take into account the inhomogeneity of the trapped fluid and make a correction to the thermodynamics property of the matter. Also, it allows studying the structure of the fluid. This approach considers the graphene nanobubble as an interesting type of matter confinement. It is unique because the confinement size adjusts due to the competition between the van der Waals and the elastic forces. Thus the matter inside is affected significantly by graphene walls. It is shown that for nanobubbles with a radius less than 50 nm, the negative excess density is presented. That can be attributed to the onset of the liquid-solid phase transition.

## 4.2 Outlook

Graphene nanobubbles are very promising in industrial and laboratory applications due to a number of their unique properties. Still, many aspects of the formation

of graphene nanobubbles are disclosed. Our theoretical studies helps to predict properties and to understand the physics of graphene nanobubbles.

For the successful application of graphene nanobubbles, the controlled synthesis of graphene nanobubbles should be developed. The ability to capture the desired matter inside graphene nanobubbles opens the door to controlled chemical reactions in strong confinement. Also, a lot of possible applications require a particular substance to be trapped. As well different methods of matter detection and observation should be applied and improved in order to study the state of matter inside such a small space, like low-energy electron microscopy and synchrotron-based photoemission electron microscopy or x-ray photoelectron spectroscopy. In molecular dynamics, the bigger systems with sophisticated potentials should be used in order to describe the interaction of water or hydrocarbons with different types of 2D crystal such as graphene or MoS<sub>2</sub>. Finally, the theoretical investigation should be focused on the development of a precise model to describe matter in such extreme confinement and to take into account liquid-solid phase transition.

# Glossary

**2D** two dimensional. [10](#)

**AFM** atomic force microscopy. [17](#)

**CNTs** carbon nanotubes. [23](#)

**DFT** density functional theory. [13](#)

**FTIR** Fourier transform infrared. [20](#)

**GN** graphene nanobubble. [10](#)

**LAMMPS** large-scale atomic/molecular massively parallel simulator. [14](#)

**LEEM** low energy electron microscopy. [21](#)

**MD** molecular dynamics. [10](#)

**STM** scanning tunneling microscopy. [19](#)

**vdW** van der Waals. [10](#)

**XPEEM** synchrotron-based photoemission electron microscopy. [21](#)

# Bibliography

- G Algara-Siller, O Lehtinen, FC Wang, RR Nair, U Kaiser, HA Wu, AK Geim, and IV Grigorieva. Square ice in graphene nanocapillaries. *Nature*, 519(7544):443, 2015.
- TF Aslyamov, ES Iakovlev, I Sh Akhatov, and PA Zhilyaev. Model of graphene nanobubble: Combining classical density functional and elasticity theories. *The Journal of Chemical Physics*, 152(5):054705, 2020.
- E Bauer. Low energy electron microscopy. *Reports on Progress in Physics*, 57(9):895, 1994.
- J Bernholc, A Antonelli, TM Del Sole, Y Bar-Yam, and ST Pantelides. Mechanism of self-diffusion in diamond. *Physical review letters*, 61(23):2689, 1988.
- Simone Bertolazzi, Jacopo Brivio, and Andras Kis. Stretching and breaking of ultrathin mos2. *ACS nano*, 5(12):9703–9709, 2011.
- Donald W Brenner, Olga A Shenderova, Judith A Harrison, Steven J Stuart, Boris Ni, and Susan B Sinnott. A second-generation reactive empirical bond order (rebo) potential energy expression for hydrocarbons. *Journal of Physics: Condensed Matter*, 14(4):783, 2002.
- Richard A Buckingham. The classical equation of state of gaseous helium, neon and argon. *Proceedings of the Royal Society of London. Series A. Mathematical and Physical Sciences*, 168(933):264–283, 1938.
- Santanu Das, Debrupa Lahiri, Dong-Yoon Lee, Arvind Agarwal, and Wonbong Choi. Measurements of the adhesion energy of graphene to metallic substrates. *Carbon*, 59:121–129, 2013.
- X Fan, EC Dickey, PC Eklund, KA Williams, L Grigorian, R Buczko, ST Pantelides, and SJ Pennycook. Atomic arrangement of iodine atoms inside single-walled carbon nanotubes. *Physical review letters*, 84(20):4621, 2000.
- Daan Frenkel and Berend Smit. *Understanding molecular simulation: from algorithms to applications*, volume 1. Elsevier, 2001.
- Andre K Geim and Irina V Grigorieva. Van der waals heterostructures. *Nature*, 499(7459):419–425, 2013.

- T Georgiou, L Britnell, P Blake, RV Gorbachev, A Gholinia, AK Geim, C Casiraghi, and KS Novoselov. Graphene bubbles with controllable curvature. *Applied Physics Letters*, 99(9):093103, 2011.
- H Ghorbanfekr-Kalashami, KS Vasu, RR Nair, François M Peeters, and M Neek-Amal. Dependence of the shape of graphene nanobubbles on trapped substance. *Nature communications*, 8:15844, 2017.
- SJ Haigh, A Gholinia, R Jalil, S Romani, L Britnell, DC Elias, KS Novoselov, LA Ponomarenko, AK Geim, and R Gorbachev. Cross-sectional imaging of individual layers and buried interfaces of graphene-based heterostructures and superlattices. *Nature materials*, 11(9):764–767, 2012.
- Jason K Holt, Hyung Gyu Park, Yinmin Wang, Michael Stadermann, Alexander B Artyukhin, Costas P Grigoropoulos, Aleksandr Noy, and Olgica Bakajin. Fast mass transport through sub-2-nanometer carbon nanotubes. *Science*, 312(5776):1034–1037, 2006.
- J Hone, C Lee, XD Wei, and JW Kysar. Measurement of the elastic properties and intrinsic strength of monolayer graphene. *science*, 321(5887):385–388, 2008.
- ES Iakovlev, PA Zhilyaev, and I Sh Akhatov. Obtaining the state of matter inside graphene nanobubble from its shape. In *Journal of Physics: Conference Series*, volume 1147, page 012006. IOP Publishing, 2019a.
- ES Iakovlev, PA Zhilyaev, and I Sh Akhatov. Adhesion energy of ethane–graphite interface: Atomistic study. In *Journal of Physics: Conference Series*, volume 1556, page 012052. IOP Publishing, 2020.
- Evgeny Iakovlev, Petr Zhilyaev, and Iskander Akhatov. Atomistic study of the solid state inside graphene nanobubbles. *Scientific reports*, 7(1):1–7, 2017.
- Evgeny Iakovlev, Petr Zhilyaev, and Iskander Akhatov. Modeling of the phase transition inside graphene nanobubbles filled with ethane. *Physical Chemistry Chemical Physics*, 21(33):18099–18104, 2019b.
- E Khestanova, F Guinea, L Fumagalli, AK Geim, and IV Grigorieva. Universal shape and pressure inside bubbles appearing in van der waals heterostructures. *Nature Communications*, 7:12587, 2016.
- Hyo Won Kim, Wonhee Ko, JiYeon Ku, Insu Jeon, Donggyu Kim, Hyeokshin Kwon, Youngtek Oh, Seunghwa Ryu, Young Kuk, Sung Woo Hwang, et al. Nanoscale control of phonon excitations in graphene. *Nature communications*, 6(1):1–5, 2015.
- Alexander I Kolesnikov, Jean-Marc Zanotti, Chun-Keung Loong, Pappannan Thiagarajan, Alexander P Moravsky, Raouf O Loutfy, and Christian J Burnham. Anomalously soft dynamics of water in a nanotube: a revelation of nanoscale confinement. *Physical review letters*, 93(3):035503, 2004.

- AV Kretinin, Y Cao, JS Tu, GL Yu, R Jalil, KS Novoselov, SJ Haigh, A Gholinia, A Mishchenko, M Lozada, et al. Electronic properties of graphene encapsulated with different two-dimensional atomic crystals. *Nano letters*, 14(6):3270–3276, 2014.
- Rosanna Larciprete, Stefano Colonna, Fabio Ronci, Roberto Flammini, Paolo Lacovig, Nicoleta Apostol, Antonio Politano, Peter Feulner, Dietrich Menzel, and Silvano Lizzit. Self-assembly of graphene nanoblisters sealed to a bare metal surface. *Nano letters*, 16(3):1808–1817, 2016.
- Changgu Lee, Xiaoding Wei, Jeffrey W Kysar, and James Hone. Measurement of the elastic properties and intrinsic strength of monolayer graphene. *science*, 321(5887):385–388, 2008.
- N Levy, SA Burke, KL Meaker, M Panlasigui, A Zettl, F Guinea, AH Castro Neto, and MF Crommie. Strain-induced pseudo-magnetic fields greater than 300 tesla in graphene nanobubbles. *Science*, 329(5991):544–547, 2010.
- Candy Haley Yi Xuan Lim, Anastassia Sorkin, Qiaoliang Bao, Ang Li, Kai Zhang, Milos Nesladek, and Kian Ping Loh. A hydrothermal anvil made of graphene nanobubbles on diamond. *Nature communications*, 4:1556, 2013.
- Andrea Locatelli and Tevfik Onur Menteş. Chemical and magnetic imaging with x-ray photoemission electron microscopy. In *Synchrotron Radiation*, pages 571–591. Springer, 2015.
- Jiong Lu, AH Castro Neto, and Kian Ping Loh. Transforming moiré blisters into geometric graphene nano-bubbles. *Nature communications*, 3:823, 2012.
- Marcus G Martin and J Ilja Siepmann. Transferable potentials for phase equilibria. 1. united-atom description of n-alkanes. *The Journal of Physical Chemistry B*, 102(14):2569–2577, 1998.
- Alexander S Mayorov, Roman V Gorbachev, Sergey V Morozov, Liam Britnell, Rashid Jalil, Leonid A Ponomarenko, Peter Blake, Kostya S Novoselov, Kenji Watanabe, Takashi Taniguchi, et al. Micrometer-scale ballistic transport in encapsulated graphene at room temperature. *Nano letters*, 11(6):2396–2399, 2011.
- Rentao Mu, Qiang Fu, Li Jin, Liang Yu, Guangzong Fang, Dali Tan, and Xinhe Bao. Visualizing chemical reactions confined under graphene. *Angewandte Chemie International Edition*, 51(20):4856–4859, 2012.
- RR Nair, HA Wu, PN Jayaram, IV Grigorieva, and AK Geim. Unimpeded permeation of water through helium-leak-tight graphene-based membranes. *Science*, 335(6067):442–444, 2012.
- GE Norman and VV Stegailov. Stochastic theory of the classical molecular dynamics method. *Mathematical Models and Computer Simulations*, 5(4):305–333, 2013.
- KS Novoselov, A Mishchenko, A Carvalho, and AH Castro Neto. 2d materials and van der waals heterostructures. *Science*, 353(6298):aac9439, 2016.

- Thomas C O'Connor, Jan Andzelm, and Mark O Robbins. Airebo-m: A reactive model for hydrocarbons at extreme pressures. *The Journal of chemical physics*, 142(2):024903, 2015.
- Jungwon Park, Hyesung Park, Peter Ercius, Adrian F Pegoraro, Chen Xu, Jin Woong Kim, Sang Hoon Han, and David A Weitz. Direct observation of wet biological samples by graphene liquid cell transmission electron microscopy. *Nano letters*, 15(7):4737–4744, 2015.
- Steve Plimpton. Fast parallel algorithms for short-range molecular dynamics. *Journal of computational physics*, 117(1):1–19, 1995.
- LA Ponomarenko, AK Geim, AA Zhukov, R Jalil, SV Morozov, KS Novoselov, IV Grigorieva, EH Hill, VV Cheianov, VI Fal'Ko, et al. Tunable metal–insulator transition in double-layer graphene heterostructures. *Nature Physics*, 7(12):958–961, 2011.
- Zenan Qi, Alexander L Kitt, Harold S Park, Vitor M Pereira, David K Campbell, and AH Castro Neto. Pseudomagnetic fields in graphene nanobubbles of constrained geometry: A molecular dynamics study. *Physical Review B*, 90(12):125419, 2014.
- WH Roos, R Bruinsma, and GJL Wuite. Physical virology. *Nature physics*, 6(10):733–743, 2010.
- Steven J Stuart, Alan B Tutein, and Judith A Harrison. A reactive potential for hydrocarbons with intermolecular interactions. *The Journal of chemical physics*, 112(14):6472–6486, 2000.
- Peter Sutter, Jerzy T Sadowski, and Eli A Sutter. Chemistry under cover: tuning metal- graphene interaction by reactive intercalation. *Journal of the American Chemical Society*, 132(23):8175–8179, 2010.
- Jerry Tersoff. Empirical interatomic potential for silicon with improved elastic properties. *Physical Review B*, 38(14):9902, 1988.
- JJPRB Tersoff. Modeling solid-state chemistry: Interatomic potentials for multi-component systems. *Physical Review B*, 39(8):5566, 1989.
- Mark Tuckerman. *Statistical mechanics: theory and molecular simulation*. Oxford university press, 2010.
- Anastasia V Tyurnina, Denis A Bandurin, Ekaterina Khestanova, Vasyl G Kravets, Maciej Koperski, Francisco Guinea, Alexander N Grigorenko, Andre K Geim, and Irina V Grigorieva. Strained bubbles in van der waals heterostructures as local emitters of photoluminescence with adjustable wavelength. *ACS Photonics*, 6(2):516–524, 2019.
- Adri CT Van Duin, Siddharth Dasgupta, Francois Lorant, and William A Goddard. Reaxff: a reactive force field for hydrocarbons. *The Journal of Physical Chemistry A*, 105(41):9396–9409, 2001.

- Michal Wojcik, Margaret Hauser, Wan Li, Seonah Moon, and Ke Xu. Graphene-enabled electron microscopy and correlated super-resolution microscopy of wet cells. *Nature communications*, 6(1):1–6, 2015.
- Jong Min Yuk, Jungwon Park, Peter Ercius, Kwanpyo Kim, Daniel J Hellebusch, Michael F Crommie, Jeong Yong Lee, A Zettl, and A Paul Alivisatos. High-resolution em of colloidal nanocrystal growth using graphene liquid cells. *Science*, 336(6077):61–64, 2012.
- Giovanni Zamborlini, Mighfar Imam, Laerte L Patera, Tevfik Onur Menten, Natasa Stojic, Cristina Africh, Alessandro Sala, Nadia Binggeli, Giovanni Comelli, and Andrea Locatelli. Nanobubbles at gpa pressure under graphene. *Nano letters*, 15(9):6162–6169, 2015.
- Huijuan Zhao, K Min, and Narayana R Aluru. Size and chirality dependent elastic properties of graphene nanoribbons under uniaxial tension. *Nano letters*, 9(8):3012–3015, 2009.
- Petr Zhilyaev, Evgeny Iakovlev, and Iskander Akhatov. Liquid–gas phase transition of ar inside graphene nanobubbles on the graphite substrate. *Nanotechnology*, 30(21):215701, 2019.